

---

# Dynamic Adaptation in Fly Motion Vision

Virginia L. Flanagan

---



München 2006

---

# Dynamic Adaptation in Fly Motion Vision

Virginia L. Flanagin

---

Dissertation  
zur Erlangung des Doktorgrades  
der Naturwissenschaften (Dr. rer. nat.)  
der Fakultät für Biologie  
der Ludwig-Maximilians-Universität München

Angefertigt am Max-Planck-Institut für Neurobiologie,  
Abteilung ‚Neuronale Informationsverarbeitung‘

vorgelegt von  
Virginia L. Flanagin  
aus Chicago, IL USA

München, den 01. Juni 2006



## Ehrenwörtliche Versicherung

Ich versichere hiermit ehrenwörtlich, dass die Dissertation von mir selbständig, ohne unerlaubte Beihilfe angefertigt ist.

Martinsried, den.....

.....

## Erklärung

Hiermit erkläre ich, dass ich mich anderweitig einer Doktorprüfung ohne Erfolg **nicht** unterzogen habe.

Martinsried, den.....

.....

Erstgutachter:  
Zweitgutachter:

Professor Dr. Alexander Borst  
Professor Dr. Benedikt Grothe

Tag der mündlichen Prüfung:

20. Juli 2006

# Table of Contents

---

<b>TABLE OF CONTENTS .....</b>	<b>5</b>
TABLE OF FIGURES.....	7
ABBREVIATIONS .....	8
<b>ABSTRACT.....</b>	<b>10</b>
<b>1 INTRODUCTION.....</b>	<b>12</b>
FLY VISUAL SYSTEM.....	13
<i>Photoreceptors</i> .....	15
<i>Lamina</i> .....	18
<i>Medulla</i> .....	19
<i>The lobula complex</i> .....	21
<i>Lobula plate tangential cells</i> .....	21
ELEMENTARY MOTION DETECTION.....	24
<i>General Principles</i> .....	24
<i>Gradient-type detector</i> .....	25
<i>The Reichardt Detector Model</i> .....	27
<i>Evidence for the Reichardt Detector</i> .....	30
ADAPTATION .....	32
<i>Efficient information transfer</i> .....	33
<i>Automatic adaptation</i> .....	36
<i>H1-cell and adaptation</i> .....	38
<i>The time course of adaptation</i> .....	41
JUSTIFICATION.....	43
<b>2 METHODS .....</b>	<b>45</b>
EXPERIMENTS.....	45
<i>Preparation</i> .....	45
<i>Electrical Recording</i> .....	47
<i>Visual Stimulation</i> .....	49
DATA ANALYSIS .....	54
<i>Stimulus-Response Curves</i> .....	55
<i>Dynamic Gain</i> .....	55
<i>Cross-Correlation</i> .....	56
MODELING .....	56
<i>Visual Pattern</i> .....	57
<i>Motion Detector</i> .....	58
TABLE OF EQUIPMENT AND SUPPLIERS.....	59
<b>3 RESULTS .....</b>	<b>61</b>
DEPENDENCE ON STIMULUS STATISTICS .....	62
<i>H1-cell firing properties</i> .....	62
<i>Stimulus-Response Function</i> .....	64
<i>Dynamic Gain</i> .....	67

	<i>Cross-correlations</i> .....	69
	DEPENDENCE ON VISUAL PATTERN.....	71
	TIME COURSE OF ADAPTATION.....	77
<b>4</b>	<b>DISCUSSION.....</b>	<b>83</b>
	GENERALITY .....	84
	<i>Examples of automatic adaptation</i> .....	84
	<i>Adaptation mechanisms in the Reichardt detector</i> .....	85
	<i>Adaptation of individual neurons and the Reichardt detector</i> .....	88
	EFFICIENCY .....	89
	<i>Efficient representations of correlations</i> .....	92
	<i>Ambiguity</i> .....	93
	DYNAMIC ADAPTATION IN MOTION DETECTION .....	94
	VISUAL PATTERNS AND NATURAL SCENES .....	97
	FUNCTIONALITY IN THE FLY VISUAL SYSTEM .....	99
	<i>Physiology of motion detection</i> .....	99
	<i>H1-cell functionality</i> .....	101
	<i>LPTCs network connectivity</i> .....	102
	CONCLUDING REMARKS.....	103
<b>5</b>	<b>REFERENCES .....</b>	<b>105</b>
<b>6</b>	<b>ACKNOWLEDGEMENTS .....</b>	<b>111</b>
<b>7</b>	<b>CURRICULUM VITAE.....</b>	<b>112</b>

---

## Table of Figures

Figure 1.1 Diagram of the fly visual system.....	14
Figure 1.2 Retinotopic organization in the fly visual system.....	15
Figure 1.3 Neural superposition and photoreceptor arrangement.....	16
Figure 1.4 Synaptic connections in a laminar cartridge.....	18
Figure 1.5 Two proposed vision pathways in the fly. ....	20
Figure 1.6 Diagram of 3 of the LPTC cell types.....	22
Figure 1.7 Two main classes of algorithmic motion detector models. ....	25
Figure 1.8 The Reichardt model for directionally selective motion.....	28
Figure 1.9 Different versions of the Reichardt motion detector. ....	29
Figure 1.10 The motion energy model. ....	30
Figure 1.11 The capacity for a neuron to maximize information ....	35
Figure 1.12 Adaptation to balanced background input. ....	37
Figure 1.13 The anatomy of the H1-cell. ....	38
Figure 1.14 Adaptation of response transients in the H1-cell. ....	39
Figure 1.15 H1-cell adaptation to the variance of the time varying velocity profile. ....	40
Figure 1.16 Information rate is invariant to stimulus entropy.....	41
Figure 1.17 The timescale of adaptation. ....	42
Figure 2.1 Fly preparation: the fly as seen from the back of the head. ....	46
Figure 2.2 The left H1-cell of the fly as seen from the back of the head. ....	47
Figure 2.3 Visual Stimulation Setup.....	48
Figure 2.4 Gaussian colored noise velocity profiles used.....	49
Figure 2.5 Velocity profiles for experiment set 3.....	52
Figure 2.6 Example 1 of stimulus with statistics ....	53
Figure 2.7 Example 2 of stimulus with statistics ....	54
Figure 2.8 The Reichardt detector model used in the simulations.....	57
Figure 3.1 Response characteristics from one fly.....	63
Figure 3.2 Overall response characteristics. ....	64
Figure 3.3 The stimulus-response functions for 3 velocity standard deviations.....	65
Figure 3.4 The maximum firing rate and corresponding velocity ....	65
Figure 3.5 Stimulus-response curves for H1-cell experiments. ....	66

Figure 3.6 Stimulus-response curves for different time constants..	67
Figure 3.7 Dynamic gain for experiments and motion detector model.....	68
Figure 3.8 Dynamic gain vs. acceleration.....	69
Figure 3.9 The normalized x-correlation between stimulus and response. ....	71
Figure 3.10 Stimulus-response correlations experiments and model.....	71
Figure 3.11 Dynamic gain of the motion detector for sinus vs. square wave .....	72
Figure 3.12 Dynamic gain of H1-cell for sinus vs. square wave.....	73
Figure 3.13 H1-cell response to higher harmonics of a square wave.....	75
Figure 3.14 Dynamic gain for square and sine wave gratings .....	75
Figure 3.15 The normalized cross-correlation for sine and square wave gratings .....	76
Figure 3.16 The effect of contrast on firing rate saturation and dynamic gain.....	76
Figure 3.17 Dynamic gain at low mean luminance. ....	76
Figure 3.18 Comparison of motion detector simulations and H1-cell gain.....	78
Figure 3.19 Motion detector gain during a switch experiment. ....	79
Figure 3.20 Dynamic gain of the motion detector to a stimulus switch .....	80
Figure 3.21 The statistics of the stimulus over a change in velocity time constant. ....	81
Figure 3.22 The statistics of the stimulus over a change in velocity standard deviation.....	82
Figure 4.1 A general model for automatic gain control.....	86
Figure 4.2 The effect of one stimulus component on another.....	87
Figure 4.3 The information rate of the H1-cell for Gaussian white noise.....	90
Figure 4.4 Information per spike as a function of lambda.....	91
Figure 4.5 Information per spike.....	92
Figure 4.6 The stimulus-response function from a gradient detector.....	96
Figure 4.7 Response of a Tm-cell to a moving grating.....	99
Figure 4.8 Electrical connections between different LPTCs in the blowfly. ....	102
Figure 4.9 Circuit diagram of the LPTCs connectivity.....	102

---

## Abbreviations

$\tau_0$	Time constant of low pass filter used to filter the velocity signal
$\sigma$	Standard deviation of the Gaussian colored noise velocity signal (zero mean)
$\tau_L$	Time constant of first order low pass filter in the full Reichardt detector model
$\tau_H$	Time constant of first order high pass filter in the full Reichardt detector model

CRT	Cathode ray tube
dB	Decibel (measuring unit)
EMD	Elementary motion detector
H1	Horizontal one (cell of the fly visual system)
HH	Hodgkin-Hukley model neuron
Hz	Hertz (measuring unit)
ICNC	Interdisciplinary Center for Neural Computation
ISI	Interspike interval
L1-L5	Laminar cell 1 to cell 5
LGN	Lateral geniculate nucleus
LIF	Leaky-Integrate-and-fire model
LPTC	Lobula-plate tangential cell
LTD	Long term depression
LTP	Long term potentiation
ND	Null direction
PD	Preferred direction
PSTH	Peri-stimulus time histogram
R1-R8	Rhamdomere 1-8, the photoreceptors of the fly
SNR	Signal-to-noise ratio
V	Volts (measuring unit)

## Abstract

---

Sensory neurons process and convey information about our surroundings, providing the physiological basis for how we interact with the external world. In order to understand neuronal responses we must identify the rules governing how sensory information is encoded. It was proposed more than fifty years ago that neural codes constitute efficient representations of the natural world (Attneave, 1954; Barlow, 1961). In an information maximization paradigm, an efficient coding strategy will match the encoded neural response to the statistics of the input signals. Adaptation of the stimulus-response function to the statistics of the stimulus is one way to efficiently encode a stimulus when the response range and resolution are limited compared to the entire range of stimulus probabilities (Laughlin, 1981). Recent work has indeed shown that adaptation to the input statistics can occur in real time (Smirnakis et al., 1997) and that this form of adaptation can be used to efficiently encode the stimulus and maximize information transmission (Brenner et al., 2000).

In this work I examined the mechanisms of dynamic adaptation in fly motion vision. The H1-cell is a large field tangential cell of the blowfly visual system that responds to motion in a directionally selective way. It also adapts its response properties to the second order statistics of an apparent motion stimulus (Fairhall et al., 2001). I measured the adaptation of the H1-cell to the variance and temporal correlations of a Gaussian low-pass filtered velocity signal that directed a sine wave visual grating. I found that the H1-cell adapted the slope, or gain, and range of its input-output function to the variance of the velocity signal over two orders of magnitude. The H1-cell also adapted its response properties to the low-pass filter time constant of the velocity signal over one order of magnitude. I compared the adaptation between flies by normalizing the gain of the stimulus-response function by the gain of the stimulus-response function during steady-state firing properties. This “dynamic gain” decreased as the velocity variance increased and broadened to cover the larger range of velocities. In contrast, as the time constant of the velocity fluctuations increased, the dynamic gain increased.

The results of these experiments were then compared with simulations of the correlation-type or Reichardt motion detector model. The Reichardt detector is an algorithmic model for

motion detection that explains the behavior of directionally selective large-field tangential cells in flies including the H1-cell, as well as directionally selective motion vision in humans (Zanker, 1996; Borst and Egelhaaf, 1989). The Reichardt detector model showed the same adaptive properties as the H1-cell in response to the same stimuli. Reichardt detector adaptation occurred without changing any of the model parameters; it was an automatic function of the dynamics of the model. This suggested that the mathematical properties of the Reichardt detector provide a mechanism for adaptation in the H1-cell of the blowfly.

This adaptation was further characterized in both the Reichardt detector model and the H1-cell. The time course of this form of velocity adaptation in the H1-cell was examined by switching between two different variances and two different low-pass filter time constants of the velocity signal. The H1-cell adapted to the statistics or the time course of the new velocity signal within two seconds after the switch. The Reichardt detector showed a similar time course for adaptation as in the experiments. The effect of the visual pattern on adaptation was also examined, using a square wave pattern in addition to the sine wave used previously. The visual pattern affects the output of an array of Reichardt motion detectors and may therefore affect adaptation in the system. The overall shape of the adaptation function with respect to the stimulus variance was not different between the two stimulus patterns. In the experiments, the H1-cell showed a consistently higher dynamic gain with a square wave pattern. The Reichardt detector model, however, had a lower dynamic gain when the square wave pattern was presented. After careful investigation of the potential causes of this discrepancy I found that the steady-state firing rate of the H1-cell saturated when a square wave pattern was used, thereby altering the normalization under experimental conditions that was not accounted for in the simulations. These results suggest that contrast saturation is an important feature of fly motion vision that has not been explained by the Reichardt detector model.

The Reichardt detector provides an automatic mechanism and mathematical explanation for adaptation in the fly visual system involving the nature of the incoming visual signals and the non-linearity in the motion detector model. Interestingly, the gradient detector model, although it is also non-linear, does not display automatic adaptation. It remains to be seen whether this type of adaptation is prominent in other sensory systems and whether it leads to and efficient and accurate representation of the natural world.

# 1 Introduction

---

We are constantly faced with motion information, either from egocentric movements or objects traveling in our field of view. This information is not, however, explicitly represented on the level of the photoreceptor; it must be computed from the local time dependent light intensity values that are encoded in the retina. Calculating the direction and velocity of an object in space is not a trivial task for the visual system; it requires multiple inputs and non-linear processing; not to mention the potential need for higher level processing such as object recognition or figure-ground discrimination. There are many different perspectives from which motion detection can be regarded. It is possible to look at the electrophysiological characteristics of motion sensitive cells, to examine the network connections that are involved in determining motion, or to look at the minimal amount of computation that is necessary for a system to detect motion information. Each of these perspectives contributes to our understanding of motion vision and is important to gain a full understanding of the complex nature of motion computation in the visual system.

From the algorithmic perspective, a number of mathematical models have been developed that describe how directionally selective motion information can be calculated from light intensity information over time. Strong biological evidence in favor of the correlation-type motion detector model has been found in both insects and in humans (Borst and Egelhaaf, 1989; Zanker, 1996; Sekuler et al., 1990). The correlation or Reichardt detector has been shown to be responsible for afterimage effects, for transient modulations that mirror the contrast frequency of the stimulus and for adaptation of decay time constants in response to a test motion pulse or step that follows an adapting stimulus. On the other hand, the Reichardt detector has not been able to account for contrast saturation in the fly.

Another way to look at motion vision is with neural coding. Neural coding examines the rules that govern how inputs are encoded into neuronal responses and what is encoded in the neural response. Neurons carry and process information; therefore it is natural to look at neural representations from the standpoint of efficiency and maximizing information. A single

neuron that is influenced by both internal and stimulus noise, has only a limited range and resolution with which it can encode velocity information. During chase behavior in the fly however, speeds can reach up to 3000 degrees per second and neuronal reaction times can be shorter than 30 milliseconds (Land and Collett, 1974). The response range of a neuron cannot cover such a large range of velocities without sacrificing information about smaller deviations in velocity. One way to circumvent this is to adapt the response properties to maximize the information about the current surroundings. Adaptation within the visual system allows for a more precise and efficient representation of the visual world under dynamic conditions.

It is still unclear how the fly visual system accomplishes directionally selective motion vision with the physiological tools it possesses. The fly visual system is composed of the retina, three regions that contain the neuronal cell bodies otherwise known as neuropile layers, and the axonal tracts that connect them. Additionally, directionally selective neurons called the lobula-plate tangential cells (LPTCs) integrate motion information over a large visual field and extend out of the third visual neuropile to the rest of the fly. Their response properties have many similarities to the output of an array of correlation-type motion detectors. The actual computational steps involved in motion detection in the fly are thought to occur in the cells upstream of the LPTCs in the three visual neuropile layers. The second neuropile layer is the first place where motion sensitive cells are found, but very few electrophysiological recordings have been done on these cells due to their small size.

In this work I will examine the dynamic adaptive response properties of the H1-cell of the blowfly *Calliphora vicina* and the mechanism for this adaptation. If the Reichardt detector is responsible for directionally selective motion then it should also be responsible for adaptation in the H1-cell. I will characterize the dynamic adaptation found in the H1-cell and test whether a similar type of adaptation is found in the Reichardt detector. This work gives further evidence that the Reichardt detector provides a sufficient mathematical description of motion detection in the fly.

---

### **Fly visual system**

In the first stage of visual processing, light enters the ommatidia or retina, exciting light sensitive cells that convert photon energy from a single point or pixel into local electrical

signals. This visual information travels from the retina to the lamina, and then through the optic chiasma to the second visual neuropile, the medulla. The signal then travels to the third visual neuropile, the lobula complex, which consists of the lobula and lobula plate. There local visual information is integrated by large field directionally selective neurons called lobula-plate tangential cells (LPTCs) and sent on to other areas of the nervous system. A diagram of the fly brain including the visual system is shown in Figure 1.1.

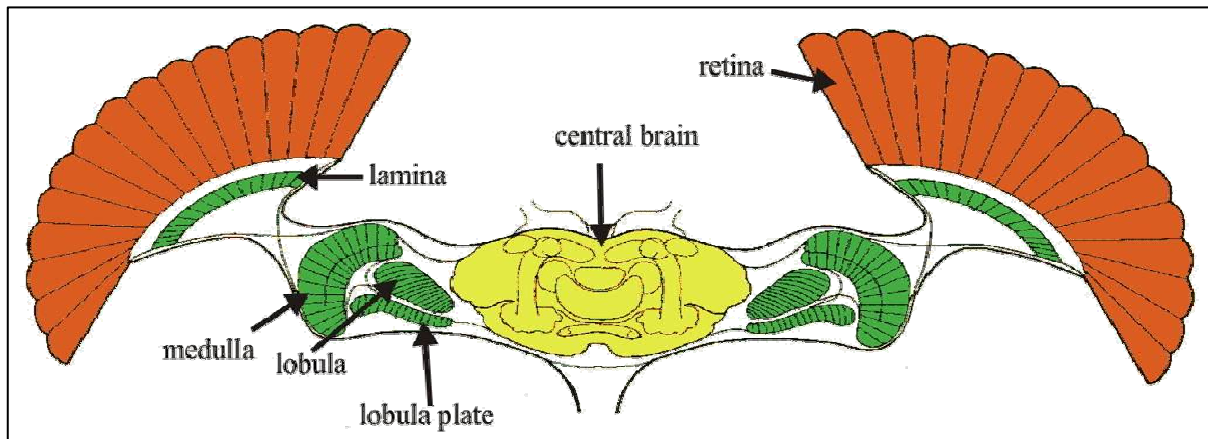


Figure 1.1 Diagram of the fly visual system. The retina is shown in red, the visual neuropile in green and the central brain in yellow. Information travels from the lateral to the medial visual neuropile layers. From the lobula complex, information can travel to the opposite eye, to the central brain or to the descending neurons that are involved in motor control. From (Borst and Haag, 2002; Borst and Haag, 1996)

The fly maintains a retinotopic image of the visual world throughout all of the visual neuropile layers. Each cell in the retina only responds to light from a small spot in the visual field, which is called its receptive field. Adjacent cells have receptive fields that correspond to nearby locations in the visual field; such that the activity patterns of neighboring cells create a pixilated 2-D picture of the local light intensity values across the field of view. This retinotopic organization is also found in the visual cortex of humans including V1 and is thought to be advantageous for neuronal computations. It allows for neighborhood relationships such as spatial correlations that are required for object recognition to be calculated with minimal wiring (Chklovskii and Koulakov, 2004). Retinotopy is an essential component in the form of spatial blurring that was recently found in the fly (Cuntz et al., 2003). The orientation of the retinotopic map is not constant throughout the fly visual system. It is preserved through the lamina, and then it is flipped in the optic chiasma such that the retinotopic map in the medulla is rotated 180 degrees. The map is rotated again this time 90 degrees in the lobula complex (Figure 1.2). Each time the map is turned, the neighborhood relations remain the same.

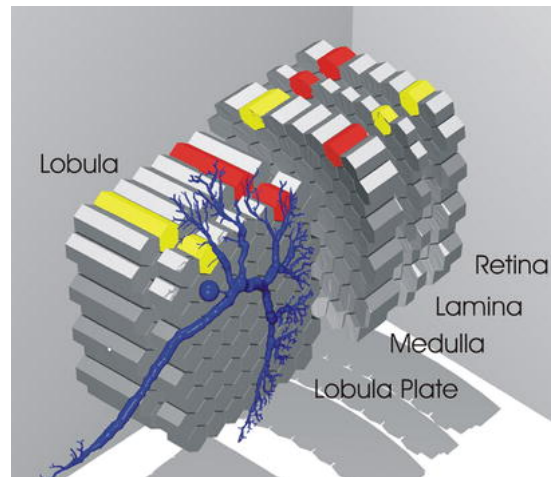


Figure 1.2 A schematic representation of the retinotopic organization in the fly visual system. The hexagonal columns in each layer represent columns of each neuropile layer. The red and yellow columns demonstrate how two parts of the visual field are represented in each neuropile layer, always maintaining neighborhood relations. The retinotopic information is then projected onto the dendrites of the lobula-plate tangential cells, here represented by the VS1-cell. From (Borst and Haag, 2002).

The majority of cells in the three visual neuropile layers are small and difficult to record from electrophysiologically; therefore most of the information about the functionality of these cells comes from experiments using radioactive 2-Deoxyglucose. In this method, radioactive 2-Deoxyglucose is taken up by only those cells that are metabolically active after the radioactive glucose is injected. The tissue is subsequently freeze dried and then viewed using autoradiography. 2-Deoxyglucose staining does not provide information about the electrical properties of individual cells but exposes which layers are active during specific visual stimulation. Golgi staining has also been used in the fly visual system to characterize cell types and to examine their fine anatomical structure. Golgi staining uses potassium dichromate and silver nitrate to stain entire neurons including spines and other fine anatomical structures, but does not provide any information about their activity or response properties. For reasons that remain unclear, this staining method randomly stains approximately five percent of the cells in a region. These staining techniques along with electrophysiological and calcium imaging data has provided extensive knowledge of the anatomy and physiology of the fly visual system.

### Photoreceptors

Flies, like most insects, have compound eyes where each facet or ommatidium is a functional unit including a lens apparatus and eight light sensitive photoreceptor cells. The lens is composed of a cornea and a cone that directs light onto the tops of seven of the eight photoreceptors. A single blowfly eye consists of approximately 5000 ommatidia (Strausfeld,

1984). In non-dipteran insects, the photoreceptor cells in each ommatidium are fused together (Figure 1.3B). Light entering a single facet will therefore stimulate all of the photoreceptors in that ommatidium. In the fly, however, the photoreceptor cells are spread around a central opening such that each cell has a unique optical axis (Land, 1997). This photoreceptor positioning makes it possible for individual cells to be activated independently from one another, depending on the angle at which the light enters the ommatidium (Figure 1.3A).

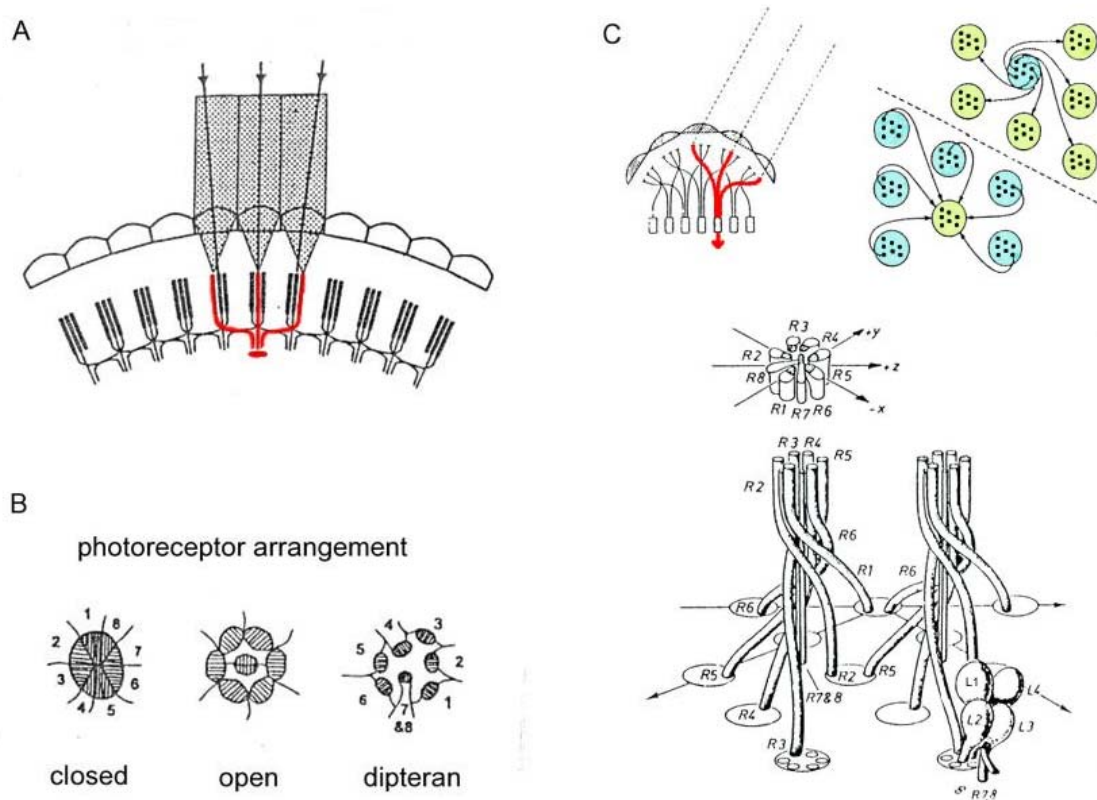


Figure 1.3 Neural superposition and photoreceptor arrangement. (A) When light enters an ommatidium after traveling through the lens it hits one of the 6 photoreceptors. The red photoreceptors are all activated by the same angle of light and then travel to the same laminar cartridge. (B) The arrangement of photoreceptors underneath the lens for different insects. The blowfly, like other dipteran insects, has the photoreceptors 1-6 around the perimeter and receptors 7 and 8 together in the center. (C) Left picture: similar to (A). Right: Laminar cartridges are in green, ommatidia in blue. 6 different ommatidia send processes from 1 photoreceptor to the same laminar cartridge. Similarly, all 6 photoreceptors from one ommatidium go to 6 different laminar cartridges. Below: A drawing of the crossing over pattern from 2 ommatidia to 12 different cartridges. Adapted from (Strausfeld, 1984).

Although a point light source in the visual field will stimulate only one photoreceptor in an ommatidium, it will simultaneously stimulate an additional five photoreceptor cells in five neighboring ommatidia. Photoreceptor cells from different ommatidia that respond to the same angle of light send their axonal processes, through a complex crossover arrangement, to the same synaptic cartridge in the lamina (Figure 1.3C) (Kirschfeld, 1972). This type of organization, called neural superposition, maintains the topographic structure of the light

signals and leads to the retinotopic arrangement of neuronal signals that exists throughout the fly visual system. The redundancy that results from having more than one photoreceptor respond to the same position in space, is thought to amplify the signal and reduce neuronal noise (Strausfeld, 1984)

Only six of the photoreceptors, otherwise known as rhabdomeres R1-6, form the outside circle of the ommatidium and have separate optical axes that contribute to neural superposition (Figure 1.3B). These six photoreceptors are called short receptors; sending their axons through the basement membrane of the retina to the first visual neuropile layer, the lamina. The short receptors send their axons to the lamina in a highly regular crossing over pattern, such that each photoreceptor from one ommatidium innervates a separate cartridge forming a ring-like structure (Figure 1.3C). The reverse is also true; a single cartridge in the lamina receives input from the photoreceptors with the same optical axis from the 6 ommatidia that form a ring around it (Figure 1.3C). These short receptors are thought to be the beginning of the primary visual pathway in the fly.

The two remaining photoreceptors, R7 and R8, in each ommatidium are generally about half as large in diameter as the short receptors; however they are called the long receptors because they send their axons from the retina through the lamina to the second neuropile layer, the medulla. R7/R8 are located in the center of the ommatidium with R7 situated on top of R8, but deeper away from the lens than the other 6 photoreceptors. Due to this positioning, the long photoreceptor cells are stimulated by all angles of light entering the ommatidium, but they are overall less sensitive to light than the short photoreceptors. In a small subset of ommatidia located in the upper medial part of the eye, the R7 and R8 receptors are enlarged and straight not twisted down their length as they typically are elsewhere in the retina. These specialized R7 and R8 cells are thought to detect polarized light (Strausfeld, 1984).

The concept of visual acuity describes the highest possible accuracy at which an organism can resolve an image. The distance between each ommatidium, or the interommatidial angle, is one of the factors that determine visual acuity in organisms with compound eyes. The interommatidial angle differs between insect species leading to different visual acuities that are generally related to the species' lifestyle. Dragonflies as predatory insects for instance, have a higher visual acuity than flies. In general, the maximal angular spatial resolution of the blowfly compound eye is about 2 degrees angular distance (Land and Eckert, 1985). In

contrast, a human with clinically “perfect” or 20/20 vision, has a visual acuity between 1/60 and 1/12 of a degree, depending on the measurement used (Pirenne, 1967; Hecht, 1931).

### Lamina

The lamina is the first neuropile layer in the fly visual system. It is a highly structured visual area consisting of repeated optical cartridges. Golgi staining in combination with electron microscopy has revealed the cellular structure and synaptic connections within the laminar cartridges. Twelve distinct cell types exist in the lamina, in addition to the axons from the photoreceptor cells (Strausfeld, 1984). There are five types of monopolar relay cells, basket-shaped dendrites from the T1-cells, two types of amacrine cells providing lateral connections in the lamina and four centrifugal neurons originating in the medulla. A summary of the connections in the individual cartridges of the lamina is shown in Figure 1.4.

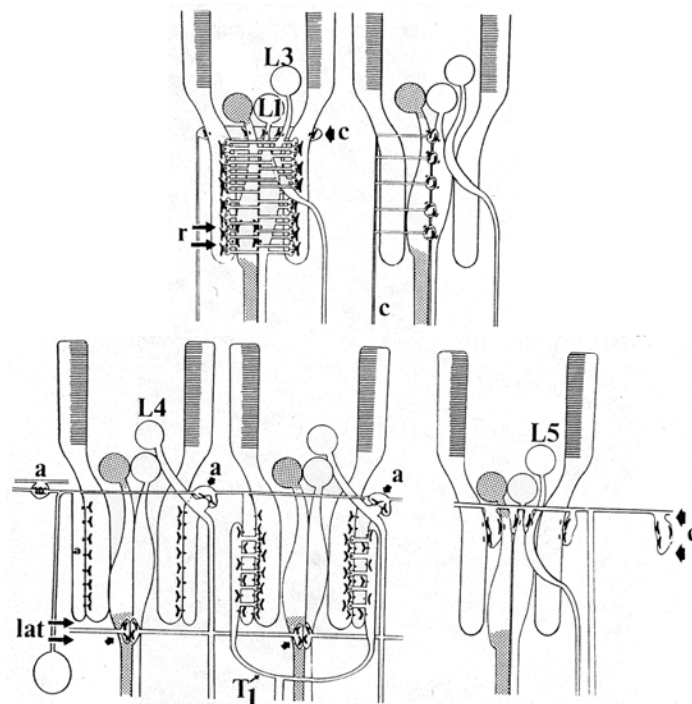


Figure 1.4 Synaptic connections in a laminal cartridge. Black Y-shaped structures indicate synapses. The L1-L3 cells connect directly with the photoreceptor cells coming from the retina. Various centrifugal cells (c) provide reafferent input onto the photoreceptors and the lamina monopolar cells (top 2 figures and bottom left figure). Amacrine cells (a) provide lateral connections between the cartridges (bottom left) and the dendrites of the T1-cells from the medulla. They also synapse on other amacrine cells and photoreceptors (bottom middle). From (Strausfeld, 1984).

Three of the monopolar relay cells L1-L3 synapse directly with the photoreceptor cells. L1 sends its axon to layers M1 and M5 of the medulla whereas L2 and T1 project to layer M2 (Figure 1.5) (Bausenwein et al., 1992). The L1 and L2 cells provide the beginning of two separate motion sensitive pathways that remain distinct throughout the visual system (Figure

1.5) (Bausenwein et al., 1992). L4- and L5-cells are local interneurons that remain in the lamina; receiving wide field inputs from the amacrine cells, which themselves provide the lateral connections within the lamina. The centrifugal cells provide reafferent input from the medulla back to the lamina and photoreceptor cells.

How do these connections affect the physiology of the cells? Lamina monopolar cells (L1-L2) have narrow and peaked receptive fields similar to those of the photoreceptors and are known to amplify the signals coming from the retina. Due to their narrow receptive fields, these cells are thought to act as spatial high-pass filters (Laughlin, 1981c). The receptive field of these cells can adapt to the mean luminance of the surrounding environment. The L3-cell receives input from the photoreceptors, but does not have any lateral or recurrent input from the lamina. It is however an output neuron from the lamina, unlike the L4 and L5 cells. Therefore, the L3-cell has the potential to represent a different set of information about the visual world that is independent from the L1-L2 cells and may therefore represent a third pathway for motion information (Strausfeld, 1984).

### **Medulla**

The medulla is organized into retinotopic columns with the same number of columns as the lamina has cartridges. Each column is also divided into ten layers that are individually distinguishable by the dendritic or axonal arborizations pattern of neurons that innervate the medulla. Cells that enter or exit the medulla have terminal branches that occur in one or more layers with very little overlap to neighboring layers. The medulla is considered the most complex of the visual neuropile layers in the fly, due to the diversity of cell types that have been found in the medulla using Golgi staining (Fischbach and Dittrich, 1989). Receptor terminals from the R7 and R8 photoreceptors end in the medulla as well as the axons from lamina monopolar cells L1-L3. In addition, approximately 40 medullar or trans-medullar cells are found in each column that connect medullar layers to one another and to downstream neuronal structures (Fischbach and Dittrich, 1989).

In *Drosophila melanogaster*, the most abundant cells found in the medulla are the trans-medullar-cells, the Tm- and TmY-cells (Bausenwein et al., 1992). Other cell types include the Y-cells and the medullar intrinsic neurons, or Mi-cells. Mi-cells branch in most of the medullar layers and can be individually identified by the layers they innervate. The Mi1-cell, for example, branches in layers M1, M5 and M10. Tm-cells have dense arborizations in

layers M3, M8 and M9, whereas TmY-cells have dense arborizations in layers M3, M5 and M8. TmY-cells and Y-cells are named for their characteristic axonal branching; the primary axon splits first into two large axonal stems that travel separately to the lobula and lobula plate. Tm-cells on the other hand have their output arborizations primarily in the lobula (Bausenwein et al., 1992).

The medulla is the first location where motion processing has been found in the fly. The 2-Deoxyglucose (2-DG) method for staining active neurons has shown layer specific staining of the medulla during motion stimulation (Bausenwein et al., 1992; Bausenwein and Fischbach, 1992). Layers M1, M2, M5, M9 and M10 are heavily stained when the fly is stimulated by a whole-field moving grating. On the contrary, M1, M5 and M7 were heavily stained when a single bar was moved across the visual field, suggesting that the layers of the medulla provide additional separation of motion pathways, in this case for different types of motion.

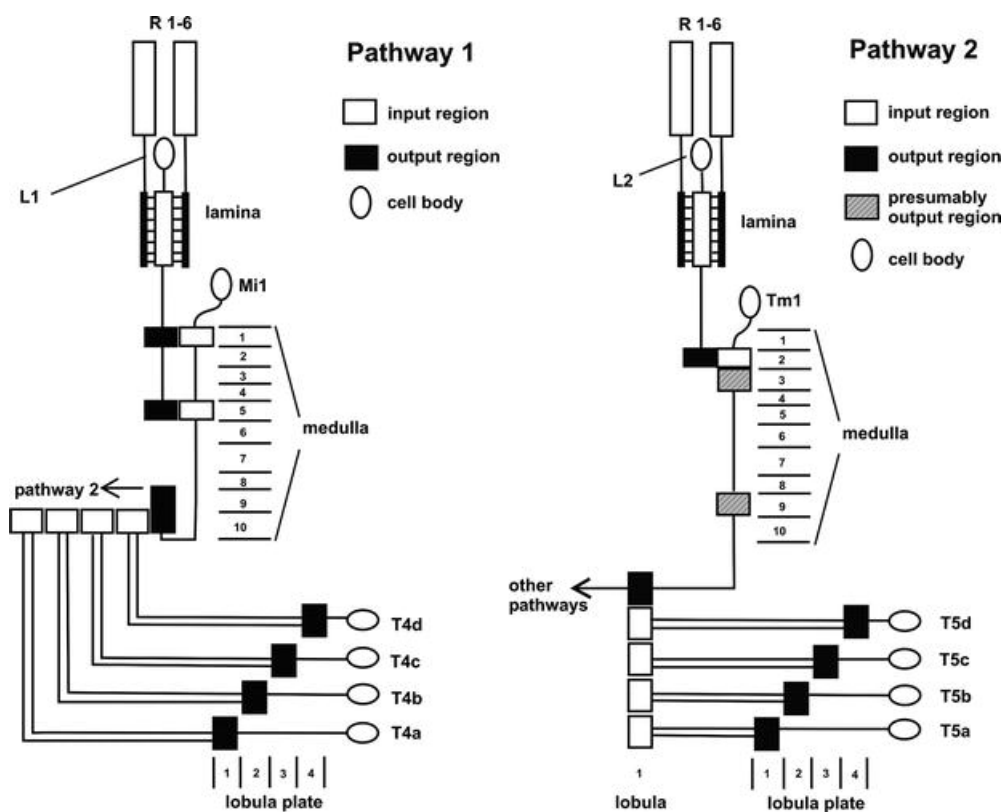


Figure 1.5 Two proposed vision pathways in the fly. The pathways start in the photoreceptors, R1-6, but then separate in the lamina through the L1 or L2 neurons. The pathways converge again in the lobula plate tangential cells. From (Bausenwein et al., 1992).

Figure 1.5 portrays the cellular composition of two proposed visual pathways found in the fly visual system. In the first pathway, L1-neurons project to layers 1 and 5 where the Mi1-cell has its dendrites. The Mi1-cell remains in the medulla and connects to a set of T4-cells,

which then innervate the lobula plate. In the second pathway on the other hand, L2-cells are thought to connect to the Tm1-cells in layer 2 of the medulla. The Tm1-cell extends into more distal layers of the medulla and then on into the lobula, where it connects with the T5-cells. T5-cells then project into the lobula plate, synapsing onto the LPTCs.

### **The lobula complex**

The lobula complex is made up of two structures, the lobula and the lobula plate. The lobula is organized in retinotopic columns, but with less columns than the previous neuropile structures and has therefore a coarser visual resolution (Strausfeld, 1989). The lobula is also divided into six layers, as opposed to the ten layers in the medulla. Three of the six layers were labeled with 2-Deoxyglucose in response to a motion stimulus (Buchner et al., 1984). The most posterior layer of the lobula contains the axonal arborizations of the Tm1 cells from the medulla as well as the T5 dendritic arborizations which are all part of the second pathway for motion vision (Figure 1.5).

The lobula plate is similar in structure to the lobula. It has only four layers but a similar number of retinotopic columns as in the lobula. Four distinct types of both T5-cells and T4-cells innervate the lobula plate, each cell type projecting to a different layer (Strausfeld and Lee, 1991) (Figure 1.5). This organization suggests that the layers of the lobula plate are responsible for different characteristics of the visual world. It was indeed found using the 2-Deoxyglucose method that each layer responds to a different direction of motion (Bausenwein et al., 1992; Bausenwein and Fischbach, 1992; Buchner et al., 1984). The four different layers correspond to the four preferred directions found in the lobula-plate tangential cells (LPTCs); front-to-back, back-to-front, up and down (Bausenwein et al., 1992; Bausenwein and Fischbach, 1992). In addition, the LPTCs themselves have their dendritic ends in the four different lobula plate layers, depending on the preferred direction of the cell.

### **Lobula plate tangential cells**

The lobula plate tangential cells (LPTCs) are a group of around 60 cells that provide the major information output from the lobula plate and the rest of the visual system. LPTCs receive feed-forward input from the retinotopically organized cells that come from the lamina, medulla and lobula. At the level of the LPTCs, visual information is no longer retinotopically organized; instead it is pooled from the local neuronal elements that synapse on to each particular cell. As the name suggests, LPTCs sit on top of the lobula plate and

extend their dendritic processes into to lobula plate, connecting to the local retinotopically organized cells there. They are relatively large cells, with unique firing properties and distinct morphology that is recognizable across flies, making them ideal for electrophysiological studies. A wealth of information exists about the response properties of LPTCs and their sensory contribution to flight control (for a review see (Borst and Haag, 2002)). The individual LPTCs can be categorized by 1) whether they respond to horizontal or vertical motion 2) the shape of their response, 3) where the neurons send their axonal projections, 4) whether they respond to large or small field motion.

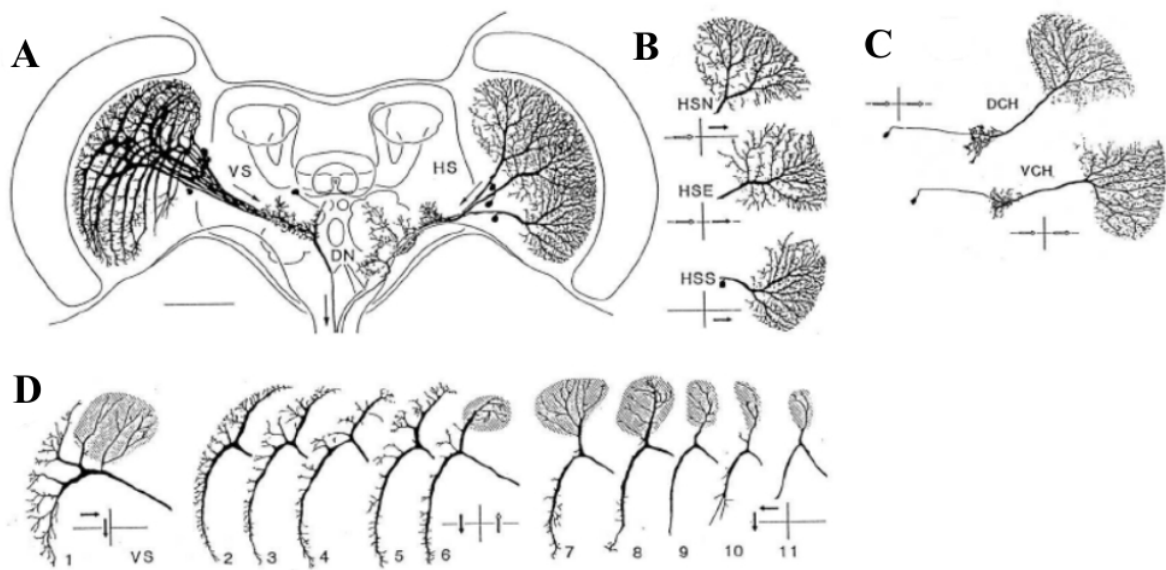


Figure 1.6 Diagram of 3 of the LPTC cell types. A) A horizontal section through the fly with the vertical system (VS)-cells drawn on the left hand side and the horizontal system (HS)-cells on the right. B) The dendritic anatomy of the 3 HS-cells in their respective positions. C) The anatomy of centrifugal horizontal (CH) cells. D) The structure of the VS-cells. Shaded zones represent dendritic regions that synapse in horizontally responsive layers of the lobula pate. Small arrows indicate the preferred direction with the vertical line representing the midline. From (Hausen, 1984).

There are three main classes of cells that respond to large field horizontal motion. These are the horizontal system (HS)-cells, the centrifugal horizontal (CH)-cells and the horizontally responsive heterolateral spiking cells (H1-Hu) (Hausen, 1982). The different horizontally responsive cell types are distinguishable from one another by their anatomy, their firing properties and the location of their output projections. Each eye has three HS-cells; the northern (HSN), equatorial (HSE) and southern (HSS)-cells, that respond to motion in the upper, middle and lower regions of the visual field respectively (Figure 1.6B). HS-cells respond to their preferred direction, which is front-to-back motion, with a graded potential depolarization and spikelets that are irregular in size. The HS-cells project to the ipsilateral

side of the central brain; however they also have electrical synapses on their dendrites that relay information to the CH-cells (Haag and Borst, 2002).

There are two CH-cells per hemisphere, named the dorsal (dCH) and ventral (vCH) cells for their respective receptive field locations (Figure 1.6C). These cells do not connect directly to columnar elements of the lobula plate, but instead receive motion information from other LPTCs (Cuntz et al., 2003; Haag and Borst, 2002). CH-cells have two types of synaptic specializations in their dendritic branches; electrical synapses that provide ipsilateral visual input from the HS-cell, and pre-synaptic GABAergic specializations that send information to small field LPTCs such as the FD-cell (Gauck et al., 1997; Warzecha et al., 1993). The axon-like structure is in fact an input region that receives information from the H2-cell on the contralateral side. The preferred direction for CH-cells is the same as HS-cells: front-to-back motion, but they respond only with a graded potential and no spikelets. Due to the separate input branch in the other hemisphere of the fly, CH-cells also respond to contralateral back-to-front motion by increasing EPSP activity.

The cellular organization of the vertically responsive LPTCs is slightly different. There are at least 10 vertical system (VS)-cells per hemisphere although an eleventh VS-cell may exist that is medial to the VS10-cell (Hengstenberg et al., 1982). VS-cells have a characteristic shape, with a T-shaped axon and dendrites that lie in a dorsal-ventral line (Figure 1.6D). The VS1-cell dendrites are located lateral to all the other VS-cells, and the consecutive VS-cells form a row from lateral to medial. In general, the VS-cells all respond strongly to downward motion each at a particular frontal-posterior position that corresponds to their location in the lobula plate, although they respond weakly to horizontal motion in the dorsal and ventral most regions of the visual field (Hengstenberg et al., 1982; Hengstenberg, 1982). VS-cells with more lateral dendritic trees respond strongest to motion in the frontal part of the visual world as seen by the fly. They also respond weakly to upward motion approximately 120 degrees horizontal to where their maximum response is. VS-cells send their axons medially to the ipsilateral side of the brain similar to HS-cells, where they connect to descending cells.

Finally, the heterolateral spiking cells are a group of either vertical or horizontal cells that connect the two visual hemispheres. These cells respond to motion with changes in their firing rate. There are cells that respond to horizontal motion (H1, H2 and Hu) and cells that respond to vertical motion (V1-V2) (Hausen, 1984). All heterolateral spiking cells have a motion direction that they respond strongest to, but most tend to have additional complex

receptive fields that involve motion in other directions. For instance, the horizontal cell H1 has a back-to-front preferred direction of motion. It also responds, however, to downward motion in the front receptive field, and to horizontal motion in the upper visual field (Haag and Borst, 2003). The H1-cell faithfully represents with its firing rate, the contrast frequency of a moving grating, and it is possible to record from the H1-cell for long periods of time. It is therefore a subject of interest for questions regarding information theory and neural coding and it also the subject of this study. A more detailed introduction to the H1-cell can be found in a separate section at the end of this chapter.

---

## **Elementary Motion Detection**

Motion detection is one of the most basic tasks that a visual system must perform. An organism is confronted with motion information whenever it is moving through space or when another object moves in its visual field. The ability to accurately determine speed and direction is also important for visual orientation and stabilization of gaze. Velocity information, however, is not explicitly represented in the output signal of a photoreceptor. Instead, at least two spatially separated inputs are required in order to measure directionally selective motion from light intensity changes that are perceived at the level of the photoreceptors. In this section I will introduce the concept of motion detection including the fundamental requirements for motion detection and a few existing models for motion detection before discussing the evidence in favor of the correlation-type motion detector as the mathematical algorithm for motion perception in the blowfly.

### **General Principles**

It is easy at first to imagine that a system designed to extract motion information could simply measure the displacement of individual objects in the visual field. This requires a more complicated system that first extracts specific elements from the visual scene, and then computes the displacement of these objects over time. However from an algorithmic point of view, object recognition is not a trivial task. As it turns out, psychophysical and behavioral experiments have shown that this is not required for motion detection (Reichardt, 1961; Braddick, 1980).

There are a few minimal requirements that are necessary for directionally selective motion (Borst and Egelhaaf, 1989). First, two inputs are required to detect motion. Motion cannot be

measured by light intensity changes at a single point; it requires at least two points of reference. For instance a single photoreceptor could not distinguish between a light flash in its receptive field and a light bar being moved over its receptive field. Secondly, in order to detect the direction of motion, the two input signals must be processed asymmetrically. If the two input channels were processed in the same way they would be completely interchangeable and the system would therefore not be directionally selective. Finally, the two asymmetrical inputs must interact in a non-linear way. In a linear system, the temporal information is lost with time averaging. A number of models for motion detection have been designed, all of which meet these three minimal criteria.

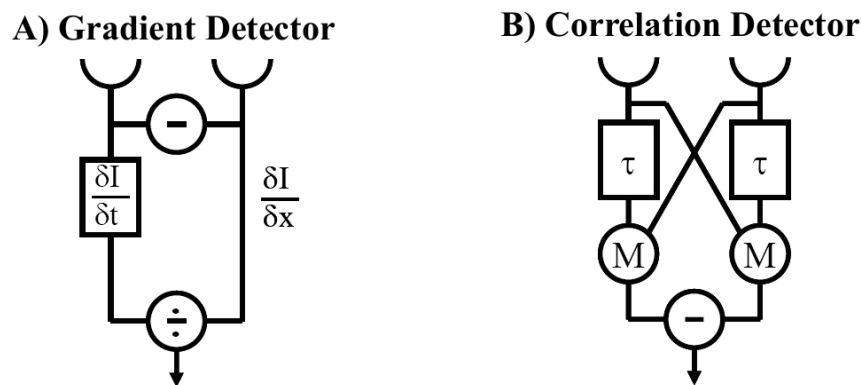


Figure 1.7 Two main classes of algorithmic motion detector models. A) The gradient detector model compares instantaneous spatial and temporal brightness changes in order to calculate motion. B) The correlation-type motion detector uses the coincidence of the two signals in order to detect motion. From (Borst, 2006).

Although the theories of motion detection are quite different from one another, they can be divided into two main categories: the gradient- or the correlation-type motion detector models. The distinction is based on the mathematically formal operations that each model uses in order to detect motion; they do not specify the biological mechanisms that perform these operations. This makes it difficult to test how motion detection occurs in the visual system and which algorithmic model accurately characterizes motion detection for a particular organism. The gradient- and correlation-type motion detectors each have unique characteristics however, that can be tested in biological systems in order to determine whether one of the algorithmic models accurately describes the physiological motion detection system in question.

### Gradient-type detector

Gradient-type motion detectors compare the instantaneous spatial brightness changes with the changes in brightness over time at a given location (Figure 1.7A). Gradient detectors were

originally developed in computer vision for the processing of video image sequences and were only later applied to biological systems (Marr and Ullman, 1981; Hildreth and Koch, 1987). The theory behind the gradient detector is based simply upon mathematics. The instantaneous temporal brightness change,  $\partial I / \partial t$ , at any given location  $x$  is proportional to the instantaneous speed  $dx / dt$  at that location such that:

$$\frac{\partial I}{\partial t} = \frac{\partial I}{\partial x} \cdot \frac{dx}{dt} \quad (1)$$

Therefore, by dividing the temporal brightness change by the spatial brightness change it is possible to recover the velocity in one spatial dimension (Borst and Egelhaaf, 1993). The negative sign for determining velocity relates to the convention that leftward motion is defined as negative and rightward motion as positive.

$$v = -\frac{dx}{dt} = -\frac{\partial I}{\partial t} \div \frac{\partial I}{\partial x} \quad (2)$$

This gradient scheme is a formalism for the relationship between the spatial and temporal brightness changes induced by motion, but it does not state how the partial derivatives representing these brightness changes are calculated. This computation is not trivial; in most cases the partial derivatives must be approximated in some way, which in turn limits the motion detection capability of the gradient detector. One way to approximate the brightness changes is to take the difference between brightness at two neighboring image points as the spatial derivative and a temporally high passed brightness signal as the temporal derivative (Buchner, 1984). More sophisticated ways of approximating the brightness changes that come much closer to the ideal gradient detector scheme have been developed in computer vision. The algorithmic gradient detector model, in contrast to the correlation model, produces a signal that measures the absolute velocity, independent of the visual pattern. However, imprecise measures of instantaneous brightness changes or physiological implementation of the gradient detector often lead to responses that no longer have this property.

Another consequence of the gradient scheme is that, because the non-linearity is divisive, the velocity estimate can become infinite. This occurs when the denominator or spatial brightness change goes to 0 when the numerator has a finite value (see Equation 2). In practice this can

happen if a spatially homogenous pattern exhibits changes in illumination that are not related to motion, for instance with a spatially homogeneous flash of light. This mathematical inconsistency can be circumvented by the addition of a small constant to the denominator. More specifically, this is accomplished by dividing by the absolute value of the partial derivative with respect to  $x$  and then adding a small constant,  $\varepsilon$ . Then the denominator is never zero, and in order to keep the sign of the velocity correct, the sign of the partial derivative is multiplied by the entire function. The final output of the detector would then look like this:

$$R = \frac{\partial I / \partial t}{|\partial I / \partial x| + \varepsilon} \operatorname{sgn} \frac{\partial I}{\partial x} \quad (3)$$

There is a wealth of evidence that suggests that the correlation-type motion detector and not the gradient detector is used in the fly to compute directionally selective motion. However, the gradient detector would be the optimal detector in terms of neural coding in the fly visual system under high signal-to-noise (SNR) conditions (Potters and Bialek, 1994). Haag et al.(2004) however, found that even during high SNR stimulation the LPTCs still responded to the temporal frequency of a pattern and not the absolute velocity suggesting that the Reichardt detector also operates in the fly at high SNR.

### **The Reichardt Detector Model**

Correlation-type motion detector models are based on a concept of delay and compare, which was first proposed by Exner (Exner, 1868). The correlation detector differs categorically from the gradient detector because it specifies how to measure the brightness changes that result from motion (Borst and Egelhaaf, 1993). In the early 1960's, Reichardt and Hassenstein came up with a formal model based upon the work from Exner (Reichardt, 1961). In the correlation detector, otherwise known as the Reichardt detector, signals from neighboring points in space are temporally filtered and then multiplied in order to produce directionally selective motion (Figure 1.7B). This is equivalent to calculating the correlation between spatially separated signals, hence the name "correlation detector." The temporal filters used in the model can vary between different realizations of the correlation-type motion detector, but the principle remains the same.

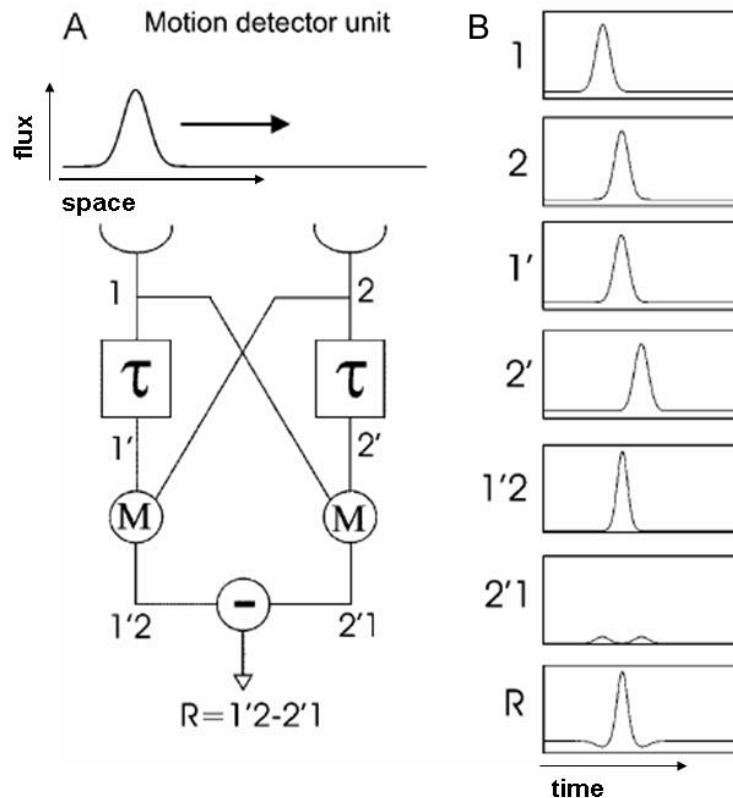


Figure 1.8 The Reichardt and Hassenstein model for directionally selective motion. The model responds with a positive signal to motion from left to right. (A) A diagram of one elementary motion detector unit consisting of two input lines and mirror-symmetrical subunits. (B) The intermediate signals from the Reichardt detector at the corresponding positions in (A). A light colored bar passes by the first photoreceptor (1) thereby stimulating it. The signal from 1 is passed through a delay and is then multiplied (M) by the unfiltered signal from 2 leading to a stronger, narrower signal (1'2). The mirror computation is done leading to a broader weaker signal (2'1) which is then subtracted from the first side, leading to a Mexican-hat type temporal response. Motion in the other direction produces a negative signal, so the system is directionally selective. From (Borst and Haag, 2002).

A simplified description of how this algorithm works is shown in Figure 1.8. One detector consists of two mirror symmetrical subunits. In one subunit the signal from two inputs that are spatially separated from one another are multiplied together after one of them has been temporally filtered; in Figure 1.8 the filter is a simple delay. If the delay is similar to the speed at which the signal reaches the second input, the multiplication amplifies the response. The mirrored subunit performs just the opposite; it separates the two signals from each other, which then become smaller through the multiplication. The final output of one elementary motion detector (EMD) is then the difference between the first and the mirror subunit. The average of an array of such detectors results in a directionally selective motion signal across the visual field. A separate array of Reichardt detectors will then be required for computing motion in each direction.

Various expansions of the Reichardt detector have been proposed to adjust the properties of the motion detection scheme to the performance of individual biological systems. More

advanced versions of the Reichardt model have been developed for the fly visual system, where the delay filter is replaced by a low-pass filter, and where the input line without any filter is replaced by a high-pass filter (Figure 1.9). Preprocessing steps can also be added to the input lines of the Reichardt detector, such as a full-wave or half-wave rectifier, or an additional high-pass or band-pass filter, which help to mimic the physiological properties of photoreceptor cells (Chubb and Sperling, 1988; Sperling, 1989; Borst et al., 2003). Reichardt detector models have been designed to work with only specific colors or patterns and have been used to explain human vision perception (Zanker, 1996; Sekuler et al., 1990).

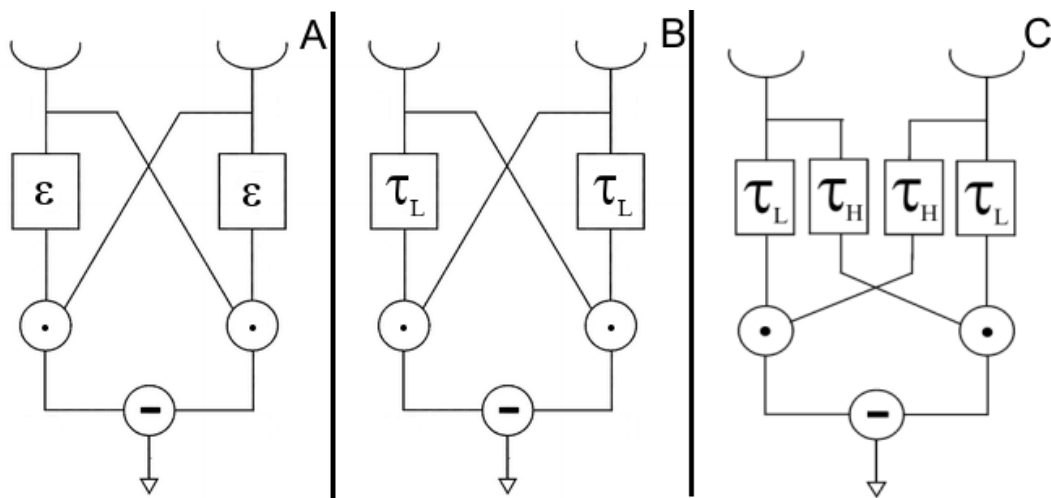


Figure 1.9 Different versions of the Reichardt motion detector. (A) The Reichardt detector with delay lines as filters. (B) The Reichardt detector model with low-pass filters in each mirror image. (C) The full Reichardt detector model with a high-pass or low-pass filter in each arm of the detector.

A very simple version of the Reichardt detector model is called the Barlow and Levick model, named after the people who used it to explain directional selectivity in rabbit retinal ganglion cells (Barlow and Levick, 1965). The model consists of two input lines, one with a delay. The signals in the two input lines are then compared using an “AND-NOT” gate instead of a multiplication. In this case, the detector is continuously active unless the two signals arrive simultaneously at the “AND-NOT” gate, then the signal is suppressed. Contrary to the traditional Reichardt detector, in the Barlow and Lewick model, the direction of motion that leads to the simultaneous arrival of both signals at the “AND-NOT” gate is the non-preferred or null direction (ND).

Another version of the correlation-type detector is the energy model (Adelson and Bergen, 1985). This model arose from the discrepancies found between the Reichardt detector model responses to a low-dimensional stimulus and the response properties in higher order visual processing, such as the orientation selectivity of area V1 in the visual cortex of cats and

monkeys. In the energy model, the input signal is filtered in parallel by two input channels that have different spatio-temporal linear filters. The filters from the two different input lines are then either added together or subtracted (Adelson and Bergen, 1985). This creates a biologically realistic spatio-temporal receptive field (Figure 1.10). Unfortunately additional computational processes are needed because the model responds to an inverse in the contrast with a change in the detected direction of motion, making it a poor directionally selective motion detector. This problem is solved by squaring the output of each channel (Figure 1.10). Despite the differences in internal architecture, the energy model is mathematically equivalent to the Reichardt detector at the level of the output (Sperling, 1989), which presents the question whether the additional complexity in the energy model is actually necessary to explain motion vision.

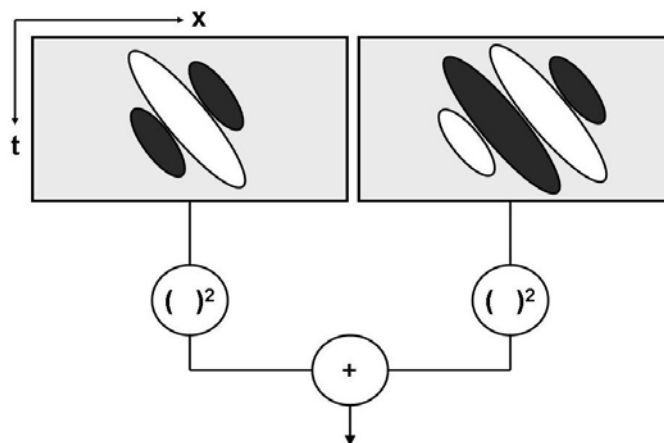


Figure 1.10 The motion energy model. Two linear filters or spatiotemporal receptive fields are 90 degrees out of phase with one another and are called a “quadrature pair.” If the responses from the filters are squared and added together they result in a phase-independent measure of local motion energy. In order to create the filters, a number of separable spatial or temporal filters can be added together. From (Adelson and Bergen, 1985).

### Evidence for the Reichardt Detector

The gradient-type and correlation-type motion detectors predict specific and different response properties to various motion stimuli. It is therefore possible to test which model most likely describes the mechanism for motion detection in individual biological systems. It has been repeatedly shown that the Reichardt detector model can explain the electrophysiological and imaging results from the LPTCs and also the optomotor response properties of the blowfly (Fermi and Reichardt, 1963; Buchner, 1976). For example, the Reichardt detector predicts that the non-averaged motion detector response i.e. the response from a single elementary Reichardt motion detector (EMD) is modulated by the contrast frequency of the visual pattern. Using local visual motion stimuli, the HS-cell modulated its

membrane potential with the same frequency as the spatial grating (Egelhaaf et al., 1989). When the visual stimulus covers the entire visual field, however, this phenomenon disappears. The Reichardt detector also shows transient responses that are modulated by the frequency of the visual pattern. Transient fluctuations in the spike rate or membrane potential of LPTCs in response to a step response also match the spatial frequency of the visual pattern (Borst and Egelhaaf, 1987; Egelhaaf and Borst, 1989).

The Reichardt detector is not a pure velocity detector; instead the mean response amplitude should depend on the structure of the pattern. For a moving grating, the response amplitude of the motion detector is a function of the contrast frequency of the visual pattern and not the absolute velocity. This means that the maximum amplitude depends on the ratio of the spatial wavelength of the brightness pattern to its velocity. Optomotor responses and electrophysiological results from the fly also show a contrast frequency maximum of approximately 2 Hz and no consistent velocity maximum (Eckert, 1980; Reichardt and Poggio, 1976).

Further evidence in favor of the Reichardt detector can be seen in spatial aliasing properties of the fly. The angular distance between the two input lines of a motion detector sets the sampling base, or the minimum spatial resolution of motion detection for the system. When the spatial pattern is below this resolution, the response of the motion detector becomes inverted signaling the wrong direction of motion. This phenomenon is called spatial aliasing or geometric interference (Götz, 1964). The lower limit before spatial aliasing occurs is, according to Shannon's sampling theorem, twice the sampling base of the system (Shannon and Weaver, 1949). In the fly, the sampling base is the interommatidial distance, which is between 1.3 and 2.6 degrees depending on the location on the eye. Indeed, spatial aliasing is found to occur below twice the interommatidial distance in the LPTCs of the fly (Eckert, 1980).

In addition, characteristics of the fly visual system that were originally attributed to movement adaptation were demonstrated to be a result of contrast frequency adaptation of the Reichardt detector model. If the H1-cell of the fly is presented with moving adaptive grating before a small test motion step is given, the decay time constant of the firing rate adapts to the velocity of the adaptive stimulus (de Ruyter van Steveninck et al., 1986). For smaller velocities, the decay time is longer, and for larger velocities the decay time is longer. They also found that the decay time constant depends on velocity and not on contrast frequency, which would be contrary to the correlation-type motion detector model (de Ruyter van

Steveninck et al., 1986). Borst and Egelhaaf (1987) showed, however, that the decay time constant also adapted to a full field flicker stimulus that was modulated sinusoidally, suggesting that contrast frequency and not pure velocity is responsible for the adaptation and is therefore consistent with the Reichardt detector model. Similar results were found in both the H1- and the HSE-cell of the fly visual system suggesting that the decay time adaptation is due to elements upstream from the LPTCs (Borst and Egelhaaf, 1987).

New properties of the Reichardt detector continue to be discovered and are used to test whether this algorithm is implemented for directionally selective motion vision in the fly. The ultimate test whether a physiological version of the Reichardt detector is implemented in the fly visual system will be to find the cells that perform the individual computational steps of the Reichardt detector; a current topic in fly vision research today.

---

## **Adaptation**

Adaptation is a widespread phenomenon in biological system that occurs on many different levels of organization, from the molecular to the population level. In the nervous system, adaptation provides flexibility of function under unstable external conditions. A neuron can be thought of as adaptive if it repeatedly responds in one way to a stimulus under prior condition A and in a different way to the same stimulus under prior condition B. In this way the neuron adapts to the prior condition by changing its response properties to the test stimulus, which remains the same. Adaptation is a useful property in the nervous system because it gives a neuron the possibility to optimize its output to the current state of the stimulus. In any system, but particularly in a system with additional noise components, the response resolution or the “detectable differences” between possible response values are not infinite and therefore limit the range and resolution at which a system can encode a stimulus. This means that the system can only encode a limited amount of input possibilities at a particular resolution. For the visual system this is particularly daunting because the overall light fluctuations are considerably larger than the response range of a neuron, but adaptation can help to surmount this problem.

For example, after stepping out into a bright day from a dark building, our eyes require a short time, on the order of tens of seconds, before they adapt to the new mean light level. This is called light adaptation and is a common form of adaptation in the visual system.

Responses from retinal ganglion cells, the output cells from the retina, already show light and dark adaptation (Smirnakis et al., 1997). Both light adaptation and the opposite, dark adaptation have a number of mechanisms, including changing the size of our iris to let in variable amounts of light and the opening and closing of cGMP mediated calcium channels in the plasma membrane of photoreceptor cells (Hodgkin and Nunn, 1988).

Retinal ganglion cells not only adapt to mean light levels but also to the variance of light fluctuations. It was shown in both the rabbit and the salamander that retinal ganglion cells adapt their response properties such that they are less sensitive to the current stimulus, for flicker stimulus patterns including checkerboard, uniform and horizontal or vertical bars (Hosoya et al., 2005). After adaptation to one of the pattern types, the ganglion cells respond more strongly to a novel stimulus than to the adaptive stimulus. Hosoya et al. (2005) found that this is most likely due to synaptic plasticity in the inhibitory synapses that are input to the ganglion cells. Using a network model connecting amacrine cells and retinal ganglion cells, they were able to show that anti-Hebbian synaptic plasticity reliably reproduces this form of adaptation.

This work focuses on the mechanisms behind motion adaptation in the visual system of the fly. In this section I will introduce the concept of adaptation as a principle for maximizing information and efficiently encoding visual stimuli. Then I will discuss mechanisms behind adaptation, in particular recent evidence that adaptation is an automatic property either of every neuron or of non-linear systems responding to dynamic stimuli. Finally, I will give a background overview of the adaptive properties of the H1-cell before introducing the purpose of this work.

### **Efficient information transfer**

A basic function of the nervous system is to relay information, either sensory or motor, to other parts of the nervous system or tissues of the body. Neural coding is the theory that explains how neurons represent information, and what rules govern how information is encoded. It is a difficult task to accurately and efficiently represent the complex dynamical signals that occur in the natural world. Attneave (1954) proposed that neural processing of information could be thought of as an optimization problem, the neural representation being an efficient representation of the input. Attneave (1954) used this concept to justify why center-surround receptive fields so often exist in early stages of visual processing, since

center-surround receptive fields reduce redundancy. He went on to explain that objects are encoded in higher visual processing stages because they are the most efficient representation at that stage (Attneave, 1954).

It has also been suggested that center-surround receptive fields in the retina increase the ability to encode spatial detail by removing the deleterious effects of intrinsic noise (Srinivasan et al., 1982). The antagonistic surround area measures the mean of the signals in neighboring receptors around the center, predicting the value of the signal in the center. The predicted value is then subtracted from the actual center value (Srinivasan et al., 1982). Therefore the value that is encoded is only a difference value, minimizing the range of values that must be encoded by the interneuron, thereby increasing the resolution of detectable values under higher noise conditions. It was also proposed that the purpose of the early visual system is to recode signals in an efficient way (Barlow, 1961). Natural signals have a large amount of temporal and spatial correlations, leading to redundancy. Recordings from the lateral geniculate nucleus (LGN) were found to be uncorrelated from one another, suggesting that the early visual system does indeed recode the inputs into a more efficient form (Dan et al., 1996).

The statistical properties of natural signals are however variable and the total dynamic range of natural stimuli is generally much larger than the range and resolution of a neural response can encode, particularly in the presence of internal noise.. Adaptation can ensure that the efficient representation is maintained for the current statistics of the natural image. Mean light level adaptation in the retina makes the retina more sensitive to other visual statistics such as the variance of the light levels at a particular point in time. In general the statistics of natural signals are stationary over small time periods of time but the statistics do change over longer time intervals (Ruderman and Bialek, 1994) making adaptation an ideal way to encode natural images.

Another way to efficiently encode a stimulus is to try and maximize the neuron's information capacity in relation to the stimulus statistics. In this case, the cell should adapt its gain function (the slope of its input output curve) to the local statistics of the visual image. But how does the system "choose" the new adapted gain function? Laughlin (1981a) suggested that the shape of the gain function is chosen to maximize the entropy of the output. This means that the stimulus-response curve should be equivalent to the probability density function of stimulus intensity values (Figure 1.11). If the stimulus-response function of a

neuron approximately follows the cumulative probability density for the stimulus, then the distances between frequently occurring intensity values will be increased and the difference between infrequent intensities decreased (Laughlin, 1981a) (Figure 1.11). It has indeed been shown that the stimulus-response curve approximates the cumulative probability density function of the stimulus and that adaptation can maximize the information carried about the current state of the stimulus signal (Laughlin, 1981a; Brenner et al., 2000).

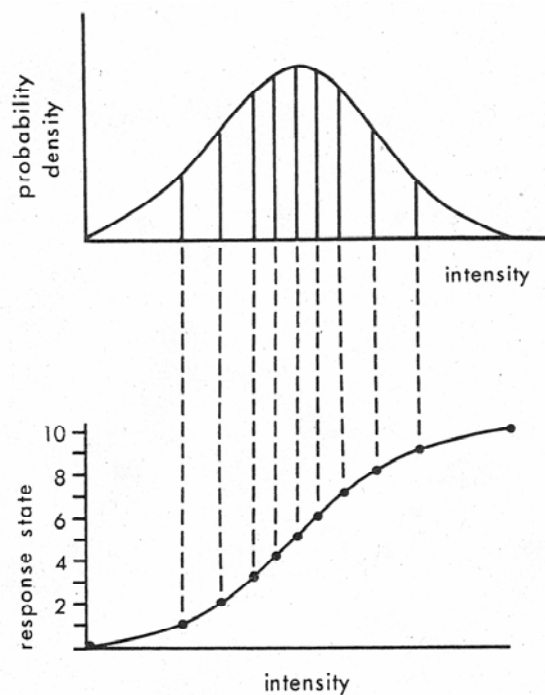


Figure 1.11 The capacity of a neuron to maximize information about the stimulus. The upper curve represents the probability density function for the stimulus. The lower curve represents the stimulus-response function that will maximize the information about the stimulus. The stimulus-response curve describes what response values will occur for each stimulus intensity value. Distances between frequently occurring intensities will be increased in the response, and less frequent stimuli will be closer together, causing all responses to occur at the same frequency, and maximizes information. From (Laughlin, 1981a).

An adaptive neural code is however, by definition, ambiguous. The output of a neuron that adapts to different stimuli may maximize the information about the one particular stimulus set but the absolute information about the nature of each stimuli is lost; the neural code is then dependent on the context in which the adaptation occurred. Assuming that the goal of neurons downstream of the adaptation is to decode the exact value of the stimulus; these downstream neurons require additional information about the stimulus in order to interpret the adaptive signals they receive. Therefore, although adaptation leads to efficient coding, ambiguities arise as to the actual nature of the stimulus, and additional information is required in order to reconstruct what stimulus actually occurred. Fairhall et al. (2001) claim that a system that adapts on multiple time scales has the ability to encode both the stimulus

and the context through multiple channels. They find supporting evidence that the timing of individual spikes or spike pairs encodes the stimulus features that are normalized by the stimulus ensemble. The interspike intervals over slightly longer time scales can encode the stimulus ensemble and the firing rate can carry information about changes in the stimulus ensemble over longer time scales. The mechanism for this type of adaptation and multiple coding scheme has, however, not been found.

### **Automatic adaptation**

In addition to the question of why adaptation exists in neural systems, it is also important to look at the mechanism behind adaptation. Adaptation was thought to occur as a result of a parameter change in the system. Long-term potentiation (LTP) and long-term depression (LTD) can both be thought of as adaptations to a strong tetanus stimulus whose mechanism, although not entirely understood, depends on  $\text{Ca}^{2+}$  fluctuations and changes in synaptic receptor proteins. In recent years however, increasingly more examples of response adaptation in the nervous system have been found in which the parameters of the system do not change at all. For instance the output of a high pass filter in response to a step in intensity will at first increase and then decrease back to the baseline level, which can be thought of as an automatic form of adaptation to the mean intensity level. The mechanisms for adaptation can be investigated from a biophysical perspective or they can be based on mathematical models for how the information is computed. Although the two appear very different in nature, both types of models have parameters that can be manipulated or characteristics that when left alone, also lead to adaptation.

It was demonstrated in the retina, for example, that spike generation in ganglion cells adapts to the variance of synaptic inputs which are in turn influenced by external temporal contrast changes (Kim and Rieke, 2003). Variable current injections into salamander ganglion cells demonstrated that increasing the variance of the current injection increased the threshold for spike generation. Kim and Rieke (2003) showed that slow  $\text{Na}^+$ -inactivation accounts for this adaptation; an increased current variance can deplete the cell of available  $\text{Na}^+$  current thereby increasing the spike generation threshold. In this case, the spiking activity is not only a function of the instantaneous membrane potential activity but also on the history of activity up to hundreds of milliseconds in the past. The  $\text{Na}^+$ -inactivation current did not itself change in response to the variance of the current injection, its slow dynamics lead to adaptive behavior under variable settings.

Another example comes from the somatosensory cortex. Using dynamic clamp techniques on rat layer 5 pyramidal neurons in slice, it was shown that changes in balanced background synaptic input can modulate the gain response of a cell to a driving stimulus (Chance et al., 2002). Excitatory and inhibitory conductances were simulated from independent Poisson spikes trains, and then used to create a balanced excitatory and inhibitory synaptic current which was then fed along with a DC driving current into the soma of the neuron. As the balanced background activity variance increased the response of the cell to the driving current decreased (Chance et al., 2002) (Figure 1.12). Model and experimental results showed that the rightward shift in the gain was due to shunting and the change in slope due to the increase in input noise (Chance et al., 2002).

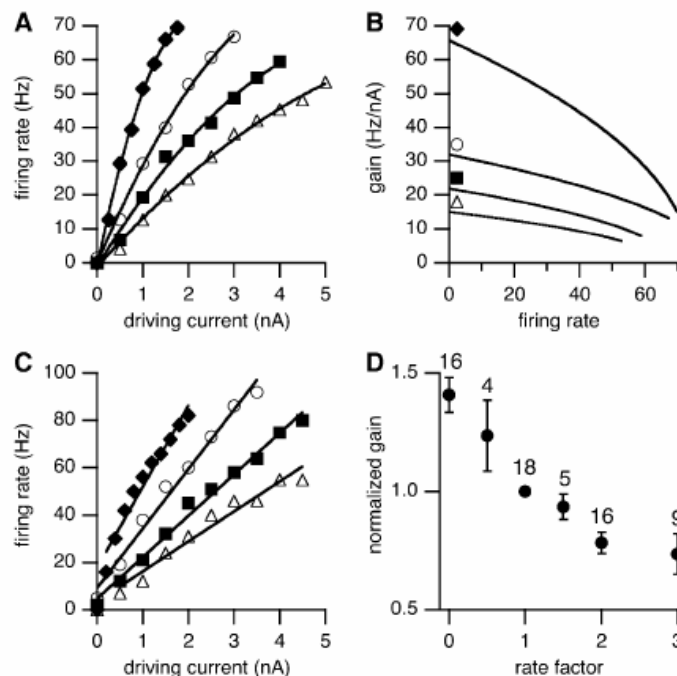


Figure 1.12 Adaptation to balanced background input. Using dynamic clamp techniques the synaptic current variance and the mean synaptic current were increased. (A) and (C) show a decreasing slope with an increasing variance and mean of the background synaptic activity. (B) and (D) plot the slope, or gain, of the stimulus-response curves. For further information see (Chance et al., 2002).

A rigorous theoretical analysis of input-output systems revealed that both Hodgkin-Huxley (HH) and Leaky-Integrate-and-Fire (LIF) model neurons adapt their response properties to the mean and standard deviation of a Gaussian white noise current input (Yu and Lee, 2003). This adaptation occurred without changing any parameters within the HH or LIF model. The LIF model was examined analytically, in order to look at whether the spike generating mechanism or the refractory period was responsible for the adaptation in response gain. Yu and Lee found that the non-linear dynamics of spike generation in a system with memory

along with the statistics of the stimulus is enough to change the stimulus-response curve in the LIF model (Yu and Lee, 2003).

### H1-cell and adaptation

Questions regarding neural coding and information have often been addressed using the H1-cell of the fly visual system as an experimental model, and it will also be the focus of this work. The H1-cell is one of the heterolateral spiking LPTCs. It has a dendritic tree that covers the entire ipsilateral visual field and axonal arborizations that cover the entire contralateral lobula plate (Figure 1.13). The H1-cell is a purely spiking cell with a baseline firing rate of around 20 Hz. It responds primarily to back-to-front motion. The H1-cell shows spiking not only in the axon but also in the dendrites suggesting that active channels also exist in its dendritic tree. It is easy to identify extracellularly due to its response properties and is stable enough to record from for hours. It is however, difficult to record intracellularly from the H1-cell due to the small diameter of its main axon. Many response properties of the H1-cell can be explained by the Reichardt detector model, suggesting that the columnar elements that are presynaptic to the H1-cell and other LPTCs represent a biological version of the output of an array of EMDs.

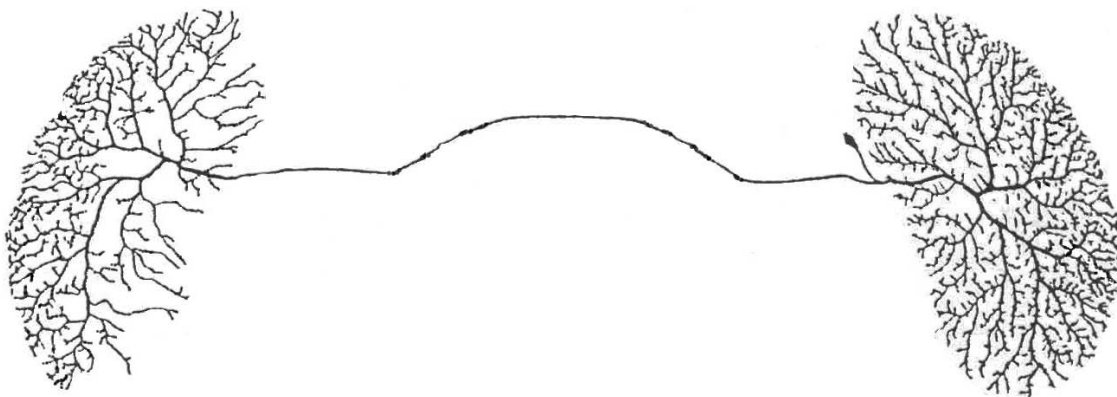


Figure 1.13 The anatomy of the H1-cell. A hand drawn picture of a right H1-cell shows the dendritic arborizations on the right side, covering the majority of the lobula plate, the electrotonically separated cell body and then the major axon that travels over the central brain to the left lobula plate, where the axon branches into a larger percentage of the lobula plate. From (Hausen, 1982)

Many forms of adaptation have been described in the H1-cell. The H1-cell responds to the onset of motion with a sharp increase in firing rate that then adapts to the mean contrast frequency of a visual stimulus; behavior that is similar to a high pass filter. It also adapts its maximum transient firing rate after motion onset to a sequences of relatively short motion pulses, such that the peak of the transient decreases with increasing pulse number (Maddess

and Laughlin, 1985). This decrease in firing rate over time is thought release the cell from saturation such that the H1-cell becomes more sensitive to fluctuations around the sustained velocity (Maddess and Laughlin, 1985). Adaptation to a constant velocity in one area of the visual field does not affect the response of the H1-cell to motion in another location, suggesting that the mechanism of adaptation occurs presynaptically to the H1-cell perhaps in the elementary motion detectors (see Elementary Motion Detection).

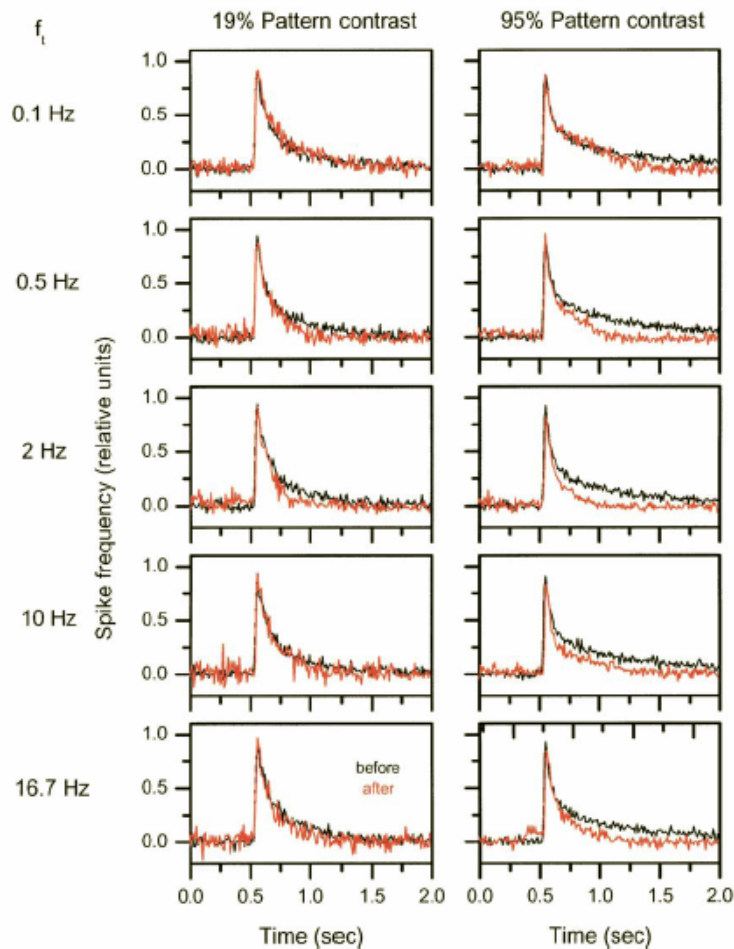


Figure 1.14 Adaptation of response transients in the H1-cell. The response of the H1-cell to a motion pulse, before and after a 3 second constant velocity “adaptive” stimulus for 5 different velocities and 2 different light contrast levels. The stimulus pattern was a square wave grating. From (Reisenman et al., 2003).

The H1-cell responds to a very brief motion pulse with a rapid increase in firing rate that then decreases exponentially back to baseline (Figure 1.14). The time constant of the exponential decay was shown to shorten after a three second adapting stimulus of constant velocity was presented (Figure 1.14). This form of adaptation, as well as adaptation to a constant velocity stimulus in the null direction and the duration of the transient oscillations at stimulus onset, were all dependent on the velocity and the contrast of the visual pattern (Reisenman et al., 2003). The mechanism for adaptation of the decay time to a stimulus pulse can be found in

the Reichardt detector. If the high-pass filter time constant from the Reichardt detector is allowed to depend on the velocity and contrast of the visual pattern, then the adaptive Reichardt detector model can explain all of these adaptation phenomena (Borst et al., 2003).

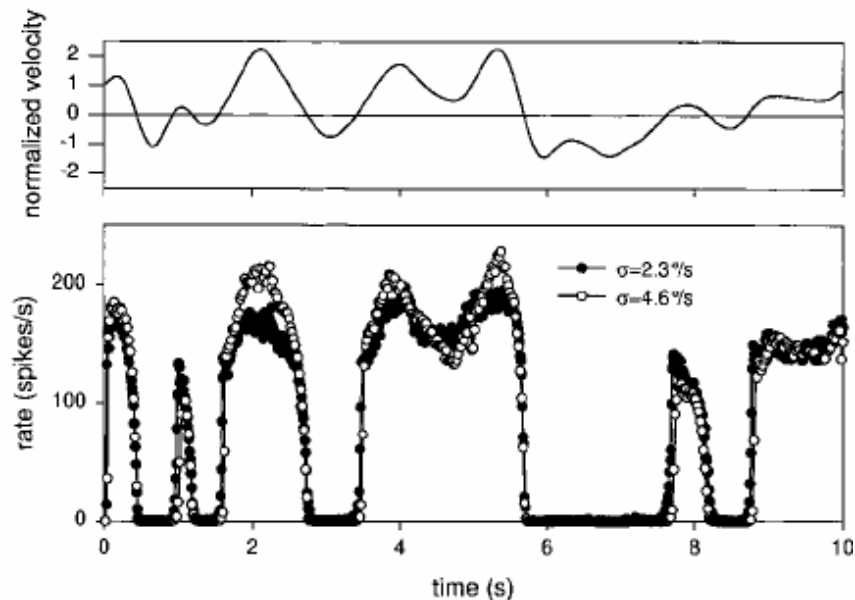


Figure 1.15 H1-cell adaptation to the variance of the time varying velocity profile. The normalized velocity profile for both standard deviations is shown in the top graph. Below is the response of the H1-cell to both velocity profiles. Although the absolute range of the velocity is doubled for the open circles, the H1-cell response to both velocity signals looks almost identical. From (Brenner et al., 2000).

The previous examples of adaptation in the H1-cell were in response to constant velocities or to transient velocity pulses. The H1-cell however, also adapts to the statistics of time varying inputs. A Gaussian white noise signal has many advantages as a stimulus. It contains all of the possible stimuli in a distribution, and it can be entirely explained by its first and second moments, mean and variance. Therefore it is often used as a dynamic, time varying stimulus for experiments on neural coding. For a sinusoidal apparent motion stimulus, the firing rate of the H1-cell adapts to the standard deviation of a Gaussian white noise velocity stimulus (Brenner et al., 2000) (Figure 1.15). The input-output curve of the H1-cell was broader and saturated at a lower firing rate for the higher standard deviation, although the difference was marginal. This difference disappeared however, if the velocity and response were normalized by the standard deviation and mean firing rate respectively (Fairhall et al., 2001). Using methods similar to principle component analysis or reverse correlation methods, various studies found that the dominant stimulus features adapted to the variance of a rapidly changing Gaussian white noise velocity signal (Brenner et al., 2000; Fairhall et al., 2001; Borst, 2003). In addition they tested whether the adaptive input-output curve indeed maximized the information transfer, by artificially stretching or contracting the input-output

relation by a factor  $\lambda$  and then measuring the information. The experimentally measured input-output curve after adaptation had the highest amount of information about the stimulus (Brenner et al., 2000).

Increasing the stimulus entropy does not affect the information rate of the H1-cell (Borst, 2003). For 3 different velocity ranges tested for Gaussian white-noise velocity stimuli, the information rate of the stimulus remained constant, although the stimulus entropy was increased. The interspike interval was slightly shifted to the right for higher velocity ranges suggesting a lower spike rate; however the information rate was not different for the 3 different stimuli tested (Figure 1.16). This suggests that the H1-cell encodes more information if the stimulus is richer and achieves this by adapting its filter to the stimulus statistics (Borst, 2003).

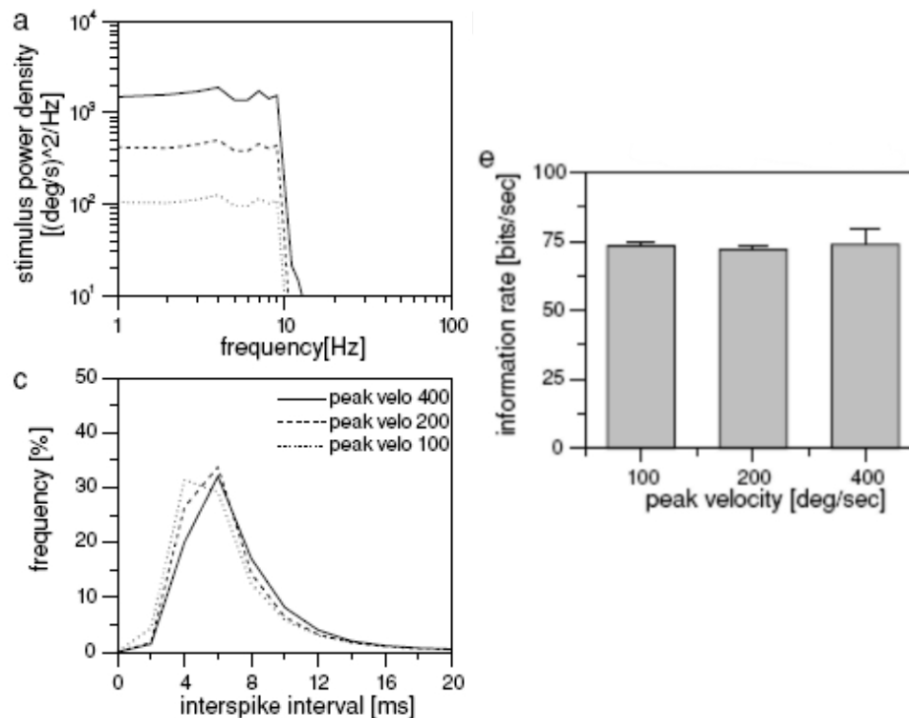


Figure 1.16 Information rate is invariant to stimulus entropy. The top left figure shows the power spectrum of the three different Gaussian white noise velocity profiles used. The bottom left figure shows the interspike intervals (ISI) for the three different velocities. The most frequently occurring ISI shifts towards larger values as the velocity range increases, showing a decrease in firing rate. The right figure shows the information rate, calculated using the direct method (Borst and Haag, 2001), for the three different velocity profiles. From (Borst, 2003).

### The time course of adaptation

Adaptation occurs on many different time scales. From the standpoint of optimal coding, a system should rapidly adapt its response properties to the new statistics of the stimulus in

order to maintain a high level of information during the switch. Retinal ganglion cells show both a fast and a slow adaptation to changes in stimulus contrast (Baccus and Meister, 2002). When retinal ganglion cells are presented with a low contrast flicker stimulus which then switches to a high contrast stimulus, retinal ganglion cells immediately increase the firing rate which then adapts with an exponential decay back to a lower firing rate (Baccus and Meister, 2002). The initial response adaptation to the new contrast occurs within 0.1 seconds and the longer decay occurs on the order or tens of seconds. Other than the firing rate, the fast effects included accelerated kinetics, a decrease in sensitivity to stimuli, and membrane depolarization. During the slower phase of adaptation no change in kinetics occurred but the membrane hyperpolarized. The contrast adaptation found was not seen in the photoreceptor cells, confirming that the mechanism was not linked to light adaptation in the photoreceptor cells, but rather to a subset of bipolar and amacrine cells that showed similar adaptive behavior.

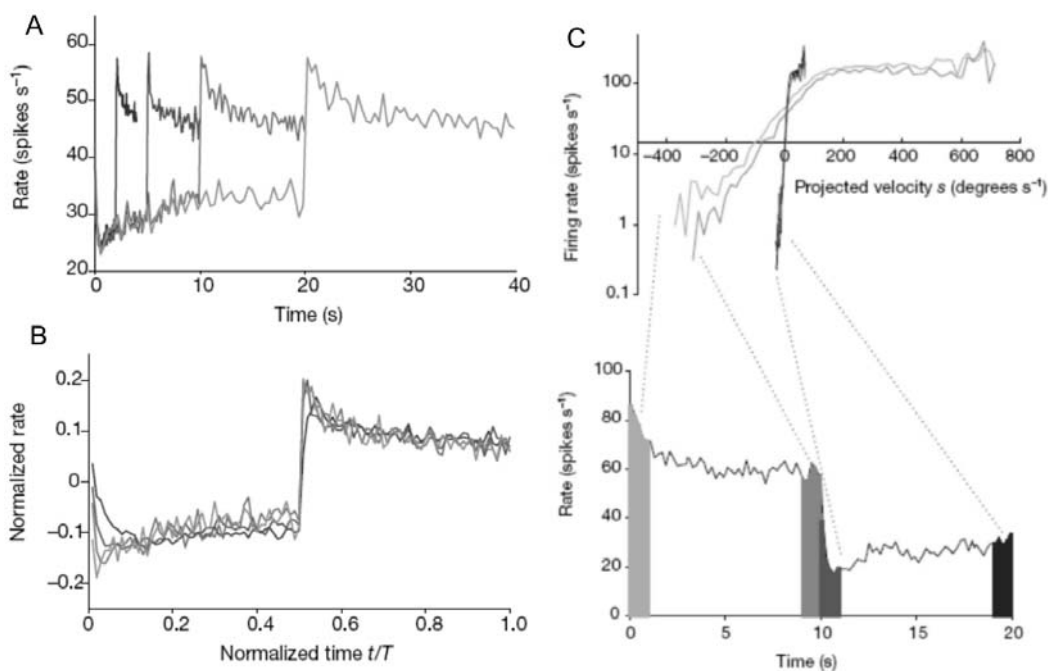


Figure 1.17 The timescale of adaptation. A) The response of the H1-cell to a switch from a low to a high standard deviation, where the switch occurred at different time points  $T = (4, 10, 20, 40)$  seconds. The time course of the slow adaptation lengthens with increasing  $T$ . B) The same curve but normalized for  $T$  and for mean firing rate. C) The input-output curves for both standard deviations one second after the switch and the last second for that stimulus. From (Fairhall et al., 2001).

In an experiment using the H1-cell of the fly, the standard deviation of a Gaussian white noise apparent motion signal was switched after variable periods of time in order to look at the time course of adaptation. The authors found that there were also multiple time scales for adaptation in the H1-cell (Fairhall et al., 2001). The H1-cell immediately changed its firing

rate to match the standard deviation of the new stimulus profile (Figure 1.17). Then, as in the retina, the firing rate gradually decreased and settled to a steady-state. The slow adaptation was also dependent on the length of the stimulus before the switch. When the first stimulus was presented for a shorter time; the slow adaptation was faster than when the first stimulus was allowed to run for longer (Figure 1.17A). In addition to the two different timescales of adaptation the authors found that the information per spike remained relatively constant through the switch, although one would predict that the system would need time to adjust to the new stimulus. The authors suggest that the stimulus and the context are both encoded in the spike train of the H1-cell and that the individual channels of information are the spike rate, the spike timing and the interspike intervals.

In summary, adaptation is a common phenomenon particularly in the early stages of visual processing that allows for the system to better cope with the current environment. Adaptation is advantageous for it allows systems to encode fine details about a stimulus even when the stimulus range is large, by adapting to the local spatial or temporal range of the stimulus. Adaptation is generally thought to occur through a change in some parameter of the system. However recent modeling and experimental work suggests that it can also occur automatically as a function of the input and the non-linearities of the system. The H1-cell adapts its firing rate to constant velocities, to transient velocity pulses as well as to dynamic velocities. Adaptation of the decay time after a motion pulse can be explained by adaptation of the high-pass time constant of the elementary motion detectors that are present presynaptically to the H1-cell. Adaptation can occur on different time scales and can be influenced by the timing of the stimulus. The mechanisms for adaptation are not very well understood and only marginally researched, however when the adaptation operates on the same time scale as the response itself, the separation between the mechanisms underlying the adaptation and those that give rise to the response becomes ambiguous.

---

## Justification

In the following work, I will use experimental and computational approaches in order to study adaptation of the Reichardt detector to a dynamic motion stimulus. I will simulate the Reichardt detector algorithm as well as recording extracellularly from the H1-cell of the blowfly in order to compare the simulations with the actual biological implementation of the Reichardt detector. The stimulus that I will use is a first order low-pass filtered zero-mean

Gaussian white noise velocity signal, in other words Gaussian colored noise, where the visual pattern is a sinusoidal grating. In particular I will investigate the following properties:

- Adaptation to the stimulus variance
- Adaptation to the temporal correlations within the stimulus
- The time course of adaptation
- Dependence of adaptation on the visual pattern

In addition, I will compare the results from the experiments and simulation work to analytical work done by Haim Sompolinsky on the output of the motion detector to a dynamically moving sinusoidal grating. This work makes an important step in the understanding of motion vision in particular the effect of dynamic stimuli on motion responses. It demonstrates the importance of mathematical algorithms for understanding complex computations in the nervous system, even when it is unclear how biologically accurate such models are. These results take us one step further to opening up the “black box” to understand the mechanisms and reasoning behind neural coding.

## 2 Methods

---

This work used a combination of experimental techniques and computer simulations in order to examine the relationship between dynamic adaptation in the Reichardt motion detector and the H1-cell of the blowfly. In the following section I will describe the methods that were used. First I will explain the electrophysiological setup used to record from the H1-cell of female blowflies. Then I will outline the visual stimulation and the reasoning behind each of the experiments. The data analysis and comparison to modeling results will also be described in detail. Finally, I will characterize the computer simulations that were done in parallel with the three different experiments. Tables of the equipment and suppliers can be found at the end of this section.

Three general sets of experiments were performed. The first set of experiments tested the dependence of gain adaptation on the statistics and temporal correlations of the stimulus. These experiments provided a comprehensive look at the absolute range of adaptation in the system. In the second set of experiments, I examined how the visual pattern itself influences adaptation of the stimulus-response function. The time course of adaptation after a switch in the stimulus statistics was studied in the last set of experiments.

---

### Experiments

The H1-cell of the blowfly visual system was recorded extracellularly in order to examine spike rate adaptation and gain control in response to the statistics of a dynamic velocity stimulus; in this case Gaussian colored noise. In this subsection I will briefly explain the blowfly preparation for extracellular H1-cell recordings, the equipment and methods used in recording spiking activity and the stimulus protocols for each of the experiments.

#### Preparation

Experiments were performed on female blowflies, *Calliphora vicina*, between the ages of 7 and 11 days old. The flies were briefly anesthetized with CO<sub>2</sub> and their dorsal thorax was attached to a small glass platform. All six legs were removed and the body cavity resealed

## Methods

with beeswax. The head and proboscis were bent forward and waxed to the ventral side of the thorax to give access to the back of the head. Right and left in the fly are defined from the dorsal side of the animal from the third person perspective such that the right eye of the fly is the eye that is on the right side of the observer if the observer is facing the dorsal side of the fly (Figure 2.1). The right head capsule was opened along the entire vertical extent, and from the most lateral limit of the head capsule to the midline (Figure 2.1). The fat body and epithelial tissue in the right head capsule were removed or pushed to the side so that the medulla and lobula plate could be seen. Wings and abdomen were then waxed together and antennae were waxed down to reduce movements that could affect electrical recordings. Case Ringers solution (Table 1) was used to keep the tissue in the open head capsule moist and in an isotonic solution.



Figure 2.1 Fly preparation: the fly as seen from the back of the head. The right eye is opened from the back and the epithelial layers and fat body tissue are removed. In the middle of the opened eye the crescent shaped medulla is visible and medial to that the lobula plate with tracheal projections covering it.

Additional Ringers solution was added to the right head capsule approximately every 30 minutes during electrophysiological recording. Brain movements due to peristaltic contractions of the gut did not significantly influence the extracellular recordings except for brief periods when Ringer was added, during which no experiments were performed. Therefore, contrary to preparation for intracellular recordings, the gut and trachea were left intact in order to reduce damage done to fly, allowing for longer recording times. With this preparation H1-cell recordings were stable for up to 8 hours, although longer recording times may have been possible if the fly was given nourishment during recording. Flies were mounted in the experimental setup in an upright position facing the visual monitor that was used for stimulation.

## Electrical Recording

All data were collected extracellularly from near the first axonal branch of the left H1-cell of the fly, whose axonal projections are in the right optic lobe (Figure 2.2). Signals were recorded with a standard tungsten electrode with a 1 M $\Omega$  impedance. Blunt glass electrodes that were pulled from thin-walled glass capillaries with an outer diameter of 1 mm, were used as ground electrodes. The tip of the ground electrode was made blunt to decrease the impedance and Case Ringers was used as the electrode solution. Ground electrodes were changed about once a week but the fluid in the ground electrode was changed daily. First, the ground electrode was inserted into the extracellular fluid in the right optic lobe dorsal and medial to the H1-cell. After the ground electrode was in the correct position, the recording electrode was inserted into the lobula plate at the approximate position shown in Figure 2.2.

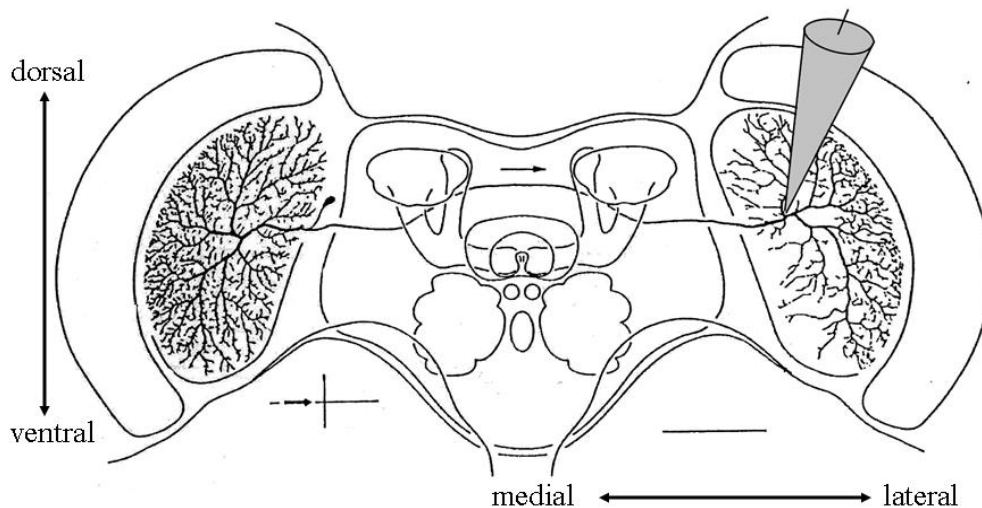


Figure 2.2 The left H1-cell of the fly as seen from the back of the head. The cell has dendritic processes that cover the majority of the retinotopic columns of the lobula plate. The axonal branches also innervate the majority of the lobula plate on the right side of the eye. Recordings were done in the approximate vicinity of the first axonal branch. From (Hausen, 1982).

The H1-cell is not visually distinguishable within the lobula plate without the aid of a colorant. Therefore the H1-cell was detected acoustically by running the recorded field potential through an audio monitor. The cell was recognized by its audible firing properties and by the X,Y,Z position of the electrode in the fly. The base firing rate of the H1-cell is of about 20 Hz and its preferred direction is from back to front on the left side of the fly. The recording electrode was positioned such that the signal-to-noise ratio of the raw spikes to the background noise was greater than two as seen after filtering and amplification on the Tektronix TDS 2002 2-channel digital oscilloscope. Cells were not used if they were 1) found

outside the general location of the H1-cell in the lobula plate, 2) found too deep in the tissue, or they 3) did not fit the firing properties of the H1-cell, including stationarity.

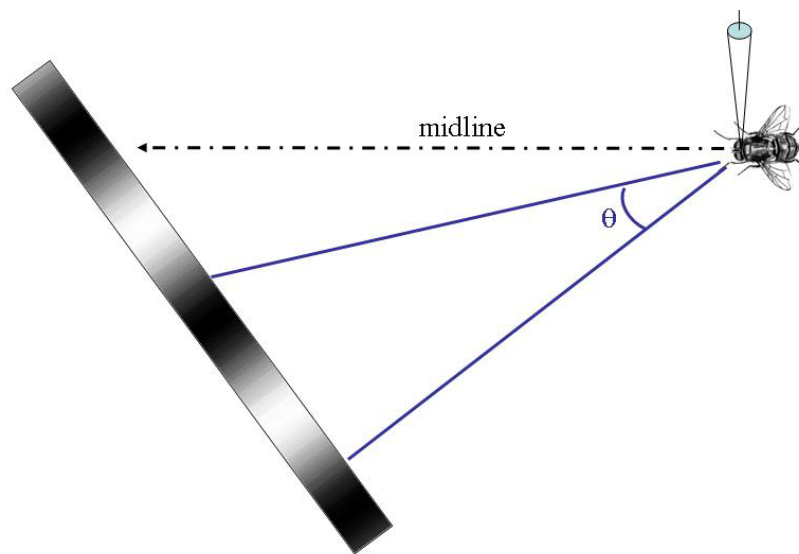


Figure 2.3 Visual stimulation setup. The fly was placed a certain distance away from the CRT monitor such that the monitor covered a large portion of the left visual field. In the first set of experiments, the fly was 7.5 cm away from the monitor, and the sinusoidal grating had a 22.0 degree spatial wavelength. In the other two experiment sets, the fly was placed 8.5 cm away from the monitor and the visual grating had a spatial wavelength of 6.5 cm corresponding to 43.3 degrees visual angle.

The raw field potential was first filtered, amplified and converted into binary spike trains before being saved to the computer for further analysis. The two signals from the recording and ground electrode were subtracted and amplified in the headstage. Afterwards the signal was amplified (by 70 dB and then by 40 dB) and then band-pass filtered (range 500-10,000 Hz and again 300-3,000 Hz). This signal was split and fed into the digital oscilloscope, to the audio monitor for locating the cell, and through a threshold device that returned a 100-mV pulse of 1.1 ms duration each time the signal was above threshold. The threshold was then manually set for each experiment such that all of the spiking events were converted into pulses and everything else was set to zero. The threshold voltage was set differently for each fly but was generally between 1.5 and 3.0 V. Noise levels tended not to vary between experiments or flies and remained below  $\pm 0.3$  V in the amplified signal. The spiking events also maintained a constant amplitude over the course of a single experiment. The binary signal was then transferred at 1.0 kHz temporal resolution to a personal computer. This response vector was saved to a single data file along with the voltage values corresponding to the velocity profile used in that particular experimental trial.

## Visual Stimulation

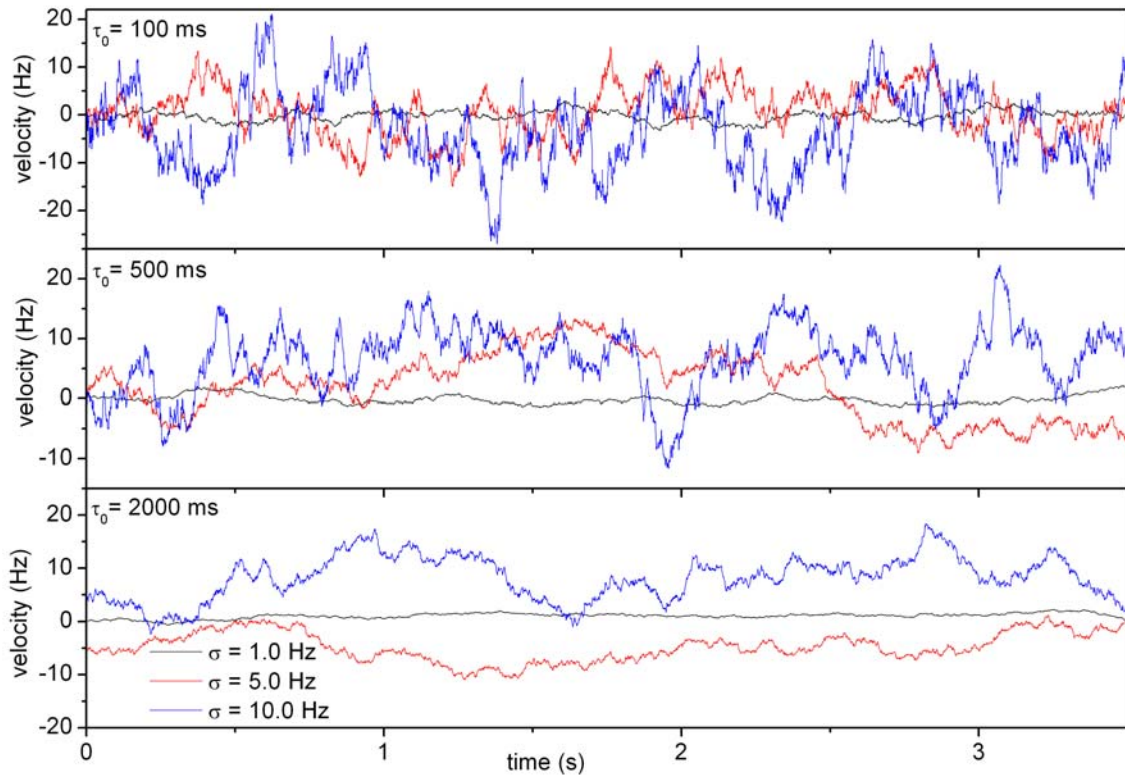


Figure 2.4 The Gaussian colored noise velocity profiles used. A total of fifteen different velocity profiles were used in experiment set 1, nine of which are shown here. Each graph represents one of the three different time constants used and in each graph three of the five different standard deviations (1.0, 5.0 and 10.0 Hz) are shown. Velocity standard deviations 0.1 and 0.1 Hz are not shown.

Flies were stimulated by a moving sinusoidal or square grating presented on a cathode ray tube (CRT) monitor with a refresh rate of 200 Hz. The visual display had a width of 13.0 cm, and a height of 9.8 cm (see Table 2). The monitor was run by a Picasso image synthesizer that set the brightness values for each point on the screen over time. The CRT monitor uses a P15 phosphor (green) light and the small dot is 0.25 mm. The velocity of the pattern depended on the experiment and will therefore be mentioned in the subsections devoted to each individual experiment type. The maximum speed was determined by the range of output voltages from the computer and the conversion rate, for an overall maximum speed of 33.3 Hz (732.6 degrees/s for experiment set 1, otherwise 1441.9 degrees/s visual angle). The image synthesizer was in turn run by the same personal computer responsible for data acquisition. The velocity profiles were entered as voltage values between -10 and 10 V, which were then converted into bit values up to 4096 and again converted into contrast frequency values in Hz. The resolution of the velocities was therefore up to 0.005 Hz, with the exception of the 0.1 Hz velocity profile which was set to be between -1 and 1 V and

therefore had a resolution of 0.0005 Hz. The stimulation and recording software were written in Delphi by Jürgen Haag. Experiments for this work were done using two slightly different distances between the fly and monitor and different wavelengths of the visual pattern (Figure 2.3); however the recording equipment and analysis techniques were the same. The following is a brief explanation of the individual stimulation protocols.

### **Experiment 1: Dependence on stimulus statistics**

This set of experiments was done in order to test the dependence of dynamic adaptation on the variance and time course of a Gaussian colored-noise velocity profile. The experiments were set up in the following way. The CRT monitor was placed 7.5 cm in front of the fly such that the screen had a horizontal and vertical extent of 65 and 80 deg, respectively. In these experiments a sinusoidal grating with 22.0 deg spatial wavelength, 63.3 % contrast, 14.0 cd/m<sup>2</sup> mean luminance was shown with a Gaussian low-pass filtered colored noise velocity profile. Fifteen different vectors of velocity values over time were generated using the Matlab programming language (see Velocity Profile p. 52) such that each stimulus had either a different standard deviation or low pass filter time constant. For each stimulus condition, approximately 100 sweeps of identical stimuli, each lasting 9.0 seconds, were presented with a 1 second pause between them. Each fly was shown stimuli with a single time constant for all five standard deviations until 100 sweeps were obtained. Then the signal stationarity and the general health of the fly were checked and the next time constant was tested. Each fly was tested using the same stimulus manifestation for each stimulus condition in order to minimize differences between flies. Example sections of the actual velocity profiles are shown in Figure 2.4. Example statistics from two velocity profiles are shown in Figure 2.6 and Figure 2.7.

### **Experiment 2: Dependence on Visual Pattern**

Experiment set 2 had a different physical setup than experiment set 1. The CRT monitor was positioned 8.5 cm in front of the fly such that the majority of the monitor was on the left side of the fly (Figure 2.3). The monitor covered a horizontal and vertical visual extent of 80 degrees and 49 degrees respectively. The wavelength of the grating was 43.3 degrees visual angle or 6.5 cm. In these experiments the sinusoidal or square wave grating had a contrast of 66.9 % and a mean luminance of 17.5 cd/m<sup>2</sup>, unless otherwise specified in the results.

This set of experiments was designed to test the dependence of adaptation on the structure of the visual pattern. The same velocity profiles were used as the previous experiments (Figure

2.4), but the shape of the visual pattern was changed between a sinusoidal and a square wave. Both square and sinusoidal patterns were always tested in each fly for as many of the velocity profiles described in Experiment set 1 as time allowed. As in the previous experiment set, each stimulus condition was repeated approximately 100 times with a 1 sec pause in between each stimulus.

The pattern wavelength was made very large so that there would be a noticeable difference between a sinus and a square grating. A square wave  $y(x)$  is the infinite sum of odd sine waves, or odd harmonics:

$$y(x) = \sin(x) + \sin(3x)/3 + \sin(5x)/5 + \sin(7x)/7... \quad (4)$$

In order for the cell to differentiate between a square wave and a sine wave, some of the higher harmonics of the square wave must be detectable. According to Shannon's sampling theory, a signal can only be measured if the sampling frequency is at least twice the frequency of the signal itself. This is also called the Nyquist limit. In the blowfly the limiting distance is the space between each ommatidium, or the interommatidial distance, which is approximately 2 degrees. This leads to a sampling frequency or Nyquist limit of 4 degrees. Therefore the first two higher harmonics (14.43 and 8.66 degrees) from a 43.3 degree visual pattern should be detectable by the fly (see Figure 3.13) for the response of the H1-cell to higher harmonics, making the visual pattern large enough to look at differences between adaptation for square and sine wave visual patterns.

### **Experiment 3: Time Course of Adaptation**

The last set of experiments had the same physical set up as experiment set 2. The wavelength of the sinusoidal grating was also 43.3 degrees and the visual pattern had the same contrast and mean luminance. In this set of experiments only a sine wave grating was used. The purpose of this experiment was to examine the time course of adaptation. Therefore, velocity profiles were created that switched either from one standard deviation to another or from one low-pass filter time constant to another. The standard deviation was switched from 0.5 to 5.0 Hz and the time constant was switched from 50 ms to 500 ms (see Figure 2.5). When standard deviation was switched, the time constant of the stimulus was 100 ms, and when the time constant was switched, the standard deviation was held constant at 1.0 Hz. A single standard deviation or time constant was shown for 10 seconds and then switched to the new standard deviation for 10 seconds. This was repeated twice with different random velocities

resulting in a 40 second velocity profile. At least 100 trials for each switch were performed for each experiment and there was no break between the trials so that ends of each stimulus waveform could also be analyzed for adaptation.

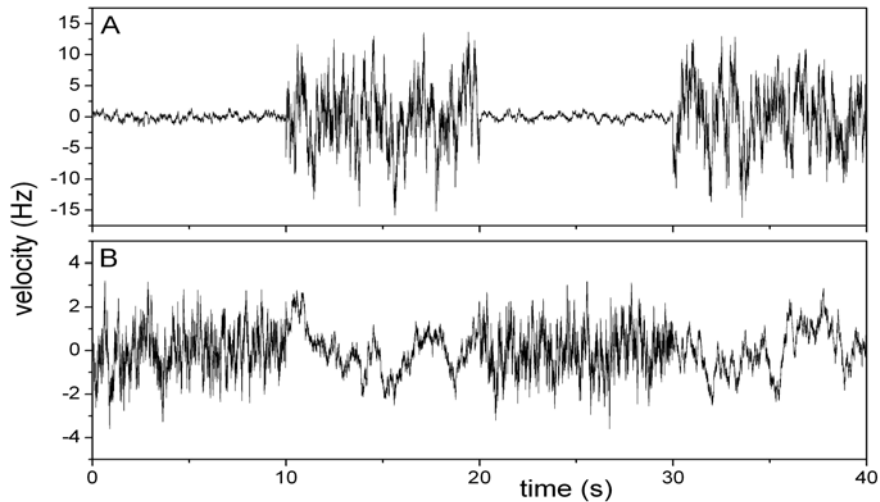


Figure 2.5 Velocity profiles for experiment set 3. Two stimulus conditions were shown to the fly. A) The velocity standard deviation was switched from 0.5 Hz to 5.0 Hz and back every 10 seconds for 40 seconds. The stimulus time constant was 100 ms. B) The velocity time constant was switched from 50 ms to 500 ms, and the standard deviation was kept constant at 1.0 Hz.

### Velocity Profile

The type of velocity profile used in this study was zero-mean Gaussian colored noise. Colored noise is Gaussian white noise with temporal correlations. Numbers were picked at random from a Gaussian distribution using the `randn.m` function in Matlab, seeded to the clock. This produced a vector of values with zero mean and a standard deviation of one. The vector was then low-pass filtered in the Fourier domain and then transformed back into the time domain. The resulting signal was stretched to the appropriate standard deviation and the mean reset to zero.

The resulting velocity vector was then checked to make sure that the higher order statistics of the vector distribution were also Gaussian (see Figure 2.6 and Figure 2.7). The skew is the third moment of a distribution, normalized by the cubic of the standard deviation and is a measure of the asymmetry of the probability distribution around the mean. A positive skew indicates that a higher proportion of the values in the distribution are located to the right of the mean, a negative skew the opposite. For a Gaussian distribution the skew should be zero; for the velocity vectors the skew was allowed to vary up to  $\pm 0.05$  around zero. The kurtosis was also checked for each velocity profile. Kurtosis is a measure of the “peakedness” of a distribution, or how much of the variance is due to infrequent extreme values. There are a few

ways of calculating the kurtosis but in this study the kurtosis is equivalent to the fourth moment of the distribution about the mean, standardized by the square of the variance. If the kurtosis is high, then the distribution is peaked and the variance in the distribution is due to infrequent extreme values; if kurtosis is low then the distribution is flat and the variance due to frequent modest size deviations. A Gaussian distribution has a kurtosis of 3.0. The kurtosis of the velocity distribution was allowed to vary around 3.0 by  $\pm 0.1$ .

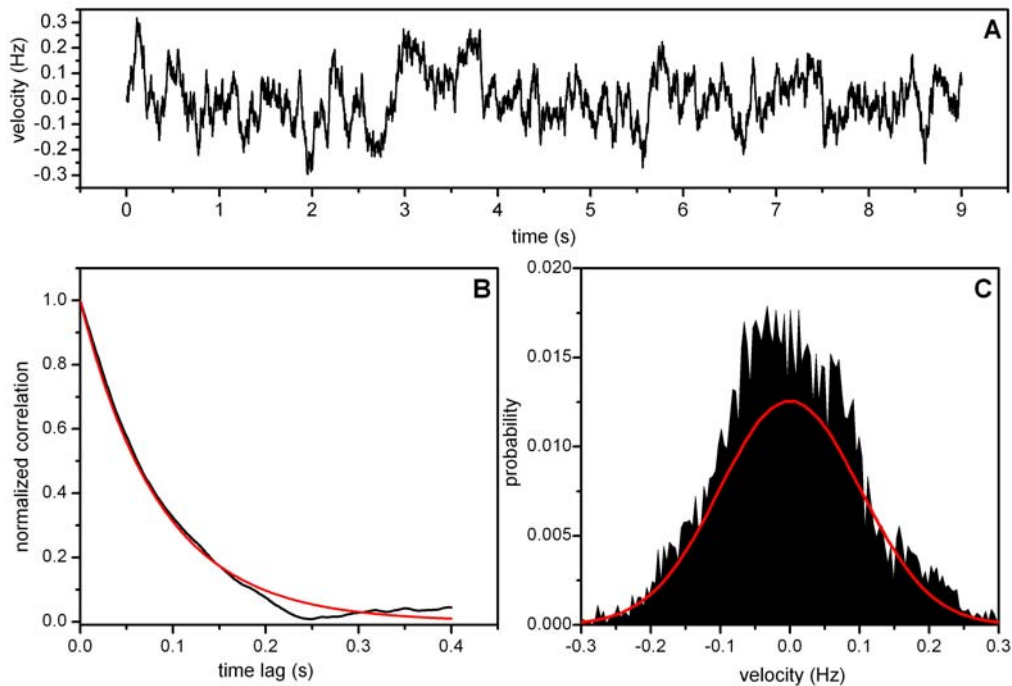


Figure 2.6 The stimulus with 100 ms time constant and 0.1 Hz velocity standard deviation. A) The entire nine second velocity stimulus. B) The cross correlation (black) of the velocity signal normalized to 1 and an exponential decay (red) with the same time constant. C) 150 bin histogram of the stimulus (black) and the corresponding Gaussian distribution (red).

The low-pass filter characteristics of the velocity signal were also checked by comparing the best fit time constant of an exponential decay to the time-lagged autocorrelation of the velocity signal (Figure 2.6 and Figure 2.7). If the best fit time constant was within 10 ms of the desired time constant, the velocity profile was used. If any of these three parameters did not fit, the entire procedure was performed on a new random distribution. Each resulting velocity profile was then converted from Hz into volts; the conversion rate for the setup used was  $1 \text{ Hz} = 10/3 \text{ Volts}$ . For the time constant of 2000 ms, the time constant was allowed to vary up to 100 ms because the velocity profile was only nine seconds long and there was not enough data points to have an accurate time course.

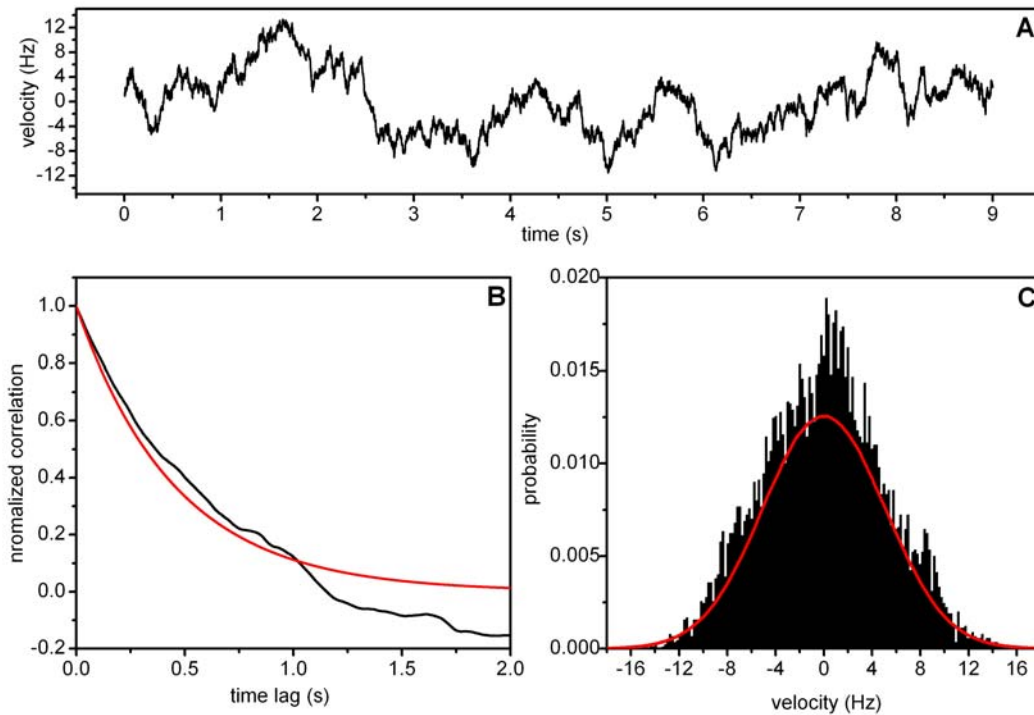


Figure 2.7 The stimulus with 500 ms time constant and 5.0 Hz velocity standard deviation. A) The entire nine second velocity stimulus. B) The cross correlation (black) of the velocity signal normalized to 1 and an exponential decay (red) with the same time constant. C) 150 bin histogram of the stimulus (black) and the corresponding Gaussian distribution (red).

---

## Data Analysis

All of the data was collected in matrix form with the first column corresponding to the velocity profile and the second column the binary response that occurred at the exact same time with 1 ms resolution. Each trial was collected in a separate file. All analysis was performed in either IDL or Matlab, and sometimes in both. IDL was generally used for analysis that took a longer time or involved many “for” loops because IDL tends to be much quicker than Matlab. For the procedures that were performed in IDL, smaller versions of the same procedures were performed in Matlab and checked for accuracy between the two programs.

For all of the experiments, the data were first cleaned up and the stimulus values converted from Volts back to Hz. The length of the spike generated pulses collected was 1.1 ms and the sampling rate of the signal that was then digitally recorded was only 1.0 ms. It therefore occurred once in a while that individual spikes were recorded in two consecutive bins. The absolute refractory period of the fly H1-cell is about 2.0 ms, which means that there should be no two spikes that occur within 2.0 ms of one another. Therefore the second spike of all

spikes that occurred within 2.0 ms of one another was removed. The average response or peristimulus time histogram (PSTH) was generated from all the trials and then binned to at least 2 ms, such that the precise spike timing was not changed by removing the one spike. The stimulus profile across trials was also checked for consistency and made into a single vector, which was also binned to 2.0 ms.

There is always a certain delay between the time the velocity is shown to the fly and the time the H1-cell responds to the stimulus. Therefore, in order to align the stimulus and response with another in time, the delay was removed. The time-delayed cross-correlation between the stimulus and the PSTH was calculated for each experiment, and time delay at the maximum cross-correlation found. Then, a piece of the end of the stimulus and beginning of the PSTH equal to the time delay were removed. The maximum cross-correlation between the resulting two signals was then at 0 ms. This time-delay or shift was calculated separately for each stimulus and each fly.

### **Stimulus-Response Curves**

In order to look at the shape of the input-output relationship, stimulus-response curves were generated for the different experiments. The stimulus velocities were sorted in ascending order and the temporal locations of each velocity were used to sort the response values into the appropriate positions. The sorted response vector tended to be very noisy and was therefore smoothed using a Savitzky-Golay least squares smoothing filter with a smoothing frame size of 201. The resulting stimulus and response vectors were then used to plot the stimulus-response curves and used for the gain calculations.

### **Dynamic Gain**

In this work, I define gain of the input-output function as the slope of the transfer function of the system or more specifically as the slope of the stimulus-response curve in a small range around zero. The gain was determined linearly by fitting a line to the stimulus-response curve over a velocity range from -0.25 to 0.5 times the standard deviation ( $\sigma$ ) of each velocity profile, except for a  $\sigma$  of 0.1 Hz where the linear part of the curve was much less in the negative velocity range (Maddess and Laughlin, 1985; Simmons, 1993; Borst and Egelhaaf, 1987). For a standard deviation of 0.1 Hz the velocity range was from 0 to 0.2 Hz. A sigmoidal fit was also used over the entire range of the stimulus-response curve but produced similar results to the linear fit and therefore the linear fit was used.

For each fly the response of the H1-cell to a constant velocity of 0.1 Hz was also measured for 5 seconds with a 1.5 second stationary visual pattern before and after the velocity step. The step velocity stimulus was presented at least 100 times to each fly and then the time shifted average response (PSTH) was calculated in the same way as mentioned above. Steady-state gain was defined as the difference between the response of the cell to the stationary pattern and the non-transient response of the cell to 0.1 Hz motion. 0.1 Hz for a 43.3 degree pattern wavelength is quite slow and the difference therefore approximates the slope of the steady-state curve at 0. The average response over the last 2 seconds during 0.1 Hz motion was subtracted by the average response over the first 1.5 seconds during the stationary stimulus and the result was divided by 0.1, producing the steady-state gain. Steady-state gain was measured once per stimulus pattern per fly, even if multiple experiments were tested in the same fly. This suggests that stationarity in the firing properties of the H1-cell was maintained throughout the entire recording period which was checked in a random subset of the flies by looking at the firing properties between experiments.

The final result, the dynamic gain was the gain in response to the Gaussian velocity profile, normalized by the steady-state gain. The dynamic gain was a value between 0 and 1 that allowed for comparison between different flies with different baseline firing rates as well as comparison with simulation results.

### **Cross-Correlation**

In order to look at the change in response speed to different stimuli, the cross-correlation between the stimulus and the response was also measured. In this case the signals were not shifted in time so that the maximum response to a stimulus occurred at the same time as the stimulus, rather they were left in the original non-temporally shifted form and the cross-correlation was calculated. The maximum of the time-delayed cross-correlation was then examined between the different experiments.

---

## **Modeling**

The same experiments as described above were also tested on the Reichardt detector model with high-pass and low-pass filtering characteristics (Figure 2.8). The simulations were also run in either IDL or Matlab and were checked for accuracy between the two programs. Simulations were used to compare the experimental results with the results expected from an

array of elementary motion detectors. The simulations were set-up such that the distance between individual motion detectors in degrees of one pattern wavelength could be specified along with the total number of motion detector units, thereby also specifying the number of pattern wavelengths that were used for the simulations. After trying a number of different combinations I settled on using one wavelength of the spatial pattern for the simulations, with 50 EMD units separated by 7.2 degrees.

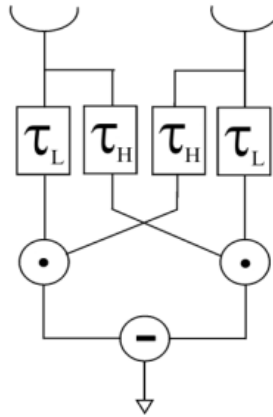


Figure 2.8 The Reichardt detector model used in the simulations. This model has in each mirror-symmetrical subunit a first order low-pass filter in one arm and a first order high-pass filter in the other arm.

### Visual Pattern

The velocity profiles were taken from the electrophysiological experiments such that for each experiment set, the velocity signal shown to the flies and to the Reichardt detector was exactly the same. The simulations were done without adding noise to the system, so that there was a unique solution for each velocity profile used. The sinusoidal pattern was generated by creating a sine wave of one wavelength with a spatial resolution of 1000 ms. A matrix was then created by shifting the visual pattern by the amount specified by the velocity that the visual pattern would move once a millisecond. For example, if the speed was 10 Hz, then the pattern would shift one wavelength in 100 ms, or in 1 ms the pattern would shift 1/100 of a wavelength. This was done for every velocity in the stimulus condition creating a 2D matrix of light intensity values with space on the x-axis and time on the y-axis. As a default, motion in the rightward direction was considered preferred direction and therefore positive motion. The resulting matrix had a temporal resolution of 1000 Hz, as in the experiments, and a spatial resolution of 0.36 degrees of the spatial pattern. This matrix was then spatially resampled to 50 so that each point was equal to the light intensity value as seen by an

individual arm of the motion detector. The resulting vector was the visual pattern used to stimulate the array of Reichardt detectors.

### **Motion Detector**

Two separate versions of the visual pattern matrix of light intensity values were low-pass filtered and high-pass filtered separately (along the spatial dimension). This was done by convolving the spatial light intensity vector at each time point by the impulse response of the filters. Both filters were first-order filters and had time constants of 20ms and 500 ms for the high- and low-pass filters respectively. The impulse response for a low pass filter is given by:

$$\frac{1}{\tau} \exp(-t / \tau) \quad (5)$$

For the first subunit of the motion detector (left hand side in Figure 2.8), each point in the low-pass filtered matrix from the first spatial value to the second to last spatial value (1 to n-1) was multiplied by the corresponding point on the high-pass filtered matrix from the second spatial value to the last (2 to n). For the second subunit of the motion detector the high-pass filtered matrix (1 to n-1) was multiplied by the low pass filtered matrix (2 to n). The second subunit matrix was then subtracted from the first subunit matrix, leading to the full EMD output for each motion detector. The full EMD output was then averaged over time leading to the average EMD output for that velocity profile and visual pattern. No additional spiking mechanism was implemented to try and mimic the spike generation in the H1-cell. The velocity vector and the full EMD output were then analyzed in the same way as the experimental data (see Data Analysis).

---

**Tables of equipment and suppliers**

<b>Table 1 Brotz Case Ringer's Solution pH 7.2</b>				
<b>Chemical</b>	<b>Mol. Weight</b>	<b>Concentration</b>	<b>Supplier</b>	
Glucose	180.16 g/mol	13.9 nM	Merck	KGaA, Darmstadt, DE
Sucrose	342.30 g/mol	73.7 nM		
NaHCO <sub>3</sub>	84.01 g/mol	20 nM		
NaCl	58.44 g/mol	110 nM		
KCl	74.55 g/mol	5.4 nM		
CaCl <sub>2</sub> -2H <sub>2</sub> O	147.02 g/mol	1.9 nM		
TRIS/HCL	121.14 g/mol	15 nM	Sigma-Aldrich Chemie	
Fructose	180.2 g/mol	23 nM	GmbH, Steinheim, DE	

Table 1 Constituents used for Case Ringers solution. New solution was made fresh approximately every 2-3 months using the above components. The Ringer's was then sterile filtered and kept at 4 °C until needed.

<b>Table 2 Electrophysiology Equipment Specifications</b>	
<b>Name</b>	<b>Properties</b>
Microscope	Eye pieces 8x, f = 100 mm
Tungsten Electrodes	1 MΩ impedance
Glass Capillary tubes	1 mm outer diameter
Micropipette Puller	Heat 479, Pull 180, Pressure 500, Velocity 100, Time 200
Visual Monitor	200 Hz refresh rate, 13 x 9.8 cm, P15 Phosphor, dot size 0.25 mm
Amplifier	3000 and 100 times
Band-pass filter	range 500-10,000 Hz and again 300-3,000 Hz

Table 2 Specifications of the electrophysiological equipment used.

<b>Table 3 Equipment suppliers</b>	
<b>Object</b>	<b>Company</b>
Micromanipulators	Narishige Japan, assembled partly by MPI-Neurobiology, Martinsried, DE
Microscope	Carl Zeiss, DE
Tungsten Electrodes	World Precision Instruments Inc., Florida, USA
Glass Capillary tubes	Science Products GmbH, Hofheimer, DE
Brown-Flaming micropipette puller (P-97)	Sutter Instruments, California, USA
Air Table and accessories	Newport Corporation, California, USA
Tektronix TDS 2002 Digital Oscilloscope	Tektronix, Oregon, USA
Audio Monitor	Grass Medical Instruments, Massachusetts, USA
Analog electronic amplification and filtering equipment	Designed by the Max-Planck Institute of biological Cybernetics, Tübingen, DE
DAS16 I/O AD/DA Board	Metabyte; Measurement Computing Co.
CRT Monitor, model 608, or 604	Tektronix, Oregon, USA
Picasso Image Synthesizer	Innisfree Inc., Massachusetts, USA
Bullmess stimulation and data acquisition software	Privately designed in Delphi (Borland) by Dr. Jürgen Haag
Dell Personal Computer	Pentium II, Intel Corporation, California, USA
Matlab versions 6.5-7.1	Mathworks Inc., Massachusetts, USA
IDL version 5.0-6.0	Research Systems Inc. Colorado, USA

Table 3 Suppliers for the electrophysiological equipment and programming software.

### 3 Results

---

H1-cell response adaptation was tested under three experimental conditions. First, the overall magnitude and shape of the H1-cell input-output function was tested in response to the velocity standard deviation and time constant using a sinusoidal grating and a low-pass filtered Gaussian white noise velocity signal. Second, the effect of the visual pattern was tested by using the same velocity signals as in the first set of experiments but in addition to the sinus grating, a square wave grating was introduced. Lastly, the speed at which the H1-cell adapted was tested by switching either the standard deviation or the time constant of the velocity signal during the experiment. The results for each of the experimental conditions were then compared with simulations of the Reichardt detector in response to the same stimuli.

The H1-cell adapted its stimulus-response function to the entire set stimulus conditions tested. The slope of the stimulus-response function decreased as the velocity standard deviation increased and increased with increasing velocity time constant. The speed at which the cell responded to the stimulus also increased as the velocity standard deviation increased. The square wave visual pattern increased the dynamic gain for all of the velocity standard deviations and time constants tested compared to a sine wave grating. The H1-cell adapted quickly to the new stimulus condition after the velocity standard deviation or time constant was switched. This suggests that the mechanism behind the adaptation also occurs on a fast time scale.

The same changes in the slope of the stimulus-response function were found in the Reichardt motion detector without any change in the model parameters. It was an automatic function of the motion detector itself. The slope of the stimulus-response function in the Reichardt detector decreased as the velocity standard deviation increased and increased with increasing velocity time constant. The Reichardt detector changed its stimulus-response function very rapidly in response to a switch in either velocity standard deviation or time constant. The only discrepancy between the experiment and the model was in the response to the square wave grating. The model adapted its slope of the stimulus-response function less for a square wave

pattern compared to a sine wave pattern. The experiments showed exactly the opposite effect. This is likely due to saturation in the firing rate that is not accounted for in the model.

In the following section I often substituted Greek letters for the different stimulus parameters that I used or for the time constants of the Reichardt detector model. These letters consistently stand for the same property throughout this work. The standard deviation of the Gaussian colored noise velocity profile is represented by the lower case Greek letter sigma ( $\sigma$ ), and the low-pass filter time constant of the Gaussian colored noise velocity profile as the lower case Greek letter tau with subscript zero ( $\tau_0$ ). The first order low-pass time constant of the Reichardt detector is represented by the Greek letter tau with subscript L ( $\tau_L$ ) and the first order high-pass filter with the Greek letter tau with a subscript H ( $\tau_H$ ).

---

## Dependence on Stimulus Statistics

The first set of experiments investigated H1-cell input-output gain adaptation in response to the standard deviation of a Gaussian colored noise velocity profile, when the visual pattern is a sinusoidal grating. The following five velocity standard deviations were used: 0.1 Hz, 0.5 Hz, 1.0 Hz, 5.0 Hz and 10.0 Hz. In addition, I tested the H1-cell adaptation in response to the time constant of a Gaussian colored noise velocity profile. Three different velocity low-pass filter time constants were tested, namely: 100 ms, 500ms and 2000ms. The results of both of these experiments were then compared to response simulations of an array of Reichardt detectors using the same stimuli as in the experiments. In this section, I will briefly mention the overall firing properties of the H1-cell to the different stimuli and then I will describe the effect of the velocity standard deviation and time constant on the stimulus-response gain function. Finally, I will discuss the correlations between the stimulus and the response and how they adapt to the velocity standard deviation, both in the H1-cell and in the Reichardt detector model.

### H1-cell firing properties

Before examining adaptation of the stimulus-response curves to dynamic stimuli, I investigated the effect of velocity standard deviation on the general H1-cell firing properties. The raw spike trains from one fly as well as the mean-over-variance curves for different standard deviations are shown in Figure 3.1 Each of the five different velocity standard

deviations tested had an entirely different sequence of preferred and null direction velocities (see Figure 2.4) which is apparent in the different raster plots.

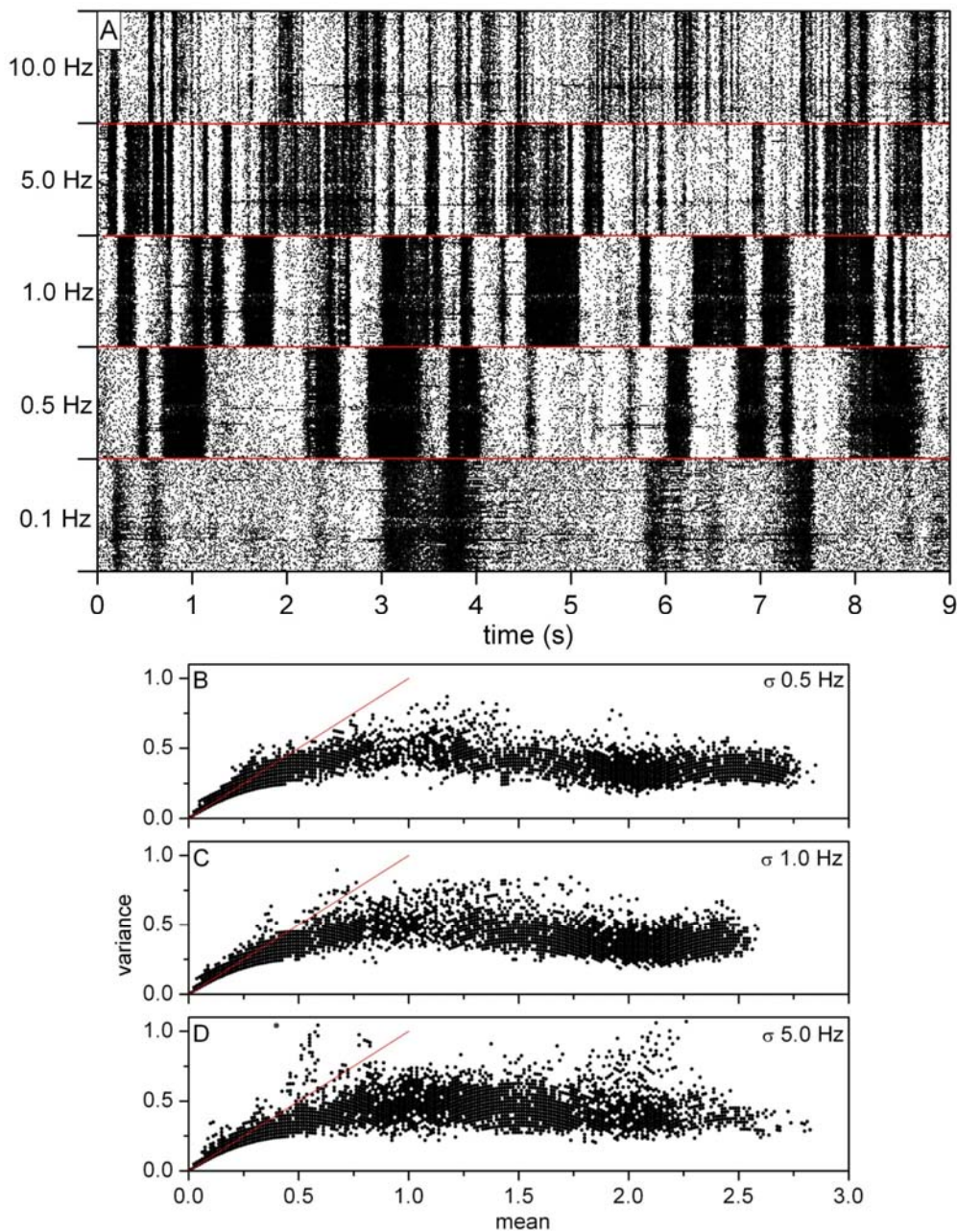


Figure 3.1 Response characteristics from one fly. (A) A raster plot with the spikes over time (x-axis) for each trial (y-axis) for all five standard deviations tested. The red lines separate the spike trains from different stimuli. (B-D) Variance over mean plots of the number of spikes per bin for the same data, for three different standard deviations, binsize 10 ms. The red line is where mean equals variance, and therefore would represent a Poisson distribution. In all cases the stimulus time constant,  $\tau_0$ , was 100.0 ms, experiment number 20050517.

The variance-over-mean plots for the different standard deviations show that the response statistics are non-Poisson, a common property for spiking cells (Figure 3.1B). Variance-over-mean plots are a measure of the variance in each bin, and a measure of whether the spike trains are Poisson and therefore random or not. The spike train was reformed into 10 ms sized

bins and the mean and variance within the bin across trials was plotted. There are only small differences between the variance-over-mean curves for each standard deviation. The general firing statistics are not shown for different velocity time constants because all three velocity time constants used were never tested in the same fly and the background firing properties differ greatly between flies making a comparison non-relevant.

The mean and variance of the firing rate for the different velocity standard deviations are shown in Figure 3.2 for all flies tested with 100 ms time constant. The mean firing rate of the H1-cell increased with increasing velocity standard deviation peaked at 1.0 Hz and then decreased again. This is interesting and perhaps predictable since the maximum response of many LPTCs occurs at 2 Hz contrast frequency. The variance of the response also increased with increasing velocity standard deviation, which peaked at 0.5 Hz and then decreased again. In some cases (see Figure 3.1A), the variance was slightly increased for 0.1 Hz standard deviation but never higher than the maximum. It is possible that the decrease in variance for the 0.1 Hz velocity standard deviation is a result of signal amplification under low noise conditions that occurs prior to the H1-cell. The stimulus-response curves also show more precisely how the H1-cell adapts to the statistics of the stimulus.

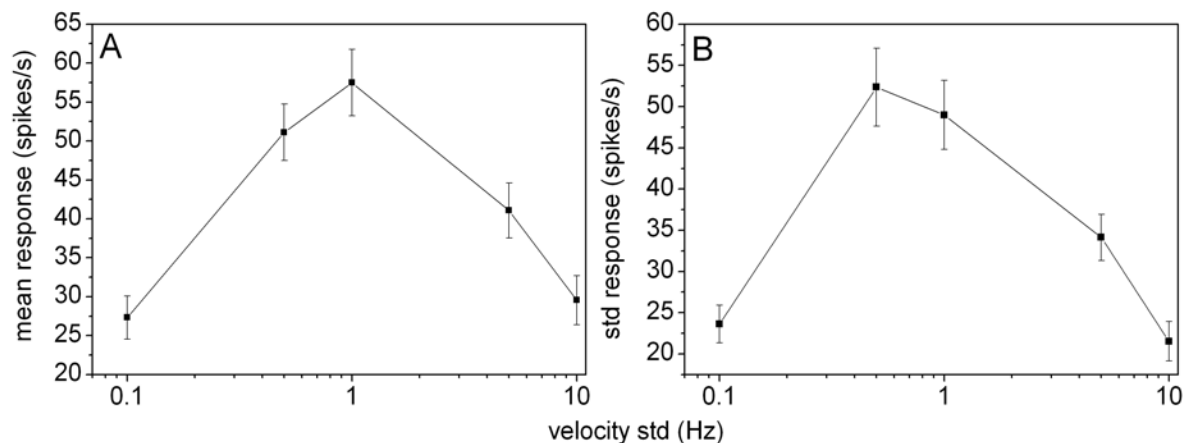


Figure 3.2 Overall response characteristics. Mean (A) and standard deviation (B) of the firing rate as a function of the velocity standard deviation. Both curves show the mean and standard error from 11 flies. The  $\tau_0$  for both curves is 100 ms.

### Stimulus-Response Function

The different H1-cell stimulus-response functions in response to Gaussian colored-noise velocity profiles are shown in Figure 3.3. The H1-cell changed its stimulus-response function depending on the standard deviation of the stimulus. For a high velocity standard deviation, the firing rate covered a broad range of velocities, corresponding to a low slope. The slope of

## Results

the response curve for a lower velocity standard deviation was then very steep, such that the cell can use its entire response range to cover a much smaller velocity range. Figure 3.3A shows the stimulus-response curves for an example experiment from a single fly chosen at random. In all of the experiments, the maximum spike rate over the whole velocity profile was the highest for 0.5 Hz velocity standard deviation and gradually decreased to the highest velocity standard deviation (A). For profiles with a smaller velocity range, the response covered the narrower range leading to a steeper stimulus-response curve. For standard deviations higher than 1.0, the firing rate was not a monotonically increasing function, instead it decreased again for higher velocities. The peak of non-monotonically increasing stimulus-response curves moved to higher velocities as the velocity range increased but the peak remained between 5 and 10 Hz velocity (B).

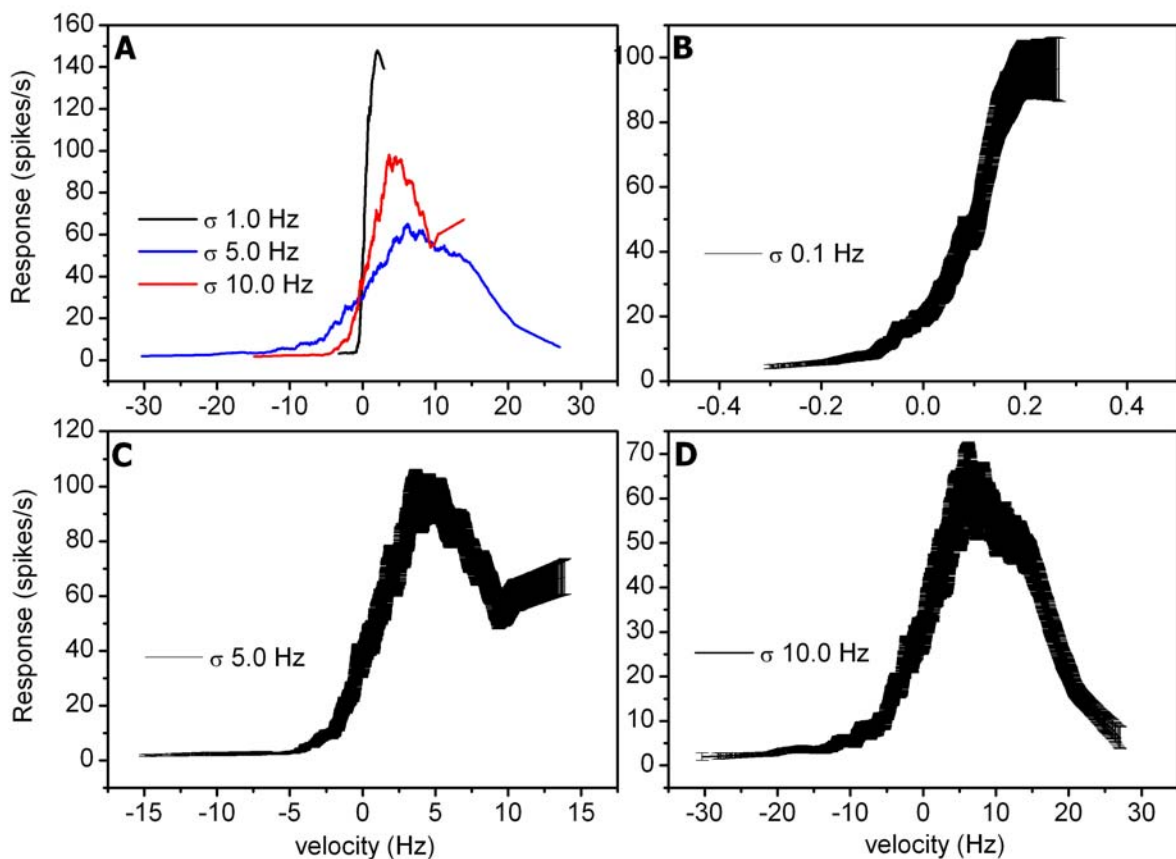


Figure 3.3 The stimulus-response functions for three velocity standard deviations. The stimulus-response curves are for velocity standard deviations of 1.0 Hz, 5.0 Hz and 10 Hz, and the velocity time constant was 100 ms.(A) An example from one fly. (B), (C) and (D) show the mean and standard error ( $n = 11$ ) of the stimulus-response curve for 0.1, 5.0, and 10.0 Hz velocity standard deviation respectively.

When the full version of the Reichardt detector was simulated using the same Gaussian colored noise stimuli, similar stimulus-response curves were produced. For small standard deviations, the Reichardt detector response curves were narrow and steep. As the standard

deviation increased, the response curve broadened and leveled out (Figure 3.5). For larger velocity standard deviations, the Reichardt detector stimulus-response curve was also non-monotonically increasing, with a shape similar to the curves from the experiments. One major difference between the model and the experiments was that the model also responds to null direction motion with a negative response. Due to the spiking nature of the H1-cell the stimulus-response curves to null direction motion at some point flattened out at zero, since negative firing rates are not possible.

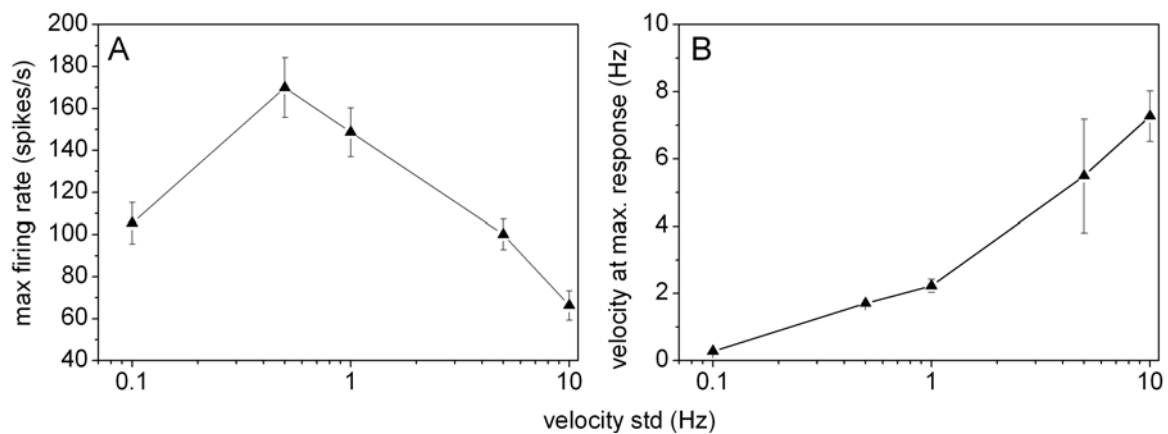


Figure 3.4 The maximum firing rate (A) and corresponding velocity at the maximum firing rate (B) for each velocity standard deviation. Filled triangles and error bars represent the mean and standard deviation respectively from 11 flies. The  $\tau_0$  is 100 ms.

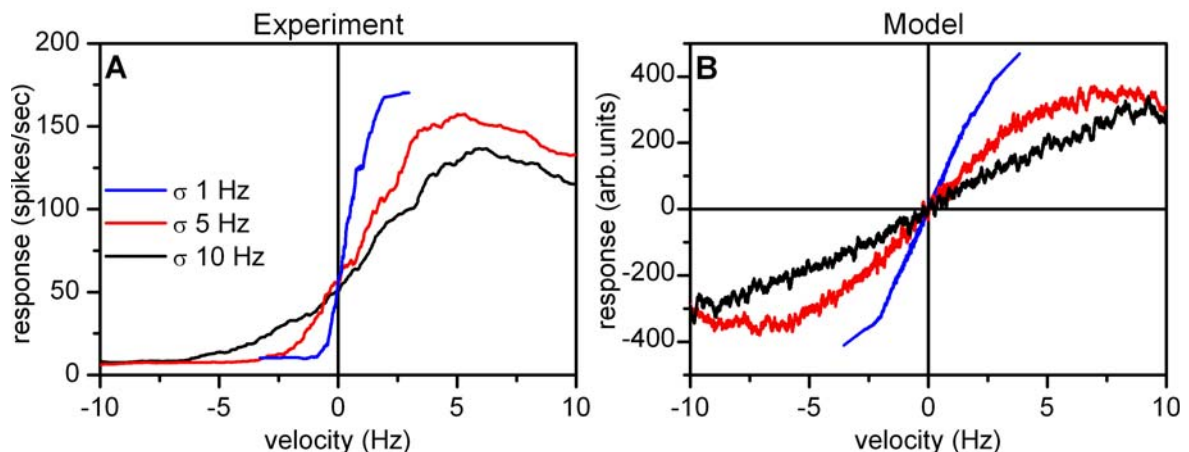


Figure 3.5 Stimulus-response curves for H1-cell experiments (A) and from the Reichardt detector model (B) with high and low pass filters in the individual arms of the detector. The H1-cell responses are means from 11 flies and the stimuli in both graphs had a time constant of 100 ms. See also (Borst et al., 2005).

The H1-cell adaptation was also tested as a function of the temporal correlations in the Gaussian colored noise profile. Figure 3.6 shows the mean stimulus-response curves for the three different stimulus correlation times, keeping the stimulus standard deviation constant at 0.5 Hz (A) and 10.0 Hz (B). It is important to keep in mind that a larger time constant

corresponds to a more slowly changing velocity profile (see Figure 2.4). The changes in response properties were less pronounced in response to the temporal correlations than they were for velocity standard deviations and generally went in the opposite direction. As the correlation time increased and standard deviation was held constant, the response curve became steeper, (Figure 3.6). The peak firing rate also tended to increase with increasing velocity time constant (Figure 3.6B) opposite to that seen in the stimulus standard deviation. For stimulus-response curves where the firing rate was no longer a monotonically increasing function, the peak firing rate shifted towards smaller velocities as the velocity time constant increased (Figure 3.6B).

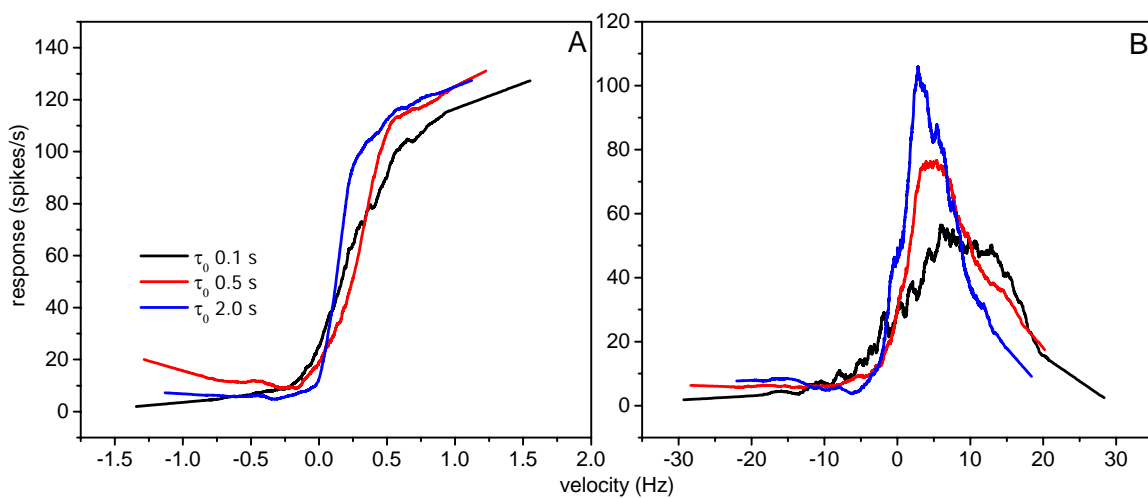


Figure 3.6 Stimulus-response curves for different stimulus time constants. The average response of the H1-cell to a colored noise velocity profile with a standard deviation in (A)  $\sigma = 0.5$  Hz and in (B)  $\sigma = 10.0$  Hz. In both graphs the signals are averaged over at least 100 trials within one fly and then between the 8 to 10 flies.

### Dynamic Gain

One way to look at stimulus-response adaptation is to compare the slope of the stimulus-response function around zero for the different stimulus conditions. Therefore, I define the dynamic gain as the slope of the stimulus-response curve around zero, normalized by the slope of the stimulus-response curve to a constant velocity in the same cell (see Methods). The dynamic gain of the H1-cell as a function of the velocity standard deviation for all three velocity low-pass filter time constants is shown in Figure 3.7. A few interesting characteristics emerge from this graph. First of all the dynamic gain never reaches 1, or the slope of the stimulus-response curve for a colored-noise stimulus is never larger than the stimulus-response curve for constant velocities. The larger the time constant, or the slower the change in velocity, the steeper the stimulus-response function and therefore the higher the

dynamic gain. In contrast if the velocity standard deviation is large, the dynamic gain is small, because the stimulus-response curve adapts to cover the larger range of velocities. The same stimuli were used to create the input to a one dimensional array of EMDs. The dynamic gain from the array of Reichardt detectors looks very similar to the dynamic gain in the H1-cell for all stimulus conditions tested in Figure 3.7. The small differences between the two curves are probably due to sampling errors in the estimate of the stimulus-response curve slope. This suggests that the underlying mechanism for the dynamic adaptation of the H1-cell is the same mechanism that is used by the Reichardt detector model. The Reichardt detector model achieved this adaptation without any change in the model parameters; it happened automatically. The simulations were done in a purely deterministic way and no noise was added, suggesting that adaptation of the stimulus-response function is an automatic outcome of the Reichardt detector model.

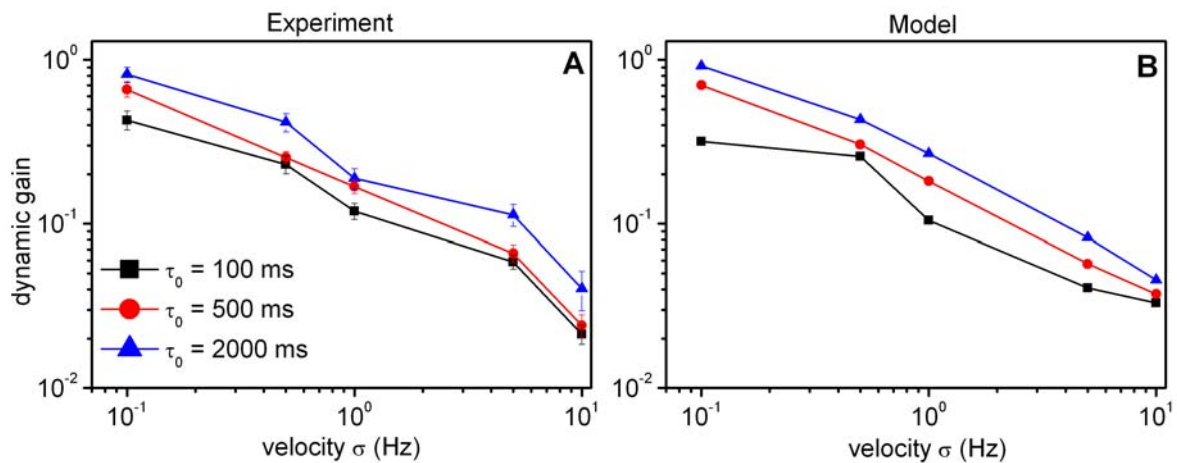


Figure 3.7 Dynamic gain for experiments and the motion detector model. (A) The dynamic gain of the H1-cell for all standard deviations and time constants tested. Mean and standard error bars for 9 flies (2000 ms), 10 flies (500 ms) and 11 flies (100 ms). (B) The dynamic gain calculated from the Reichardt motion detector model (Figure 2.8) for the standard deviations and correlation times tested in the experiments.

Since the effect of time constant and standard deviation act against each other, it is possible that the adaptation of the system functions responds to acceleration and not just to motion. If a stimulus was doubled in velocity but at the same time made twice as slow, then the change in velocity over time, or the acceleration would be the same. If adaptation responded only to acceleration then the dynamic gain curves should line up if the standard deviation of the velocity is normalized by the velocity time constant. Figure 3.8 shows the same curves as before but this time plotted vs.  $\sigma/\tau_0$ . The curves however do not line up either in the experiments or in the model suggesting that the system is not just responding to acceleration.

## Results

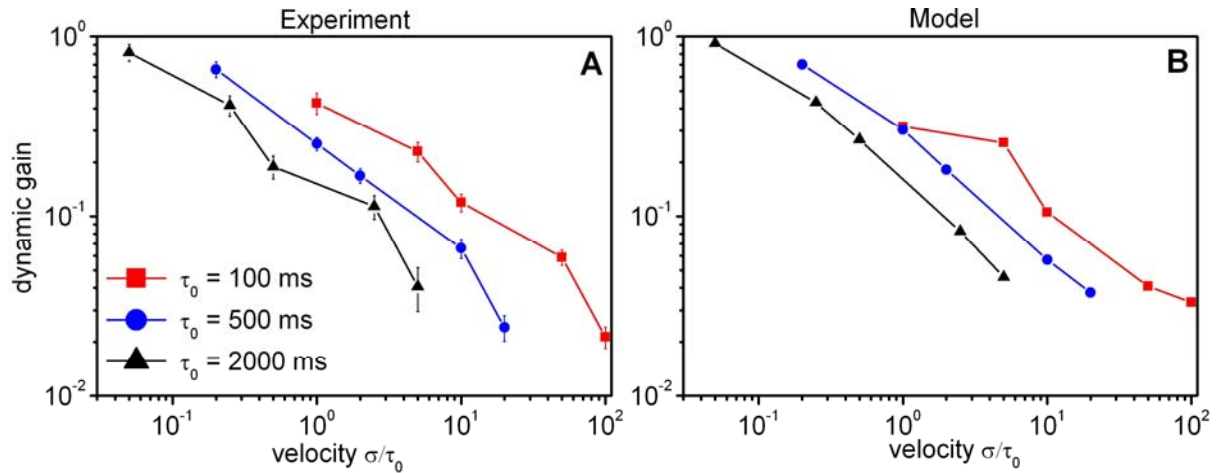


Figure 3.8 Dynamic gain vs. acceleration. The same plots as Figure 3.7 only plotted ( $\sigma$ ) over ( $\tau_0$ ) as a measure of acceleration. (A) and (B) show the results for experiments and model respectively.

## Cross-correlations

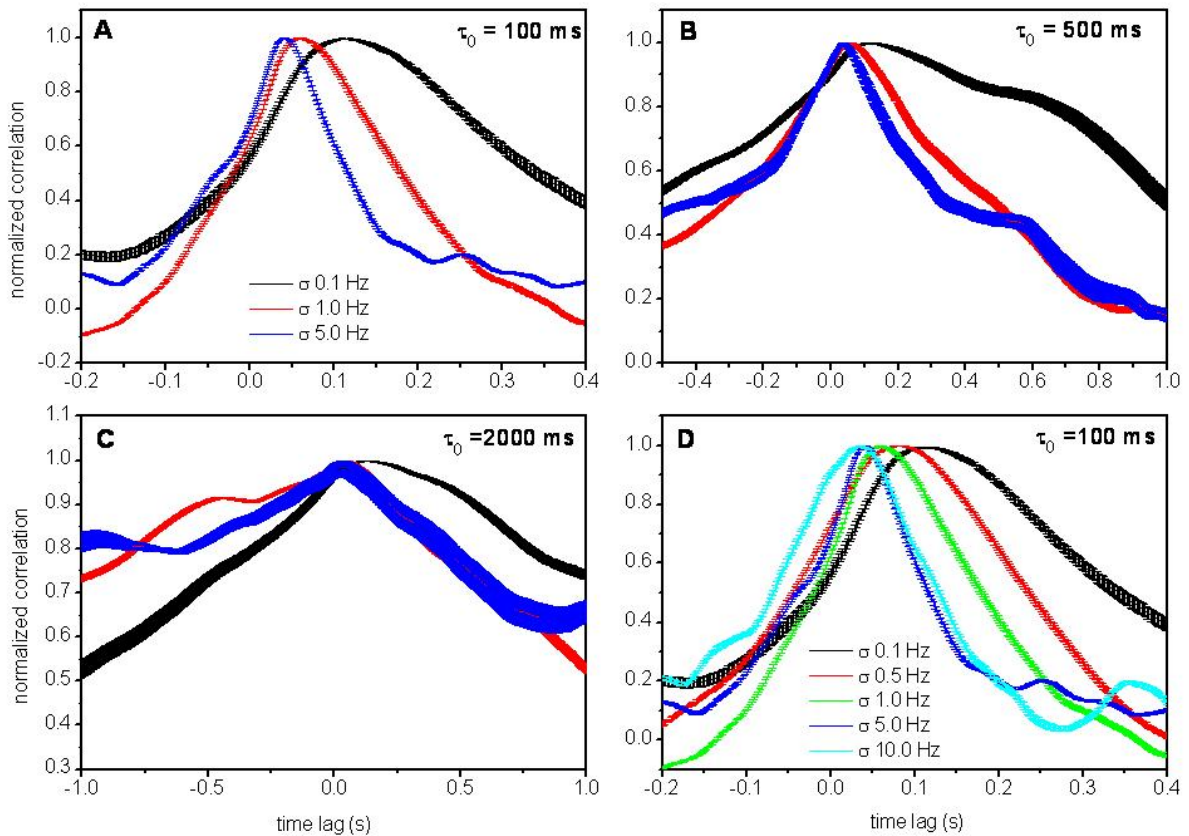


Figure 3.9 The normalized cross-correlation between stimulus and response. For all curves the mean and standard error of the mean are shown from 11, 10 and 9 flies for (A), (B) and (C) respectively. (D) shows the cross-correlation for all of the different standard deviations tested within  $\tau_0=100$ ms.

Part of the data analysis involved taking the cross-correlation between the stimulus and the response in order to measure the stimulus-response function where the response to a stimulus is at its maximum. The time-lagged cross-correlation between the stimulus and response is a measure of how strongly the two signals are correlated at different time points. It is also

considered a measure of how much delay exists between the stimulus presentation and the H1-cell response. In other words, the time lag at which the cross correlation has a maximum is generally viewed as the delay from when the stimulus occurs to when the cell fires a spike in response to the stimulus. The cross-correlations also changed for different velocity standard deviations. Figure 3.9 shows the time-lagged cross correlation between stimulus and response for the different stimuli presented. The time delay at the max-correlation between the two signals changes with the standard deviation ( $\sigma$ ) and with the time constant ( $\tau_0$ ) of the stimulus. The time delay decreases with increasing standard deviation. In addition, the cross correlation function is broader for smaller deviations and then becomes narrower as standard deviation increases (). This is a confirmation that the shape of the cross-correlation is not entirely dependent on the temporal correlations in the stimulus, because the temporal correlations in this case are the same. The peaks of the cross-correlation curves become more concurrent as the stimulus time constant ( $\tau_0$ ) increases and the cross-correlation function broadens, for all standard deviations. This is probably due in part to the broadening of the stimulus auto-correlation, which is just an exponential function with a time constant equal to the low-pass filter time constant ( $\tau_0$ ). This adaptation in the temporal relationship between the stimulus and response suggests that the H1-cell adapts not only its gain function to the statistics of the stimulus but also the speed at which it responds. With this form of adaptation the cell can respond more quickly to a fast changing stimulus, and slower to a slowly changing stimulus.

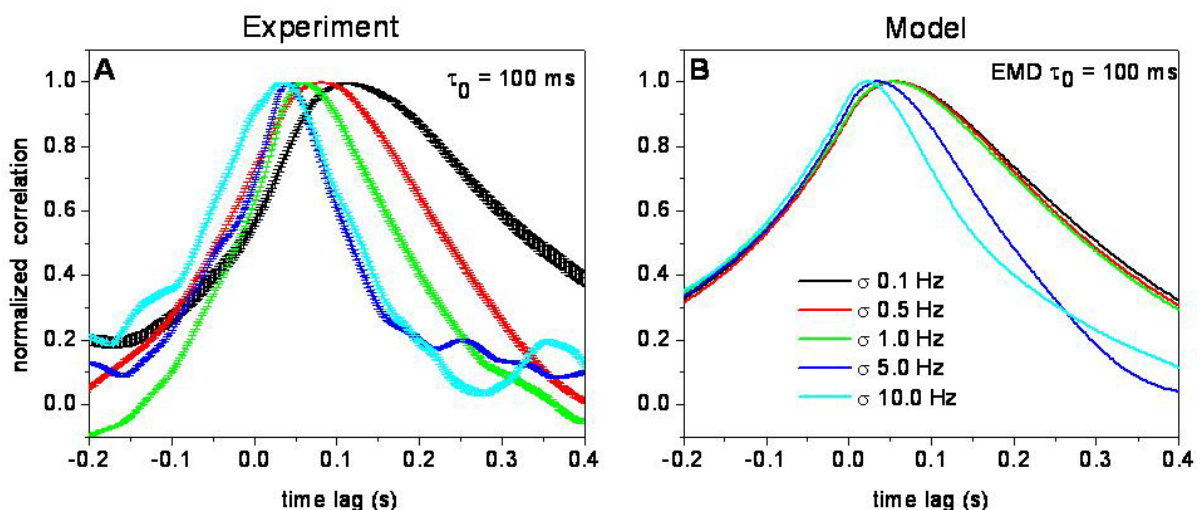


Figure 3.10 Stimulus-response correlations experiments and model. (A) shows the same results as in for  $\tau_0 = 100$  ms, mean and standard error for 11 flies. (B) shows the cross-correlation between the same stimuli as in (A), and the resulting EMD response.

The adaptation in the stimulus-response cross correlation was also found in the Reichardt detector model ( ) As the standard deviation ( $\sigma$ ) was increased, the peak cross-correlation between the stimulus and the response became smaller, and the overall time-lagged correlation function was narrower. In addition, larger stimulus time constants had a broader cross correlation function and the difference in the location of the peak cross correlation for different stimulus standard deviations ( $\sigma$ ) was diminished. The delay in the Reichardt detector model was much less than in the experiments. This could be due to additional delays due to physiological processes that are in the fly visual system that are not represented by the motion detector. This adaptive property is again an automatic function of the Reichardt motion detector and occurs without any change in the model parameters.

### Dependence on Visual Pattern

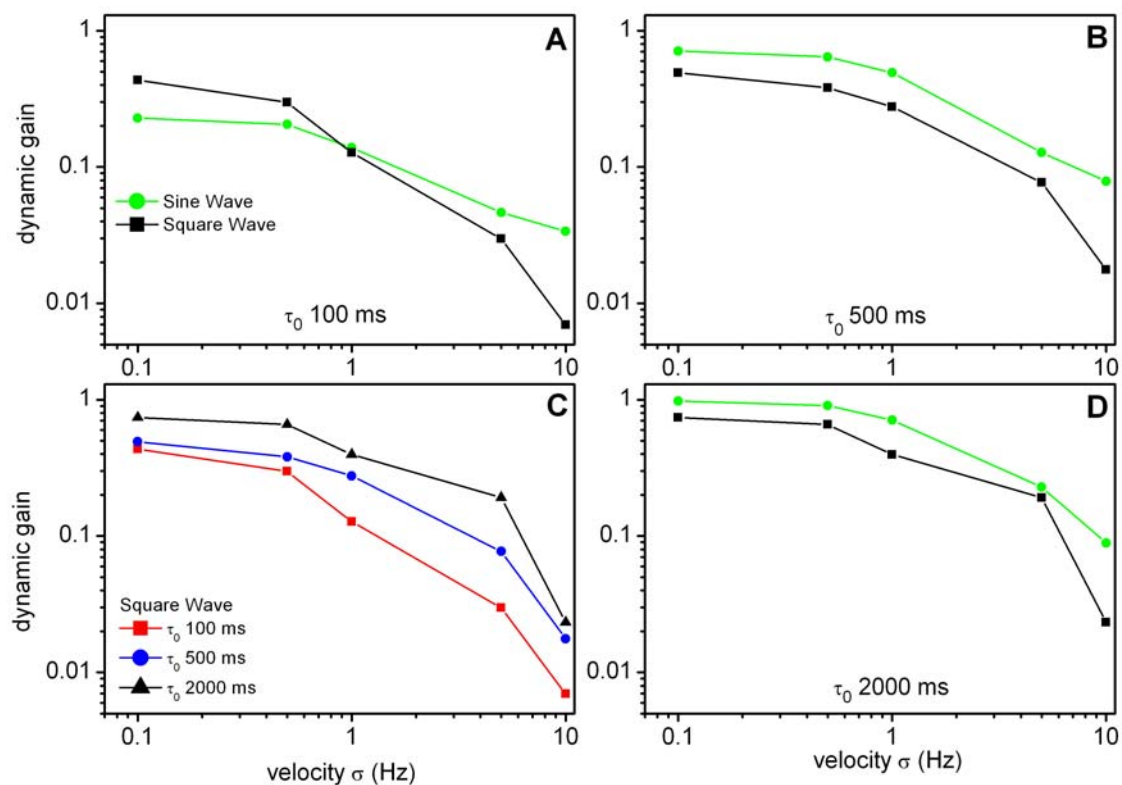


Figure 3.11 Dynamic gain of the motion detector model for a sinus and a square wave visual pattern. The modeling results from an array of the full Reichardt detector for the exact same stimuli used in the experiments but with a square wave pattern (C). (A) shows the model dynamic gain for both stimulus patterns for  $\tau_0 = 100$  ms, (B)  $\tau_0 = 500$  ms, and (D)  $\tau_0 = 2000$  ms.

The automatic property of dynamic adaptation in the Reichardt detector suggests that some inherent characteristic of the detector model is responsible for the adaptation. Only a non-linear system can respond to inputs in an automatically adaptive way. Therefore I looked into

the possible sources of non-linearity in the Reichardt detector model. The visual pattern is one source of non-linearity in the model that is easily manipulated. Therefore I examined the response of the H1-cell and the motion detector to different visual patterns. shows the dynamic gain of the EMD simulations when either a sinusoidal grating or a square grating was given. The velocity profiles were the same used for the previous experiments, and no photon or internal noise was added. In general, the sinusoidal grating produced a higher gain than the square grating, suggesting that adaptation was stronger for a sine wave pattern. The slope of the dynamic gain curve with respect to velocity standard deviation was similar for both sinusoidal and square wave patterns; both showed an inverse relationship between velocity standard deviation and dynamic gain (). The dynamic gain also increased with an increasing velocity low-pass filter time constant for both square and sine wave patterns, although the square wave dynamic gain was consistently lower than that of the sine wave (C).

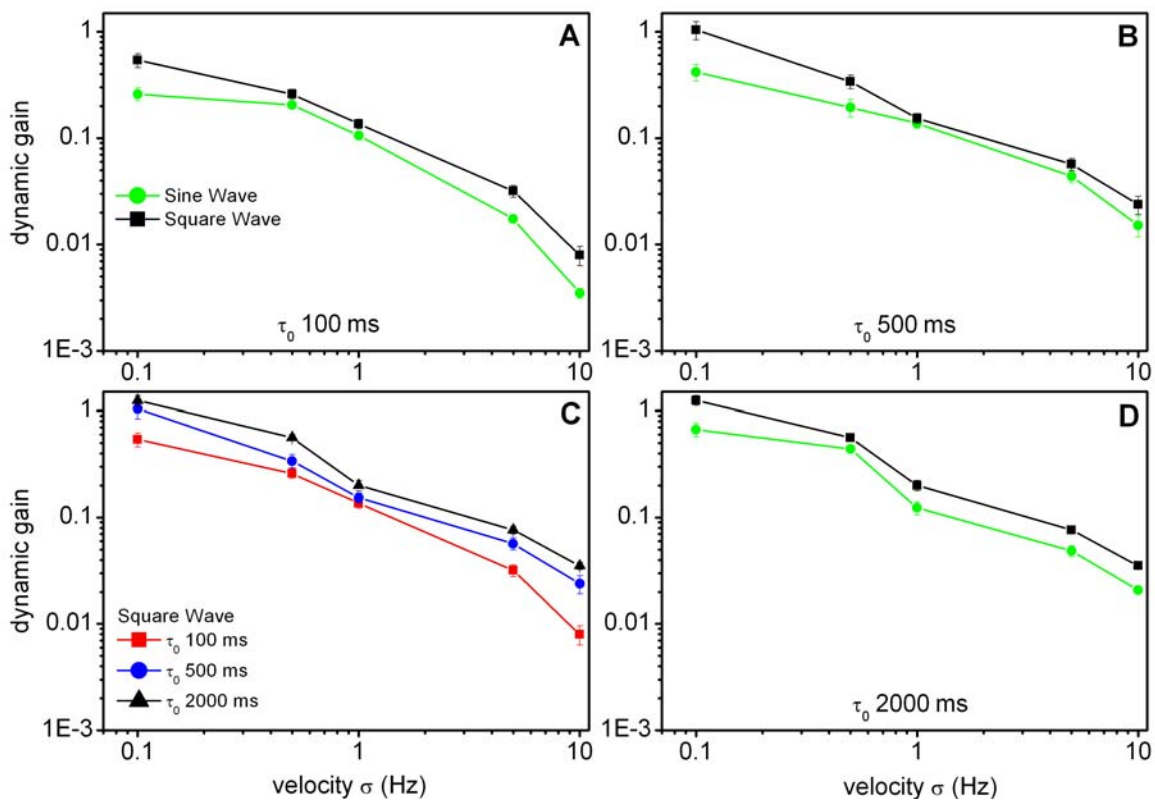


Figure 3.12 Dynamic gain of H1-cell for sinus and square wave visual patterns. (A) Mean and standard error of the mean for  $n = 8$ , stimulus time constant  $\tau_0 = 100$  ms. For (B) and (D)  $n = 6$  flies, and the stimulus was low-pass filtered with time constants  $\tau_0$  of 500 ms and 2000 ms respectively. (C) shows the entire experimental results for the square wave visual pattern.

The same stimuli were also tested in the H1-cell. For all stimuli tested, the square wave dynamic gain was consistently higher than the sine wave dynamic gain (). This is the opposite of what was found in the Reichardt detector simulations. In addition, the square wave

dynamic gain for a 2000 ms  $\tau_0$  and a 0.1 Hz  $\sigma$  was higher than one. Simulations and modeling work suggest that the dynamic gain in the Reichardt detector should never be higher than one. All other characteristics of the dynamic gain were in agreement with the Reichardt detector model. The shape of the dynamic gain with respect to velocity standard deviation was similar in the Reichardt detector and in the experiments.

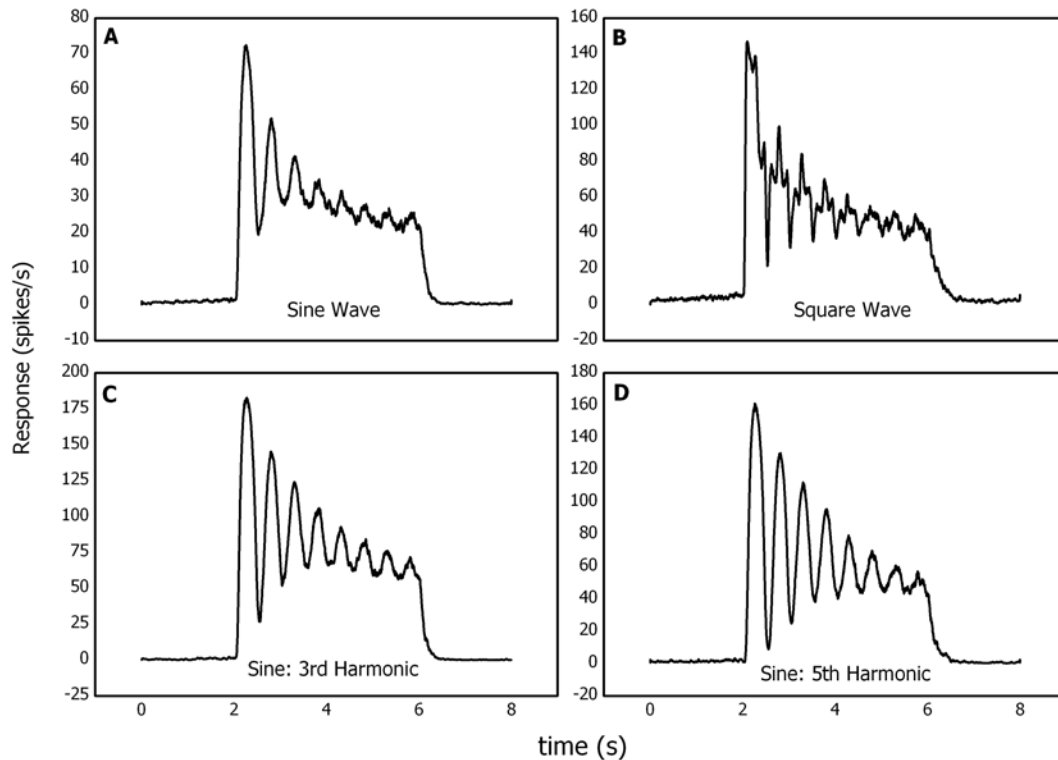


Figure 3.13 H1-cell response to higher harmonics of a square wave. The response of the H1-cell to a full size sine (A) and square wave (B) were measured along with the response to a sine wave that was a third (C) and a fifth (D) of the original wavelength, which correspond to the third and the fifth harmonic of the square wave. Data shown here are from responses averaged over 200 trials for one fly.

I then looked into possible explanations for the discrepancy between the model and the experiments. First I examined the difference between the sinusoidal and square wave patterns in the fly. In order for the cell to respond uniquely to the square wave instead of just to a sine wave, the higher harmonics of the square wave must be above twice the interommatidial distance, or the Nyquist limit of the system. I therefore tested the response of the H1-cell to a step in velocity for a sine wave, square wave, and its higher harmonics. Figure 3.13 shows the response of the H1-cell to a step velocity function of 2.0 Hz, which is the optimal contrast frequency for the H1 (Eckert, 1980). The response of the H1-cell to a sine wave differed from the response to a square wave. The higher harmonics of the square wave are visible in the response PSTH of the square wave (B). Then a velocity step of 2 Hz was shown to the fly using a sine wave pattern with wavelengths equal to the 3<sup>rd</sup> and 5<sup>th</sup> harmonic of the square

wave (C&D). It is possible to see that the H1-cell also responds to the 3<sup>rd</sup> and 5<sup>th</sup> harmonic of the square wave. Therefore the discrepancy between the model and the experiments is not due to sampling problems between the sine and the square wave.

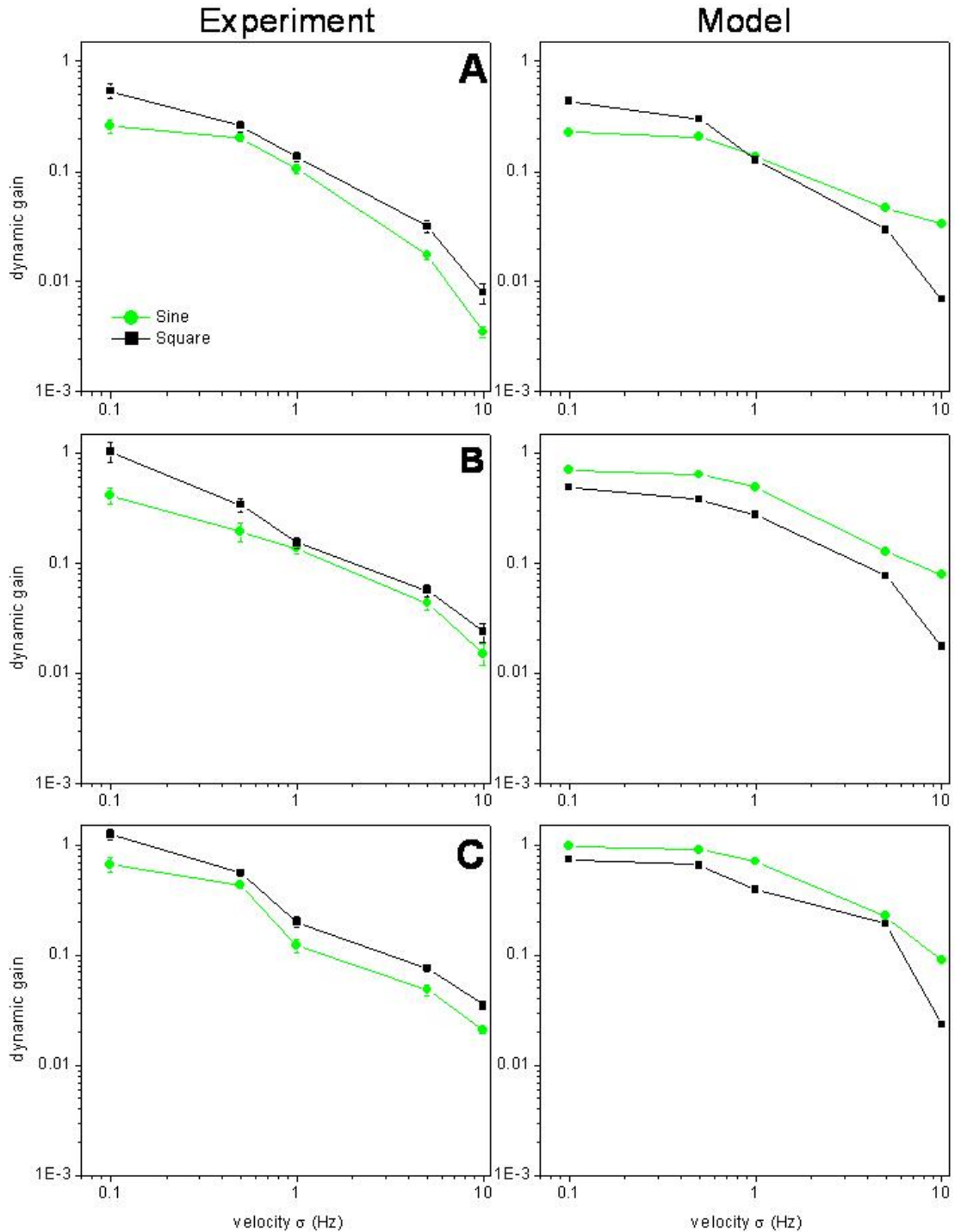


Figure 3.14. Dynamic gain for square and sine wave gratings experiments and simulations. The same curves as in and Figure 3.12 for velocity time constants of (A)  $\tau_0$  100 ms, (B)  $\tau_0$  500 ms, and (C)  $\tau_0$  2000 ms. In the experiments, the square wave gain was always higher than the sine wave gain, for all velocity standard deviations and time constants tested.

Figure 3.14 shows difference between the dynamic gain for both the square and the sine wave from the model and the simulations as a comparison. Strangely enough, adaptation in the stimulus-response cross-correlation was the same between the simulations and the experiments. shows the normalized cross-correlation between the stimulus and the response for a sine wave and for a square wave. The time delay between the stimulus and the response is shorter for a square wave pattern than for a sine wave pattern. The results for all standard deviations and stimulus time constants look very similar between the model and the experiments. The simulations predict that the sine and square wave pattern stimulus-response cross-correlation should have similar peaks, but that the downward slope after the peak is steeper for the square wave than for the sine wave pattern, which was also found in the experiments (Figure 3.15). The experiments show an overall delay or rightward shift in the cross-correlation, but this is most likely due to additional delays between the retinal input and the H1-cell output that are not specified in the motion detector model.

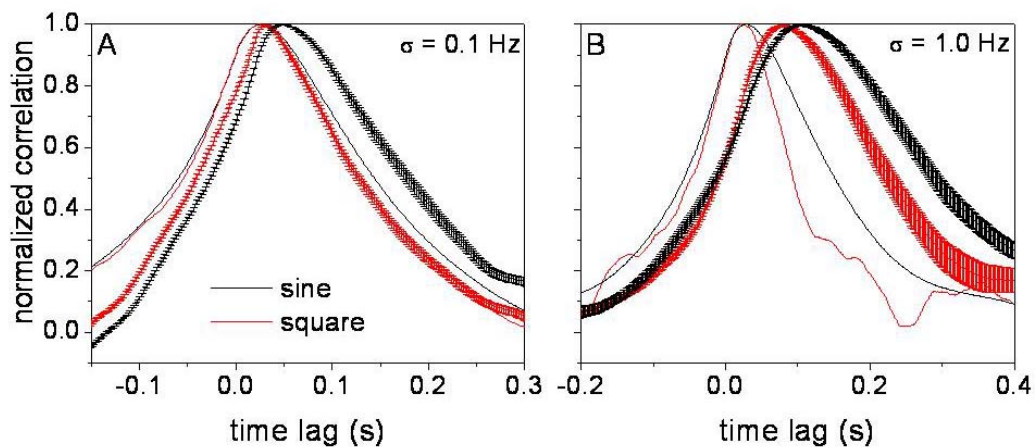


Figure 3.15 The normalized cross-correlation for sine and square wave patterns. The thin lines represent the model results and the lines with error bars represent the mean and standard error from 8 flies. In both graphs  $\tau_0 = 100$  ms; and  $\sigma = 0.1$  and  $1.0$  Hz for (A) and (B) respectively.

Another possible explanation for the discrepancy between the model and the experiments is due to saturation of the firing rate when the square wave pattern was used, particularly in response to the constant velocity. The square wave function leads to an extremely high firing rate in the step response and it is therefore possible that the firing rate saturated for the square wave pattern, leading to higher dynamic gain values. I retested 3 flies for the difference between the sine and the square grating at a low contrast (10%) and found no difference in the relative locations of the curves (Figure 3.16). When performing the experiments, I noticed that the H1-cell seemed to respond to the square wave in general much better than a sinusoidal wave, particularly at low light levels or contrast levels. The H1-cell responded to

motion of a square wave pattern at much lower contrast values than to motion of a sine wave pattern.

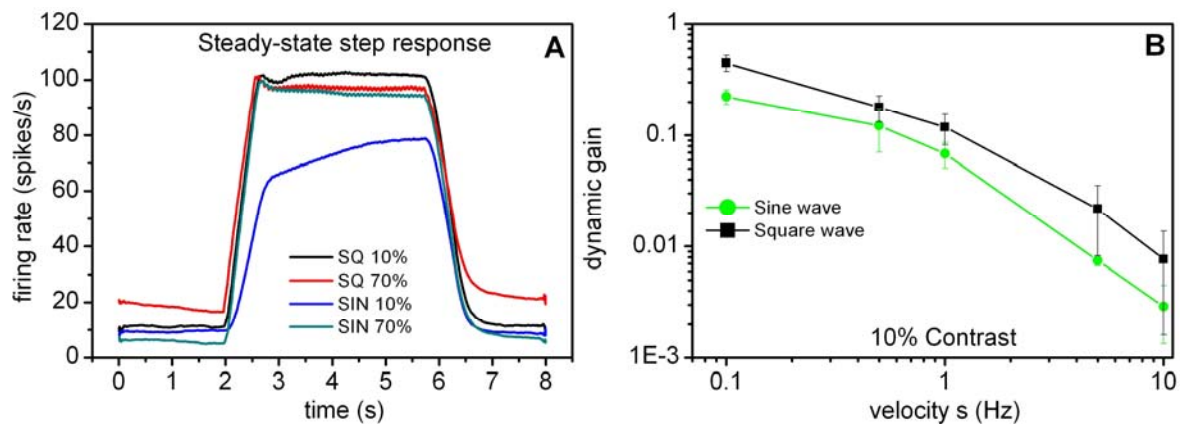


Figure 3.16 The effect of contrast on firing rate saturation and dynamic gain. (A) the four curves represent the mean PSTH for 3 flies in response to a step in velocity from 0 to 0.1 Hz. The PSTH for a square wave is as high for 10% contrast as for 70% suggesting that the firing rate saturated. (B) dynamic gain at 10% contrast. Mean and standard error for 3 flies are shown for a 100 ms velocity time constant.

Therefore I looked again at the firing rate in response to a velocity step from the three flies that were tested for both high and low contrast. I found that the firing rate for the square wave visual pattern was as high for a 10% contrast pattern as it was for a 70% contrast pattern, suggesting that the firing rate was saturating (Figure 3.16A). The constant velocity stimuli were used for the dynamic gain normalization, so that I can compare across flies. If the firing rate is saturated for a square wave pattern then the denominator for the dynamic gain is not large enough and the dynamic gain will be higher than expected. The square wave dynamic gain was in fact higher than predicted. It was impossible to find a single contrast in which the square wave did not saturate that sine wave pattern still elicited a response from the H1-cell to motion.

I therefore switched from contrast to mean luminance in order to try and eliminate the firing rate saturation for square wave stimulus with constant velocity. I examined the firing rate in response to a number of different mean luminance values for both sine and square wave patterns in order to find a mean luminance and contrast combination where the response to the square wave pattern did not saturate but the response to the sine wave was robust. I found that the response of the H1-cell did not saturate at 4.5 cd/m<sup>2</sup> mean luminance and 82% contrast. Therefore I performed the same experiments as before on three flies and found that the dynamic gain for a square wave grating was still higher than a sine wave, although the firing rate did not saturate. The dynamic gain for a sine wave and a square wave under these conditions were closer to one another than before, but they still did not match the results from

the Reichardt detector simulations. Therefore there must be some other mechanism that is affecting adaptation in the H1-cell that is not specified in the Reichardt detector model.

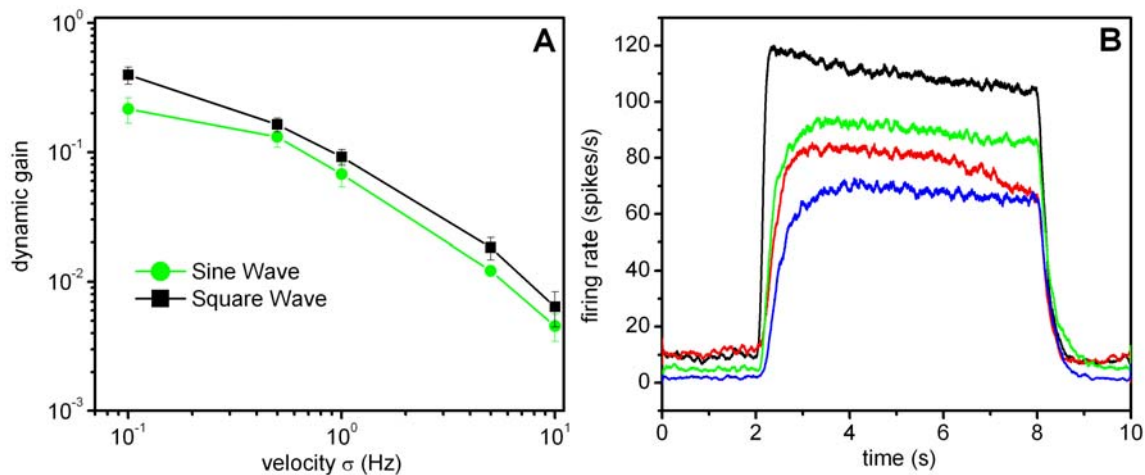


Figure 3.17 Dynamic gain at low mean luminance levels. (A) The dynamic gain as a function of velocity standard deviation for a sine and a square wave pattern. Mean and standard error for three flies are shown at  $\tau_0 = 100$  ms. (B) The PSTH for a square and a sine wave in response to a constant velocity. Black and green lines represent the response to a square or sine wave respectively at  $10.5 \text{ cd/m}^2$  mean luminance and 98% contrast. Red and blue lines represent the response to a square or sine wave respectively at  $4.5 \text{ cd/m}^2$  mean luminance and 82% contrast.

It is possible that there are some features of the adaptation that I found here that are due to the cellular spiking mechanisms or to other mechanisms that are not directly related to the Reichardt motion detector. Although the experiment and simulation results were not consistent with one another, it is still possible that the mechanism for dynamic or automatic adaptation in the H1-cell of the fly visual system.

---

## Time Course of Adaptation

The dynamic gain control of the elementary motion detectors has the potential to occur on very fast time scales, due to the fact that no parameter needs to be modified in the system. In order to look at the time scale of automatic adaptation, I performed an experiment where the velocity standard deviation was switched 0.5 Hz and 5.0 Hz and the time constant was kept constant at 100 ms throughout the experiment. I also switched the velocity time constant from 50 ms to 500 ms, setting the variance to 1.0 Hz to examine the time scale of adaptation to the temporal correlations of the velocity profile. One standard deviation or time constant was shown for 10 seconds before switched to the other standard deviation/time constant and then after another 10 seconds the entire 20 seconds was repeated with a new set of randomly

generated velocity values. Trials were presented to the fly without a pause between them such that the beginning and end of each stimulus could also be used for the analysis.

Figure 3.18 shows the dynamic gain for a switch in both standard deviation and time constant for the experiments and the model. The dynamic gain in Figure 3.18 was calculated over two seconds in order to have an accurate estimate of the stimulus statistics and the stimulus-response curve. Similar results were also found when the gain was calculated using one second of the stimulus and response, only the fluctuations in dynamic gain for each second were greater. For both ( $\sigma$ ) and ( $\tau_0$ ), the experimentally calculated dynamic gain changed immediately after the switch in the stimulus properties. The only time when the dynamic gain took longer to adapt was when the velocity time constant was changed from 50 ms to 500 ms (Figure 3.18C). The same was true for the Reichardt detector model. When simulated with the same velocity profiles, the dynamic gain of the Reichardt detector looked very similar to the dynamic gain found in the experiments.

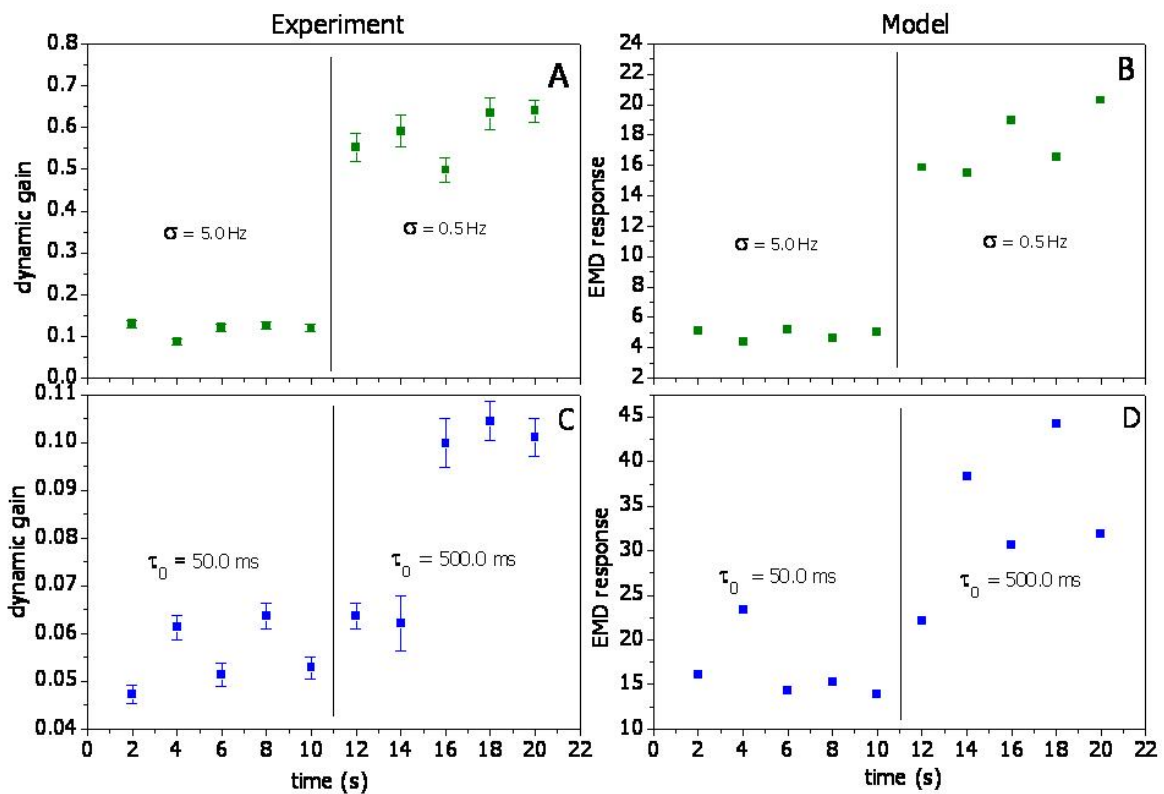


Figure 3.18 Comparison of motion detector simulations and H1-cell gain in response to a switch in either standard deviation or correlation time. (A) Mean and SE for 11 flies of the dynamic gain for a switch from 0.5 Hz  $\sigma$  to a 5.0 Hz  $\sigma$  ( $\tau_0 = 50.0$  ms). (B) The response of a simulated one dimensional motion detector array to the exact same stimuli as used in the experiments. (C) Mean and SE for 10 flies of the dynamic gain for a switch from  $\tau_0 = 50.0$  ms to 500.0 ms ( $\sigma = 1.0$  Hz). (D) Same as in (C) but for the simulation Reichardt detector array.

## Results

One problem with the method for calculating dynamic gain was that the dynamic gain was highly dependent on the part of the stimulus that it was calculated from. This is due to sampling issues; the dynamic gain was calculated over two seconds of time and these two seconds did not always contain all or even a large number of the total possible stimuli, making the statistics over the current time window much different than the overall statistics of the signal. Therefore I simulated the motion detector array with 300 different velocity signals all with the same properties, to get an idea how the motion detector performs in general to a change in either the velocity standard deviation or time course.

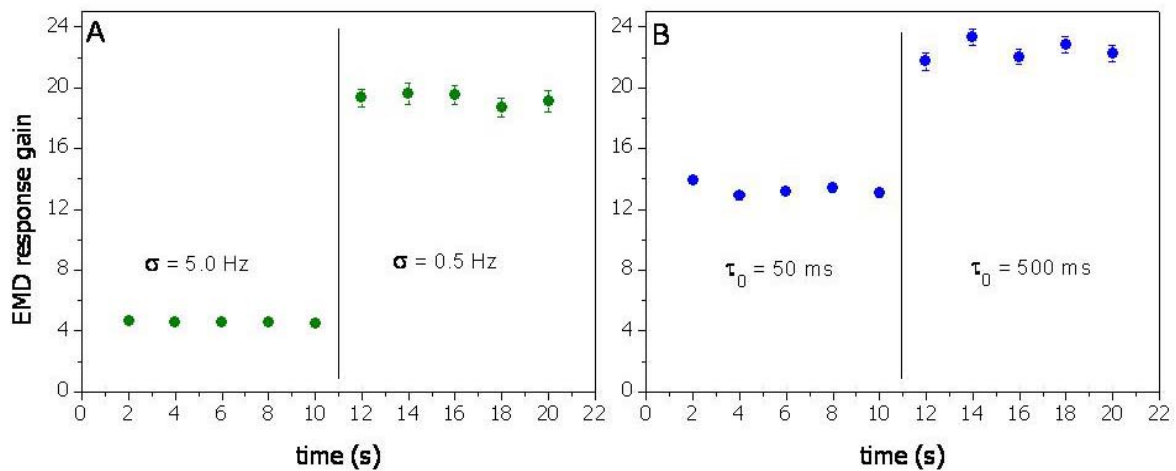


Figure 3.19 Motion detector dynamic gain during a switching experiment. 300 different random stimuli of 20 seconds long were used as inputs to the full Reichardt detector model. (A) The  $\tau_0$  was 100 ms and the  $\sigma$  switch was from 5.0 Hz to 0.5 Hz. (B) The  $\sigma$  was 1.0 Hz and the  $\tau_0$  switched from 50 ms to 500 ms. Mean and standard error from the 300 repetitions are shown.

These simulations show that the variations within a single standard deviation are probably due to the sampling problems and that the gain is relatively constant over time for a single standard deviation and time constant. The switch in gain from one standard deviation to the next appears to occur sometime within the first 1-2 seconds after the switch, and the overall deviation in time and between trials is very small. It is also interesting to note that the change in gain for an order of magnitude change in velocity time constant is much smaller than the gain change for an order of magnitude change in velocity standard deviation.

Pooling stimuli and responses over two seconds after a switch in the properties of the stimulus is not very informative about the time course of adaptation after a switch. Therefore I used 500 permutations of the same stimuli used in the experiments to calculate the dynamic gain in the Reichardt detector on faster time scales. Using a 100 ms window I examined the time course of the dynamic gain after a switch in both directions. Figure 3.20 shows the

## Results

dynamic gain over the full 10 seconds after a switch in either velocity standard deviation or velocity low-pass filter time constant with 100 ms time resolution. In all cases the dynamic gain of the Reichardt detector went to zero at the over the switch. For a switch in the velocity standard deviation, when the standard deviation was switched from 0.5 Hz to 5.0 Hz the gain rose quickly to a peak in approximately 400 ms and then settled back down to a steady value within one second (Figure 3.20A). The dynamic gain remained constant over the remaining nine seconds. When the standard deviation was switched from 5.0 Hz to 0.5 Hz the dynamic gain rose more slowly, and did not reach a peak. The dynamic gain slowly leveled off but there were large fluctuations in the dynamic gain throughout the whole ten seconds.

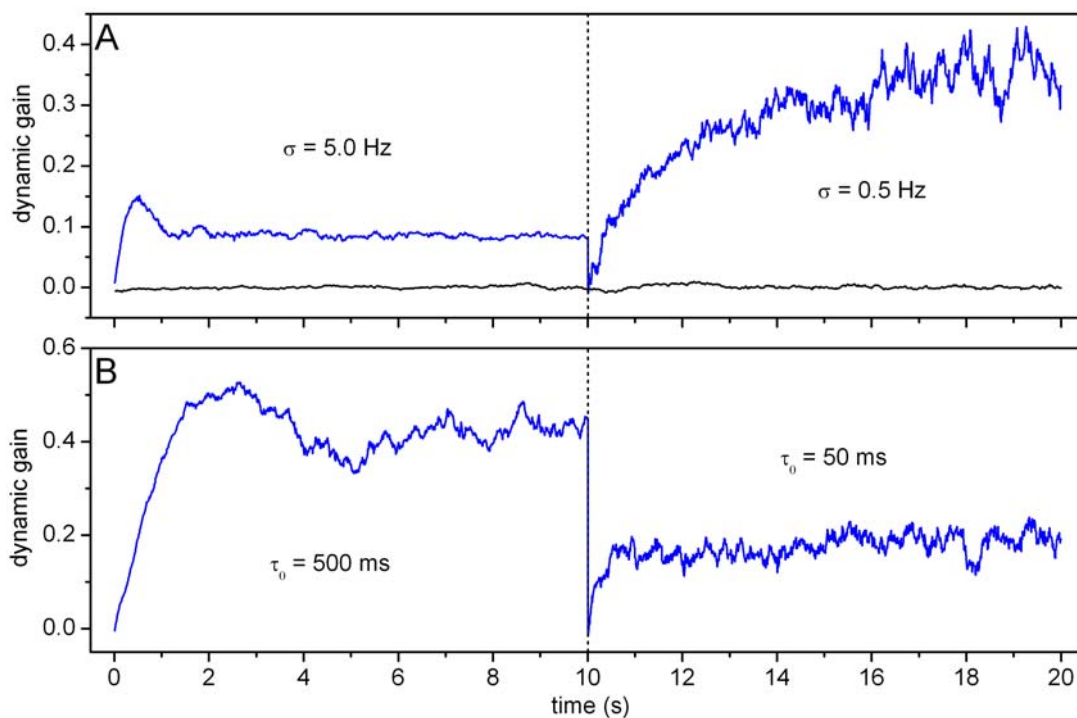


Figure 3.20 Dynamic gain of the Reichardt detector in response to a switch in the velocity standard deviation or time constant. 500 different random stimuli were used as inputs and the gain was calculated with a sliding window of 100 ms. (A) The dynamic gain in response to a switch in velocity standard deviation (blue curve). As a control the gain was calculated for the stimulus-response curve when the stimulus was switched (black curve). (B) The dynamic gain in response to a switch in velocity time constant.

For a switch in the velocity low-pass filter time constant, when the time constant switched from 50 ms to 500 ms, the dynamic gain of the Reichardt detector rose from 0 relatively slowly to a peak dynamic gain at around two seconds. Then the dynamic gain decreased slightly and settled on a constant value within four seconds. When the velocity time constant was switched from 500 ms to 50 ms, the gain rose quickly without overshooting and settled on a value within 600 ms (Figure 3.20B). In addition, I performed a control to see whether the dynamic gain values and fluctuations over the switch were really a function of the

parameters that I tested. I took the response from one standard deviation and the stimulus from the other standard deviation and calculated the dynamic gain again. The dynamic gain of the control remained approximately zero over the entire course of the control, using 100 ms time bins, suggesting that the temporal fluctuations of the gain are in fact an effect of the standard deviation and the temporal correlations in the velocity (Figure 3.20A).

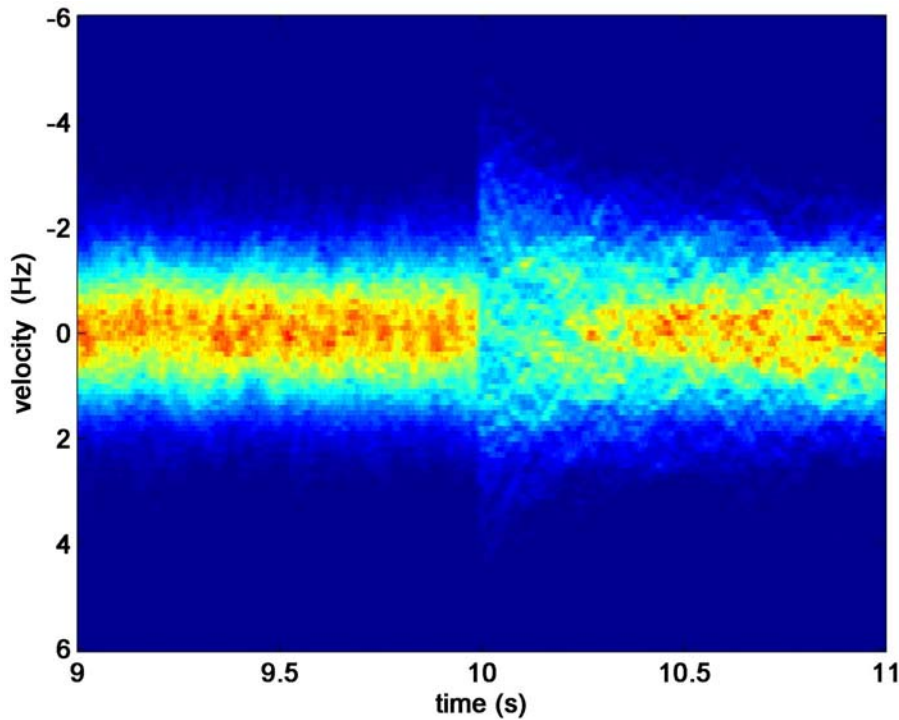


Figure 3.21 The statistics of the stimulus over a change in velocity time constant. The probability density function for the stimuli used in Figure 3.20B across the switch in velocity time constant from 500 ms to 50 ms at 10 seconds. A sliding window of 20 ms was used to pool the stimulus values.

In addition to the change in dynamic gain over the switch in velocity standard deviation or velocity temporal correlations, I examined the probability distribution of the velocity profile across the switch. Figure 3.21 and Figure 3.22 show the probability density function one second before and one second after the switch in velocity low-pass filter time constant and velocity standard deviations respectively. The probability density function does not change significantly during a switch in the velocity temporal correlations. The probability density function broadens slightly at the switch (Figure 3.21), but no large change is expected because the variance of the velocity profile remains the same. During a switch in the velocity standard deviation on the other hand, there is a strong change in the probability density function over the switch. The probability density function becomes much more peaked because the entire range of the distribution is still broad from the 5.0 Hz standard deviation velocity profile but there are significantly more small values from the 0.5 Hz standard

deviation velocity profile (Figure 3.22). The distribution over the switch is therefore highly non-Gaussian. This peak was present for a switch in either direction (data not shown).

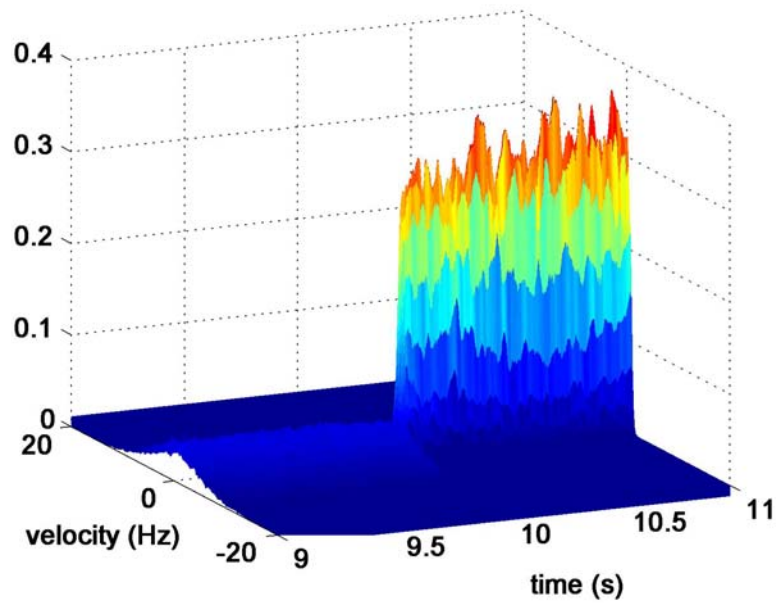


Figure 3.22 The statistics of the stimulus over a change in velocity standard deviation. The probability density function for the stimuli used in Figure 3.20A across the switch in velocity standard deviation from 5.0 Hz to 0.5 Hz at 10 seconds. A sliding window of 20 ms was used to pool the stimulus values.

## 4 Discussion

---

In this work, I examined the adaptive properties of the H1-cell and the Reichardt detector in response to the statistics and temporal correlations of a dynamic stimulus, namely a Gaussian colored noise velocity profile. I found that the H1-cell and the Reichardt detector model adapted their stimulus-response function to both the standard deviation and the temporal correlations by changing the slope or the gain of the function. I also showed that the cross-correlation between the stimulus and the response adapted to the statistics and temporal correlations of the stimulus, both in the model and in the experiments. The degree of the stimulus-response curve adaptation was dependent on the visual light intensity pattern and not just to velocity. Finally I demonstrated that this dynamic gain adaptation in the Reichardt detector model switches over time in a similar way as in the H1-cell experiments, and I characterized the time course of adaptation in the model. These experiments demonstrate, in my opinion that the Reichardt detector model accounts for dynamic gain adaptation in the H1-cell of the blowfly.

In this section, I will discuss the significance of my findings on different areas in Neurobiology. The dynamic gain adaptation found in this work is an inherent property of the Reichardt detector. I will examine the theoretical basis for this adaptation in the Reichardt detector model. I will look at previously studied examples of automatic adaptation and discuss general principles that lead to dynamic adaptation without parameter change. The results from this work will also be examined from the standpoint of efficiency in neural coding. I will address the question whether the different forms of dynamic adaptation that I found result in an efficient code. The results will be compared to previous adaptation found in the H1-cell to see if they are in agreement. The concept of ambiguity in an adaptive neural code will also be addressed here.

The results will then be used to argue that the Reichardt detector continues to be the most accurate model for motion detector in the fly and perhaps in many other systems. I will discuss analytical work done with Haim Sompolinsky to find an analytical solution to adaptation in the Reichardt detector. Then adaptation in the gradient detector scheme will also be shortly examined. I will then address the discrepancies found between the Reichardt

detector and the H1-cell and discuss the potential causes of the discrepancy. The results on the visual pattern will also be examined in the context of natural scenes. I will then talk about the physiology of the fly visual system and how it relates to the results found. I will discuss the putative location of the motion detector in the fly visual system and the properties of the H1-cell that might also influence the results found in this work. Lastly I will explain the functionality of the H1-cell in the larger context of LPTCs. In particular, I will look at how dynamic gain adaptation may affect the role of the H1-cell in the larger network.

---

## Generality

In contrast to the commonly accepted view that adaptation requires a change in parameters, the Reichardt detector adapted its response properties to the standard deviation and time constant of the velocity profile without any change in the system. This finding raises the question whether the Reichardt detector model is unique in its ability to adapt to the stimulus without a parameter change, or whether this is a general principle that may be found in other sensory systems. If this is a general principle it also raises the question what is the minimal set of operations that are required for such a system to adapt automatically, and what specific features of the Reichardt detector model lead to this form of adaptation.

## Examples of automatic adaptation

Other scientists have discovered gain adaptation and proposed mechanisms for automatic gain adaptation in different sensory systems. Dynamic clamp experiments in somatosensory layer 5 pyramidal cells of the rat were given background variable synaptic currents as well as a driving current (Chance et al., 2002). These cells exhibit change the stimulus-response curve for the driving current in response to balanced background current injection. Increasing the variance of the variable background current increases the noise in the cell which changes the slope of the input-output function. As the background variance increases, the stimulus-response curve for the driving current broadens. In addition an increase in the variance of the background synaptic current also increases the conductances which shifts the input-output-curve for driving current to the right (Chance et al., 2002).

Another biophysical mechanism for dynamic gain control was proposed for contrast adaptation in salamander retinal ganglion cells (Kim and Rieke, 2003). Variable current injections were performed where the variance of the current injected was changed and the

stimulus-response function adapted. The authors suggest that a slow  $\text{Na}^+$  inactivation causes the amount of  $\text{Na}^+$  to depend on the past history of action potentials and subthreshold voltages. Increasing the variance of Gaussian input current fluctuations therefore reduces the available amount of  $\text{Na}^+$  which in turn increases the threshold for spike generation (Kim and Rieke, 2003). The results of these experiments were then examined using a Hodgkin-Huxley model neuron with ionic currents known to be present in retinal ganglion cells. This study and the previous one both propose physiological mechanisms that lead to adaptation without any change in the parameters of the system, or cells in this case. Therefore inherent adaptation of the stimulus-response function in response to variable inputs is not just a mathematical principle; it also occurs as a direct result of physiological phenomena.

Model neurons themselves also appear to have automatic adaptation mechanisms for stimulus-response function adaptation in response to variable inputs. A leaky integrate-and-fire model (LIF) was found to have dynamic gain control in response to the mean and variance of Gaussian white noise inputs (Yu and Lee, 2003). A benefit of the LIF model is that it is possible to look at the analytical sources for the model's behavior. The authors analytically examined the model with respect to adaptation and found a mathematical explanation for adaptation in the neuron. A combination of the linear and non-linear components of the LIF leads to a saddle node bifurcation point at a specific mean input value. This mean value determines when the model cell begins to spike. As the variance of the input signal is increased, the probability that the voltage crosses threshold leading to a spike also increases and therefore the bifurcation point shifts towards lower mean input values. The input-output function adapts as a result of the automatic shift in the bifurcation point.

### **Adaptation mechanisms in the Reichardt detector**

Finding an analytical solution to the response of the Reichardt detector to a sinusoidal grating with Gaussian velocity inputs is not as simple as in the LIF model, although a generalized form has been found (Borst et al., 2005). In addition, the formulas are complicated enough that it is difficult to have an intuitive feeling for what properties of the Reichardt detector lead to dynamic adaptation. A simple model neuron was constructed in order to gain an intuition for the possible mechanisms of adaptation in the Reichardt detector model (Borst et al., 2005). The stimulus ensemble consisted of several correlated Gaussian variables  $s_i$ . In reality the correlations may come from the statistics of the stimulus itself or from preprocessing that

occurs in the photoreceptors. The signals are then passed through a non-linear squashing transfer function  $f(s_i)$  and then linearly summed to produce the output (Figure 4.1).

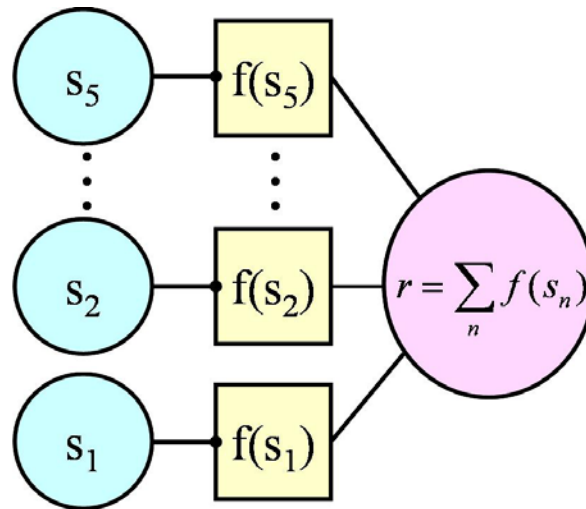


Figure 4.1 A general model for automatic gain control. Gaussian distributed correlated inputs  $s_i$  with the same variance and correlations are fed through a non-linear transfer function and then are linearly summed at the end. This leads to automatic gain control as a function of stimulus variance and standard deviation similar to what was found in the Reichardt detector. Adapted from (Borst et al., 2005).

The effect of the standard deviation or temporal correlations can be made clear by looking at the response to a single variable, for instance  $s_2$ . The response of the model neuron to the value of  $s_2$  is not only dependent on the direct response to  $s_2$ ,  $f(s_2)$  but also on contributions from the other stimuli,  $f(s_i)$ . The relative weight of the contributions from other stimuli depends on the variance of the stimuli and on the correlations between the stimuli. Adaptation arises therefore through the change in the significance of the additional stimuli to the overall response of the neuron to a single stimulus.

This phenomenon is represented graphically in Figure 4.2. The probability distribution of a given stimulus  $s_2$  is a function of the stimuli around it. Figure 4.2A shows the original probability distribution for  $s_2$  (black dotted curve) and the corrected probability distribution when  $s_1$  is fixed to a certain value and there are correlations between the inputs. The probability curve is narrowed by a factor of  $\sqrt{1-c^2}$  where  $c$  is the correlation coefficient between  $s_1$  and  $s_2$ , and shifted in the direction of  $s_1$ . In other words, the probability of having  $s_2$  is in a specific location with a narrower range due to the fact that  $s_1$  is specified and the two values are correlated. In this case the correlation coefficient is 0.5. The resulting stimulus-response curves are shown in Figure 4.2B. The authors suggest that in the case of motion detection the different inputs  $s_i$  can be seen as the velocities at different times with

correlations that depend on the low-pass filter time constant used (Borst et al., 2005). The non-linearity in the experiments is then the visual pattern itself, in this case a sinusoidal grating.

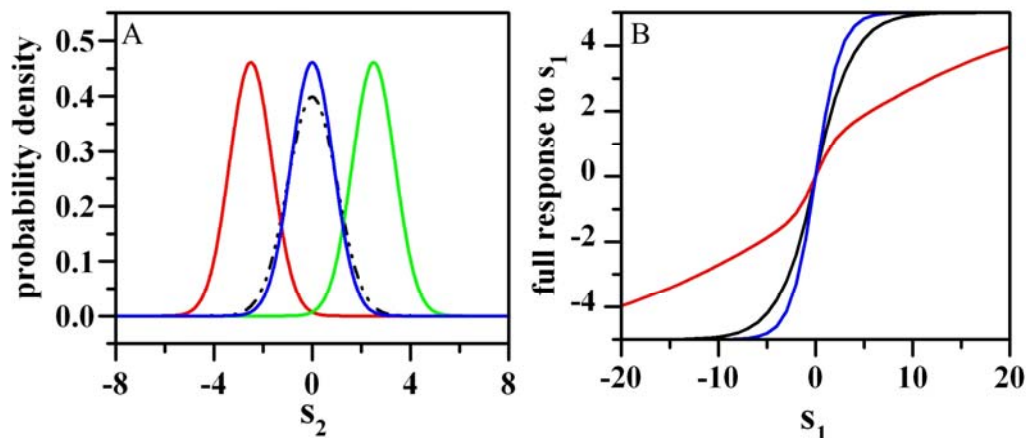


Figure 4.2 The effect of one stimulus component on another (from model in Figure 4.1). (A) The probability of stimulus  $s_2$  occurring when stimulus  $s_1$  is known and the stimulus components are correlated. The black dotted curve is the original probability density for  $s_2$ . The red, blue and green curves are the probability densities for  $s_2$  when  $s_1$  is 0, -5.0 or 5.0 respectively. (B) The resulting stimulus-response function for varying standard deviations and correlation coefficients:  $\sigma = 1$ ,  $c = 0.5$ , black,  $\sigma = 10$ ,  $c = 0.5$ , red and  $\sigma = 1$ ,  $c = 0.8$ , blue. From (Borst et al., 2005).

Another way to understand dynamic adaptation of the stimulus-response function is to think of the stimulus-response function as a dimensionality reduction. The Reichardt detector does not just respond to the velocity at one specific time, but it responds to the entire stimulus ensemble from that specific time to a point back in time that is determined by the filtering properties of the Reichardt detector. Additional correlations in the stimulus will alter the relative contribution of the previous stimulus velocities to the response of the Reichardt detector at that particular time. The stimulus-response curve reduces the response of the motion detector or H1-cell from a multi-dimensional representation of the response of the system to a particular set of velocities, down to the response of the system to the velocity at a single point.

The general model proposed in (Borst et al., 2005) only looks at the filtering and non-linear properties of the stimulus itself. There exist, however, additional filtering properties and a non-linear multiplication step in the Reichardt detector model that could greatly influence the outcome of the system. It would therefore be interesting to see what happens to automatic gain control when the system is more complex. One way to test this would be to place two of the simplified models in series to see if additional properties arise that are not present in the simplified model. Similarly one could examine dynamic adaptation in the Reichardt detector

model when the stimulus correlations are removed. The simplified model presented suggests that the correlations in the stimulus are responsible for dynamic adaptation. The filtering properties of the Reichardt detector introduce correlations in the signal that could also lead to dynamic adaptation. Therefore, by removing the correlations in the stimulus it would be possible to separate the stimulus mechanisms from the Reichardt detector mechanisms for dynamic adaptation.

In principle the simplified model of dynamic gain shows us: 1) that the visual pattern itself, if non-linear, can have a large effect on the stimulus-response function and 2) that the principle of automatic gain control, that is adaptation without any change in internal parameters, could very well be found in many other systems. Indeed these principles have already been described in a number of other sensory systems. It appears as if there are multiple mechanisms available for a system to achieve dynamic gain control and it is very possible that more than one mechanism can be operating simultaneously. Two unifying properties are present in all of the examples of dynamic gain control above:

- The response of the system at one time point depends on the past history of inputs to the system (in the LIF model the voltage was dependent on the previous inputs with a time constant based upon the capacitative properties of the neuron) and
- The system has at least one non-linear computation that gives the system the possibility for chaotic behavior.

### **Adaptation of individual neurons and the Reichardt detector**

This presents the question whether the Reichardt detector is really the appropriate level of abstraction for the experimental results found in this work. I believe that previous evidence in favor of the Reichardt detector in the fly visual system combined with the similarity between the dynamic gain found in the simulations and in the experiments all speak in favor of the Reichardt detector model. Understanding the general principles of dynamic gain control does however provide clues as to where discrepancies between the model and the experiments could arise.

If the generic mechanisms for dynamic adaptation are correct, then every neuron has the capability to automatically change its transfer function in response to the statistical properties and time course of dynamical inputs. Then the question arises whether all cells exhibit

dynamic adaptation. If spike generation causes dynamic adaptation then the H1-cell has an additional mechanism for adaptation that is not explained by the Reichardt detector alone. This additional adaptation could explain some of the discrepancies between the H1-cell adaptation and the adaptation of the Reichardt detector model. It will be important to look at adaptation to the statistics of a velocity stimulus when a Reichardt detector and a spiking cell are placed in parallel. In addition, if all spiking cells exhibit adaptation then it is unclear whether any absolute information can be transmitted in the nervous system. The question of ambiguity will be addressed in the following section.

---

## Efficiency

Adaptation in the nervous system allows for a system with a smaller dynamic range than the sensory input to adjust its transfer function to the current statistics of the sensory input. This not only allows for the system to cover the entire range of the sensory input but also allows the system to code for the stimulus in an optimal way, maximizing the information about the stimulus that is carried in the response. It was proposed that a neuron maximizes its information capacity about a specific stimulus when it adapts its stimulus-response function to the statistics of the stimulus distribution (Laughlin, 1981a). My work demonstrated that the H1-cell and the Reichardt detector changed their stimulus-response curve to the statistics of the stimulus; in particular they broadened or narrowed the response range with respect to the standard deviation of the stimulus. Therefore, the adaptation found in this work may provide a method to optimize the information between the stimulus and the response in the fly visual system.

It was previously found in the H1-cell that increasing the stimulus entropy and stimulus strength by increasing the stimulus variance does not change the information rate between the stimulus and the response (Borst, 2003). The dynamic gain adaptation found in this work is a likely explanation for the constant information rate over different stimulus entropy values. The question remains whether the mutual information is still constant over the larger range of velocity variances and over different velocity time constants that were tested in this work. This question was not specifically addressed in this work but there are a few hints about the possible information rate of the H1-cell in the nature of the stimulus-response curves for different stimuli.

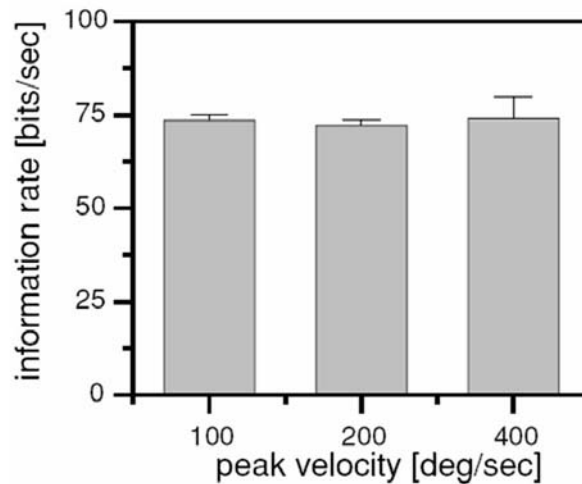


Figure 4.3 The information rate of the H1-cell in response to Gaussian white noise in the velocity signal. The three different bars correspond to velocity standard deviations of 3 Hz, 6 Hz and 12 Hz for peak velocities of 100 deg/sec, 200 deg/sec and 400 deg/sec respectively. From (Borst, 2003).

If the transfer function or the stimulus-response curve of a neuron is a monotonically increasing function that corresponds to the cumulative probability distribution of the input signal, then the information capacity of a neuron is maximized for that particular stimulus (Laughlin, 1981). In this case, the responses to frequently occurring stimuli are more spread out leading to a higher resolution for frequent stimuli than for infrequent stimuli. The stimulus-response function in this work was not always monotonically increasing. For standard deviations of 1.0 Hz and higher, the response of the H1 dropped off towards the higher velocities. This would suggest that the information capacity of the H1-cell is not constant over all of the velocity standard deviations tested in this work. For lower standard deviations, the stimulus-response curve was monotonically increasing, and therefore the information capacity for standard deviations less than one may be maximized. The information rate calculated in (Borst, 2003) was from velocity standard deviations that are higher than 1.0 Hz. Therefore it is possible that for smaller standard deviations, the information rate increases. Interestingly, the drop-off in response amplitude for higher stimulus standard deviations is also predicted by the Reichardt detector. Therefore the drop-off for higher velocities may have biological efficiency advantages that we do not understand yet.

Other studies have already demonstrated that the stimulus-response curve for a Gaussian white noise stimulus does in fact maximize the information about the stimulus (Brenner et al., 2000). In that study, the measured stimulus-response function was stretched or contracted by a constant ( $\lambda$ ) and the information per spike calculated for the new stimulus-response

relationship. Brenner et al. (2000) found that the experimentally obtained stimulus-response curve ( $\lambda = 1$ ) had the highest information in bits about the stimulus for all of the velocity standard deviations tested (Figure 4.4).

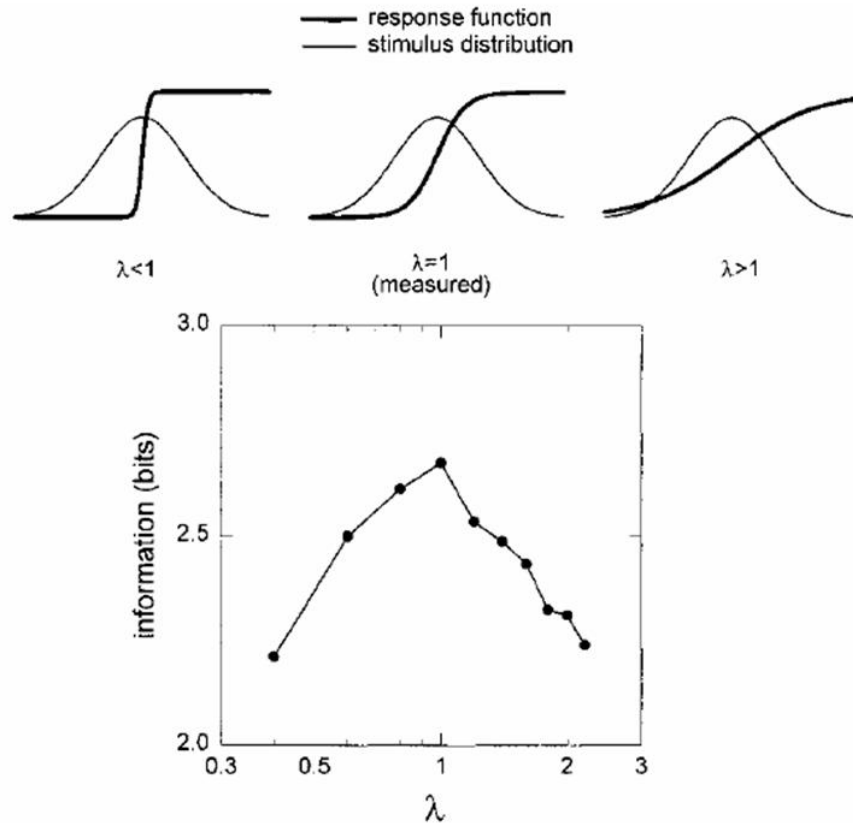


Figure 4.4 Information per spike as a function of lambda. The stimulus-response function was stretched or contracted by a factor lambda, and the resulting mutual information was calculated. The measured stimulus-response function resulted in the highest information rate. From (Brenner et al., 2000)

An additional question is how the information rate changes during a switch from one standard deviation to another. When switching from one adapted state to another it is easy to imagine that the information about the stimulus will decrease during the switch. However, it was found that when the stimulus was switched between two different standard deviations, the information in bits per spike remained almost constant (Figure 4.5). The switch from a higher standard deviation to a lower standard deviation (open circles in Figure 4.5) resulted in a slight decrease in information just after the switch. The authors claim that this is due to noise in the photoreceptors that make it more difficult to detect the change from a high to a low standard deviation within a time window of about 40 ms (Fairhall et al., 2001). This phenomenon is also understandable in the context of automatic adaptation of the motion detector. Adaptation to the velocity standard deviation occurs in the Reichardt detector without any change in the parameters of the model, and therefore has the ability to occur

immediately, maintaining the information rate during a switch between two standard deviations.

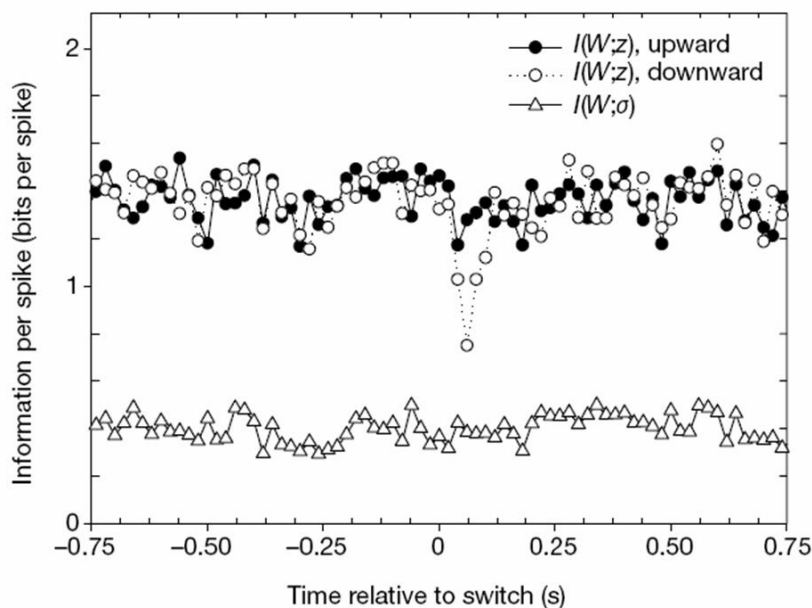


Figure 4.5 Information per spike (information rate divided by firing rate) as a function of the time relative to a switch in stimulus standard deviation. Information per spike was calculated around a switch in the standard deviation. The information in each word  $W$  about the probe  $z$  used is plotted for an upward switch in standard deviation and a downward switch in deviation. The information per spike in each word about the standard deviation was also plotted. Adapted from (Fairhall et al., 2001)

Examining the influence of the shape of the stimulus-response curve on the possible information rate is another topic that should be addressed both theoretically and experimentally. The amount of data collected in this work was too small in order to calculate the information rate or information per spike found in the experiments; however it will be an important step for the future.

### Efficient representations of correlations

There is little research on what constitutes an efficient representation of a stimulus with respect to the temporal correlations in the stimulus; most of the research on dynamic adaptation of the stimulus-response curve relates to the variance of the stimulus. In this work however, I also examined the effect of the low-pass filter time constant of the stimulus on adaptation of the stimulus-response curve. It is unclear whether adaptation to the temporal correlations of the stimulus results in an efficient code. The experiments and the results of the Reichardt detector show that the stimulus-response curve becomes steeper as the temporal correlations within the stimulus increase. This is perhaps related to the fact that the system has a probability of correctly knowing what the next velocity will be, or at least the range of

possible velocities, when the temporal correlations are high, and therefore the stimulus-response curve becomes narrower, in order to have a better resolution for the velocities that are most likely to occur. This would be consistent with the theory that neurons maximize their information capacity (Laughlin, 1981a).

Changes in the cross-correlation between the stimulus and the response were also found in this work. As the stimulus standard deviation increased, the time to the peak cross-correlation shortened. The maximum cross-correlation is the time at which the correlations between the stimulus and the response are highest. The time at which the cross-correlation is at its maximum is also a measure of the time it takes for the system to respond to the stimulus. From this perspective, larger stimulus standard deviations lead to a faster response from the H1-cell and the Reichardt detector. It is potentially advantageous for the fly to be able to respond more quickly at higher speeds, which could potentially explain why this phenomenon exists in the fly, assuming the system is optimally designed. The Reichardt detector on the other hand is only a mathematical model, suggesting that there are also theoretical reasons why the system responds more quickly to a higher standard deviation that have not been discovered yet.

### **Ambiguity**

An adaptive neural code allows the nervous system to maximize the information about the outside world, but it also leads to ambiguity in the interpretation of a signal. The signals themselves become only relative and not absolute and more information is needed about the input in order to reconstruct the absolute nature of the signal. Fairhall et al. (2001) suggested that the contextual information could be contained in other aspects of the code. The interspike interval, or the precise spike timing could contain the contextual information, as opposed to the firing rate, which is what they used to calculate the information rate. From the perspective of the fly however, it is not clear that information about absolute velocity is necessary. I would argue in the case of the H1-cell and in motion signals, that the relative speed of objects in the visual field is really the only important information for the system. If velocity information is necessary for the fly, then there are also additional vision pathways that are separate from the primary motion pathways that could encode for absolute velocity. The L3 neurons of the lamina for instance are physiologically separate from the rest of the cells in the lamina, except for the photoreceptor cells, because they have no connections to interneurons

such as the amacrine cells or centrifugal cells. They could represent a visual pathway that is independent of the Reichardt detector system.

If the simple model describing the mechanism behind dynamic adaptation in the Reichardt detector is correct (Borst et al., 2005), as well as the results from the leaky integrate-and-fire neuron (Yu and Lee, 2003), then every neuron in the nervous system has the potential ability to adapt to the statistics of dynamically varying inputs. This poses the question whether information can at all be encoded in the responses of neurons. Perhaps adaptation is part of the normal state of the system, and the absolute stimulus values are not encoded by neurons. Similarly, there is evidence that neurons have multiple states in which some could be adaptive and some non-adaptive. Numerous studies, however, suggest that the stimulus-response curve and the firing rate are not the only sources of information in the neural code and that spike timing and groups of spikes can encode information in a manner that is not understood yet (Victor and Purpura, 1996; Van Rullen and Thorpe, 2001).

---

## Dynamic adaptation in motion detection

This work suggests that the full version of the Reichardt detector with low-pass and high-pass filtering characteristics is the best model for explaining dynamic adaptation in the H1-cell of the fly. The HPLP Reichardt detector shows dynamic adaptation to the variance and temporal correlations of a Gaussian colored noise velocity profile that is very similar to results from the H1-cell. It also adapts its response time to the variance and temporal correlations in much the same way as the H1-cell. However this does not explain how other models for motion detection compare to the Reichardt detector. Therefore, in this section I provide evidence from other versions of the Reichardt detector and from the gradient detector that the HPLP Reichardt detector best explains dynamic adaptation in fly motion vision.

The relationship between dynamic gain and the stimulus properties was analytically examined using the low-pass only version of the Reichardt detector (H. Sompolinsky unpublished). The LP Reichardt detector shows much less adaptation both to the velocity standard deviation and to the velocity time constant, however it does provide a more analytically tractable approximation to dynamic gain adaptation in the Reichardt detector. The approximation for the adaptation of the Reichardt detector to the velocity standard deviation and time constant is as follows:

$$G_{dyn}(\sigma) \approx \frac{(\tau_0 / \tau_L)^2}{(\tau_0 / \tau_L)^2 + (\tau_0 / \tau_L) + 4\pi(\sigma\pi)^{4/3}} \quad (6)$$

$G_{dyn}$  is the dynamic gain, or the slope of the stimulus-response curve at zero, normalized by the slope of the response of the Reichardt detector to velocity steps close to zero.  $\tau_L$ ,  $\tau_0$  and  $\sigma$  stand for the detector low-pass filter time constant the velocity low-pass filter time constant and the velocity standard deviation respectively. The formula is not ideal to describe the full gain of the Reichardt detector, but it does expose interactions between the stimulus parameters tested and the dynamic gain that were also found in the experiments. The dynamic gain is inversely related to the velocity standard deviation, which is seen in the experiments and the simulations. The effect of the stimulus time constant actually depends on the ratio between the velocity low-pass time constant and the time constant of the detector. If this ratio is small, i.e. if the velocity changes rapidly within the time-window set by the low-pass filter, the gain is strongly reduced. If the ratio is large, implying that the velocity changes slowly within the low-pass time-window, the gain approaches steady-state gain and therefore no adaptation occurs.

The low-pass version of the Reichardt detector model only explained a small percentage of the dynamic gain found in the experiments; the dynamic gain was much less pronounced for higher velocity standard deviations. There are other realizations of the Reichardt detector model for instance where only 50 % of the second input channel is high-pass filtered or where there is an extra high-pass filter or band-pass filter in each of the input arms (Borst et al., 2003). However neither of these models worked nearly as the HPLP model when tested for the adaptive time constant of the impulse response. I did not test these models explicitly in this work nor did I look at their response to dynamic adaptation because they already did not explain adaptation of the decay time for an impulse response (Borst et al., 2003).

Since all of the experimental results found in this study were supported by simulations done in the Reichardt detector model, it appears that the Reichardt detector is the mechanism behind dynamic adaptation in the H1-cell of the fly, and that the dynamic adaptation occurs without any change in the parameters of the model. However previous work has also shown that the high-pass filter of the Reichardt detector adapts to a constant velocity stimulus, thereby changing the decay time of the H1-cell response to a motion pulse (Borst et al., 2003). This presents the question what the purpose of the high pass filter time constant

adaptation is for when adaptation can occur without any parameter change in the system. Adaptation of the high pass filter time constant occurred when the stimulus was transient, not in a dynamic situation such as Gaussian white noise.

It was proposed that the Reichardt detector is implemented in the fly visual system under low signal to noise conditions but that the gradient detector is much more suitable for motion detection in high signal to noise situations (Potters and Bialek, 1994). Recent work has shown however, that the contrast frequency dependence of the Reichardt detector was found in the LPTCs also in high SNR conditions (Haag et al., 2004). The gradient detector was recently tested for dynamic gain to the statistics of a Gaussian colored noise stimulus, the same type of stimulus used in this work. It was shown that the gradient detector shows no dynamic adaptation to the velocity standard deviation (Figure 4.6) (Borst, 2006).

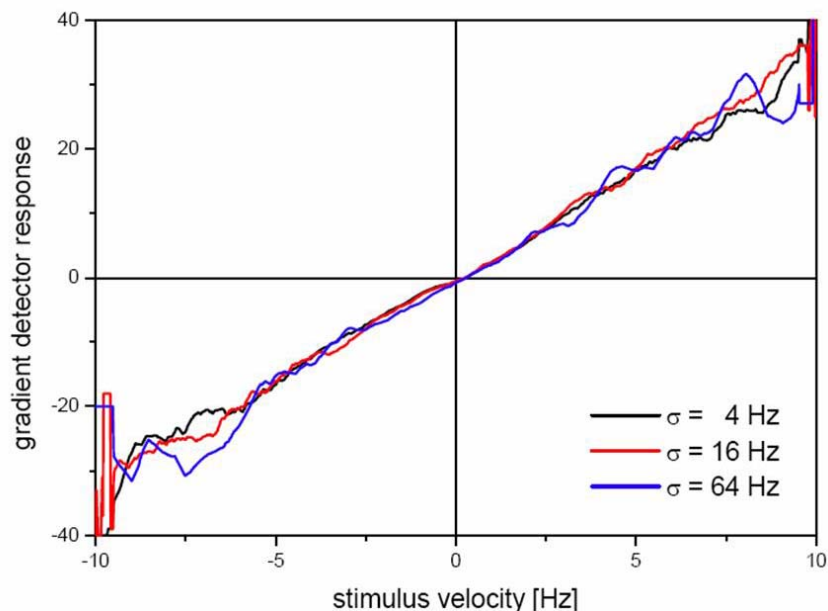


Figure 4.6 The stimulus-response function from a gradient detector with Gaussian white noise inputs. The gradient detector shows no adaptation in its stimulus-response function to the standard deviation of the velocity. Adapted from (Borst, 2006).

Therefore the gradient detector is most likely a poor model to explain motion detection in fly vision, and perhaps to explain motion vision in other organisms as well. Since the gradient detector does not adapt to the statistics of the stimulus it is certainly not an optimal motion detector for dynamic stimuli. Therefore, the only model that appears to behave in the same way as the H1-cell data with respect to dynamic adaptation is the full HPLP version of the Reichardt detector model (Figure 2.8).

---

## Visual patterns and natural scenes

The effect of the stimulus pattern on the stimulus-response adaptation provided inconsistent results between the model and the experiments. It looked as if this was a result of contrast saturation in the fly, but it turned out that although this decreased the difference between the experiments and the simulations, it did not entirely compensate for the discrepancy. When mean luminance was changed and the H1-cell in response to a square wave pattern did not saturate the square wave dynamic gain was still slightly larger than the sine wave dynamic gain. The opposite response was found in the Reichardt detector model. This problem illuminates the fact that the light properties of the visual stimulus, particularly the contrast are also very important in dynamic adaptation in the fly.

It is known that contrast plays a large role in the output of both the Reichardt detector and the LPTCs. For instance, adaptation of the H1-cell response to a motion pulse is highly dependent on contrast (Reisenman et al., 2003). The analytical expression for the response of an array of Reichardt detectors to constant motion and to motion onset depends on the square of the pattern contrast (Egelhaaf and Borst, 1989). Results from electrophysiological experiments in the fly and in other organisms have different results. Peak and steady-state responses of the HS-cell saturate with increasing pattern contrast (Egelhaaf and Borst, 1989). HS-cells also elicit contrast adaptation, the cells are less responsive to a low contrasts after a high contrast adaptive stimulus is given (Harris et al., 2000). Therefore it is natural to expect that contrast will play a role in the dynamic adaptation found in this study.

It is difficult to compare experiments with each other when the structure of the visual pattern was different. Similar experiments have been performed that test for adaptation to the statistics of a stimulus in the H1-cell of the fly but with an apparent motion stimulus and not with actual motion as was used in this work (Brenner et al., 2000; Fairhall et al., 2001). In the apparent motion stimulus the light intensity values  $I(x,t)$  for the light or dark colored bars were represented by:

$$I(x,t) = \bar{I} \cdot (1 + s(t)\sin(kt) + c(t)\cos(kt)) \quad (7)$$

Where  $\bar{I}$  is the mean light intensity,  $k/2\pi$  the spatial wavelength and  $s$  and  $c$  Gaussian white noise probability distributions (Bialek and de Ruyter van Steveninck, 2005). It is unclear how to compare this stimulus and other potential stimuli to for instance the stimulus

that was used in this work (the formula can be found in (Borst et al., 2005)). Therefore it is not too surprising that the Reichardt detector adaptation and the H1-cell adaptation to different visual stimuli were not the same. More theory is needed in order to understand the differences between visual stimuli.

Along this same line of thought, a theory for visual stimuli is of growing importance in order to understand the response of visual system cells to natural stimuli. Natural signals have very different visual and statistical properties from the sinusoidal gratings that have been presented here. They have high temporal and spatial correlations and complex spatial structure (Dan et al., 1996; Mante et al., 2005). It has been suggested that neurons in the visual system are specialized to process natural images. In the LGN for instance it was shown that cells decorrelate natural images in order to remove redundancy (Dan et al., 1996). Neural filters have also been shown to be adapted for natural scenes (Sharpee et al., 2006). Naturalistic velocity stimuli have also been used in order to examine the fly visual system (van Hateren et al., 2005). Therefore it will be important to see how both the H1-cell and the Reichardt detector model respond to more naturalistic stimuli and whether adaptation of the stimulus-response curve is still similar between the two systems

One outcome of (Borst et al., 2005) is that the non-linear nature of the sinusoidal grating actually plays a role in automatic adaptation according to the general model and to the analytical expression for the Reichardt detector. It would be interesting to know if the effect of visual pattern on motion detection has a continuous function space, i.e. whether commonalities between stimulus patterns can be found that reliably lead to the same motion detector response. Other large-field moving visual patterns are, however, generally not as mathematically tractable as the sine wave. One reason why a square wave was used in these experiments was that a square wave is the sum of the original sine wave and its higher harmonics. In my experiments only the first two higher harmonics were detectable by the H1-cell (see ) thereby reducing the complexity of the stimulus even more. The next step in analyzing the effect of the visual pattern on dynamic adaptation will be to add each harmonic separately to the visual pattern to see how each harmonic affects the stimulus-response function. This could clarify the difference between the LPTC and Reichardt detector responses to different stimulus patterns and the role of the sinusoidal grating in dynamic adaptation.

---

## Functionality in the fly visual system

What is the function of dynamic adaptation in the H1-cell in the context of the LPTC network and fly motion vision? Is there physiological evidence for the computational processes of the Reichardt detector in cells presynaptic to the lobula plate tangential cells? This work demonstrated that the dynamic adaptation found in the H1-cell can be explained by the Reichardt detector model. Therefore dynamic adaptation should be present in all of the LPTCs in the fly. This section will look at the cellular organization of the fly visual system in the context of the results found in this work.

### Physiology of motion detection

Gain control in sensory systems has often been approached from a ‘black box’ perspective; describing the phenomenon of gain control and its importance in information maximization. But the mechanism behind gain control has rarely been studied. The work presented here provides a potential mechanism for gain control in the H1-cell of the fly visual system. The mechanism that was found however, is based on an algorithmic model; it is a mathematically tractable scheme for detecting motion. The question remains as to the physiological basis for the mathematical model in the visual system of the fly and how significant the individual computational steps in the Reichardt detector are to the dynamic gain control found in the H1-cell.

As previously mentioned, cells in the medulla are the first to be stained with 2-deoxyglucose in response to motion (Bausenwein and Fischbach, 1992), suggesting that this is the first location of motion responsive cells in the fly. Intracellular recordings from the cells of the medulla would be more informative about what type of cellular responses these cells have but the recordings are quite difficult. Recent work has shown that Tm cells that connect the medulla with the lobula respond to motion in all directions with membrane potential fluctuations that are the same temporal frequency as the visual pattern (Figure 4.7). Other Tm cells of the medulla respond to a moving grating in each direction with a hyperpolarization (Douglass and Strausfeld, 2003). T2 and Y-cells that also connect the second and third neuropile layers respond to flicker motion with an “on” and “off” response and respond with spike-like activity to moving gratings, also irrespective of direction.

What are the predicted responses in the subunits of the Reichardt detector? In the Reichardt detector model, the response of a single unit after the multiplication step would be

orientationally selective and fluctuate with the temporal frequency of the spatial grating. The subtraction and integration steps are thought to occur in the LPTCs, and evidence for local inhibitory and excitatory inputs support this hypothesis. The subunits before the multiplication step should not respond specifically to motion signals. It is still unclear how the filtering steps occur in the neuropile layers preceding the LPTCs. Electrophysiological and modeling research continues to find possible mechanisms for computation in individual neurons. It is possible to imagine that the opening and closing of specific ionic channels could approximate linear filtering properties, depending on the activation and inactivation properties of the channel. In addition, both shunting inhibition and threshold generation have been shown to approximate the multiplicative step of the Reichardt detector (Torre and Poggio, 1978; Grzywacz and Koch, 1987; Srinivasan and Bernard, 1976).

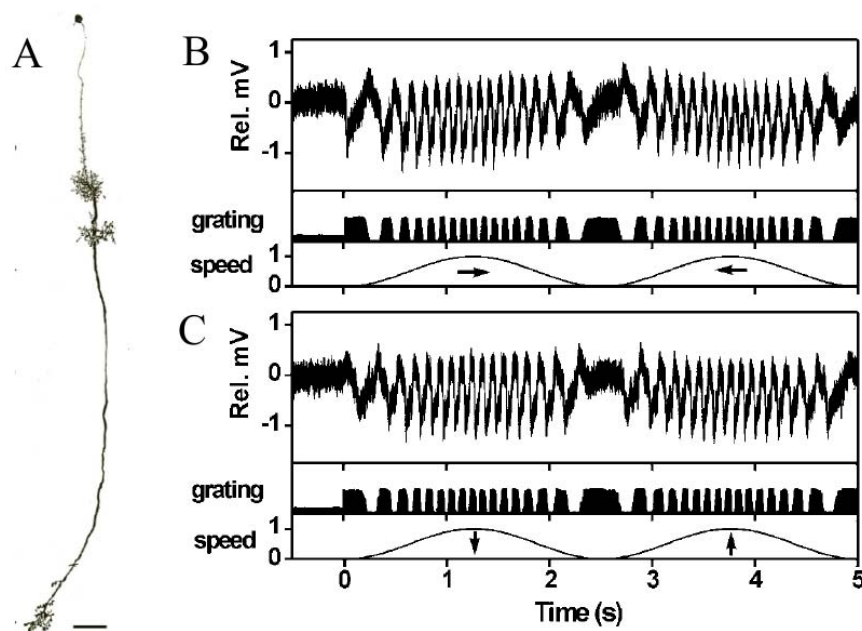


Figure 4.7 Response of a Tm cell to a moving grating. (A) The anatomy of the transmedullar cell recorded from; its dendrites are bunched in two different medullar layers. (B) The response of the Tm cell to horizontal motion and (C) to vertical motion in both directions where the speed of the moving grating was sinusoidally varied between 0 and 200 deg/sec. Adapted from (Douglass and Strausfeld, 2003).

All of these examples show responses to motion irrespective of direction, and therefore do not explicitly give evidence in favor of the Reichardt detector. It is possible that the original input signals are combined and then separated at a later stage leading to orientation selectivity. These experiments are difficult to do and therefore the sample size is very small. A current direction of research into the local motion detector is to try and patch the medullar cells and then to anatomically type the cells recorded from. The key is to determine the

different cells types that exist and build up a database of their response properties in order to see where motion detection in the fly visual system occurs.

**H1-cell functionality**

The H1-cell responds primarily to motion from back to front on the ipsilateral side of the fly. It is known to receive inhibitory input from the CH cells on the ipsilateral side and to provide excitatory input to the HS and CH cells on the contralateral side (Figure 4.8). Therefore the H1-cell is ideally placed to respond to differences in optic flow. The major difference in optic flow stimuli is whether both eyes receive motion input in the same direction (rotation) or in the opposite direction (translation). Using 2 monitors one on each side of the eye, the difference in response properties of the H1-cell to rotational and translational motion were tested. The H1-cell did not respond to preferred or null direction velocity steps presented only on the contralateral side. It responded strongly to preferred direction velocity steps in the contralateral eye and to rotational and translational velocity steps (Farrow, 2005). There was however very little difference between the magnitude of the response to rotation and translation. When a white noise velocity profile was presented to the H1-cell however, the response of the H1-cell to rotational motion was much higher than the response to translational motion. The H1-cell distinguishes between rotational and translational motion for dynamic stimuli.

	HSN	HSE	HSS	dCH	vCH	H1	VS fron	VS med	VS lat
HSN n=9	X	●●● ●●● ●●●	●○○ ○○○ ○○○	●●● ●●● ●●●	●○○ ●○○ ●○○	○○○ ○○○ ○○○	○○○ ○○○ ○○○	○○○ ●○○ ○○○	●●● ●●● ●●●
HSE n=6	●●● ●●●	X	●●● ●●●	●●● ●●●	●●● ●●●	○○○ ○○○	○○○ ○○○	○○○ ●○○	○○○ ●○○
HSS n=5	●○○ ○○○	○○○ ○○○	X	●○○ ○○○	●●● ●●●	○○○ ○○○	○○○ ○○○	○○○ ○○○	●○○ ○○○
dCH n=3	●●● ●●●	●●● ●●●	●○○	X	●●● ●●●	○○○	○○○	○○○	●●● ●●●
vCH n=3	○○○ ○○○	●●● ●●●	●●● ●●●	○○○ ○○○	X	○○○	○○○	○○○	○○○

Figure 4.8 Electrical connections between different LPTCs in the blowfly. Neurobiotin (a dye that can pass through electrical synapses but not through chemical synapses or membranes) was injected into the 5 LPTCs shown in the rows. The resulting staining is shown in the columns. Empty circles represent no staining and the strength of the staining represented by the grey level. The H1-cell was stained when Neurobiotin was injected into HSE, dCH and vCH cells. Adapted from (Haag and Borst, 2005).

It is not clear whether the major purpose of the H1-cell in the LPTC network is to distinguish between rotational and translational dynamic stimuli, but dynamic gain adaptation would then allow the H1-cell to adapt to the variance of the current velocities. Normal flight patterns of the fly can lead to speeds that change from around zero degrees/sec to hundreds of degrees/sec (Lindemann et al., 2003). Under these circumstances it would be beneficial for the H1-cell to adapt its firing properties to the statistics of the stimulus. If the H1-cell is responsible for looking at differences between the two eyes then this would also suggest that the H1-cell only needs the relative velocity information that is provided in the firing rate of the cell through dynamic adaptation and that ambiguity does not pose a problem.

### LPTCs network connectivity

Within the horizontal system, it was recently shown that the CH cells do not receive their visual information directly from the local motion detectors but rather through electrical dendro-dendritic synapses with overlapping HS cells (Cuntz et al., 2003; Haag and Borst, 2002; Farrow et al., 2003). As a result of the local nature of the input and output synapses and the properties of electrical synapses, the resulting local signal in the CH-cell is a low-passed version of the original signal (Cuntz et al., 2003). The CH cell then has inhibitory synapses on the FD-cells, small field cells, and that this connection is a method for feature detection (Cuntz et al., 2003; Haag and Borst, 2002). A picture of the full horizontal connectivity is shown in Figure 4.9.

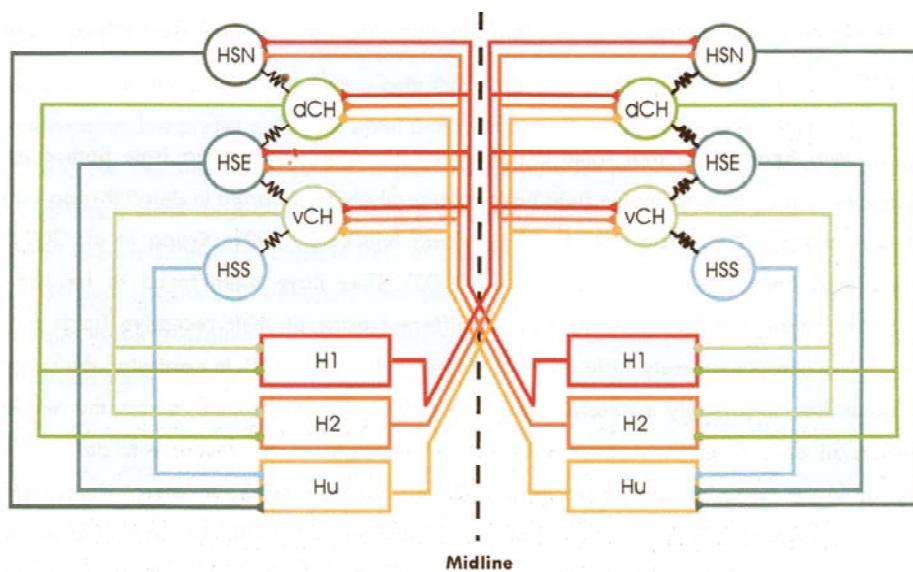


Figure 4.9. Circuit diagram of the connectivity between horizontal LPTCs in both hemispheres. The HS and H1-Hu cells receive input from the local motion detectors. Excitatory connections are shown with triangle and inhibitory with circle endings. Black resistors indicate the electrical coupling between the HS and the CH cells. Triangle endings indicate excitatory connections, circles indicate inhibitory connections. From (Farrow, 2005).

The receptive fields of the LPTCs are often complex, and show responses to more than one direction. This is thought to be due in part to the neural circuitry between the LPTCs. These connections can be both within an individual lobula plate or can connect the lobula plates from the two hemispheres. Connections within a lobula plate can also be dendro-dendritic or also axon-axonal. The network connections between LPTCs are thought to be important in optic flow and course control. It is not clear how dynamic adaptation will play a role in the functionality of the LPTC circuitry. If LPTCs all do turn out to show dynamic adaptation then it is possible that we will have to rethink the way in which the fly visual system encodes information.

---

## Concluding remarks

The H1-cell of the fly visual system adapts its input-output function to the standard deviation and the correlations of the velocity stimulus for Gaussian colored noise velocity signals. This form of adaptation was found to occur very fast and to depend on the spatial pattern presented. The same type of dynamic gain control was found in the response properties of the Reichardt detector without any change in the model parameters; it happened automatically. Based on other work on dynamic gain control and general models of gain control I suggest that there are 2 basic principles required for a system to exhibit gain control: 1) a system that responds to the past history of the stimulus and 2) a non-linear function.

This work leaves many questions unanswered but it also opens up new questions that can easily be tested. Some of the open questions that should be addressed include:

- The effect of the spiking mechanism in the H1-cell on dynamic adaptation
- The generality of dynamic adaptation to other non-Gaussian stimulus distributions
- The physiological implementation of the Reichardt detector in the fly visual system

In addition it will be important to untangle the different levels of dynamic adaptation by looking for gain control in other LPTC neurons and by using other perhaps less complicated stimuli that will prevent the non-linear nature of the sinusoidal grating from influencing dynamic gain in the motion detector. There is no general theory of nonlinear systems. A nonlinear system with memory can be quite surprising. In particular, it can produce any

## Discussion

output signal in response to any input signal. Throughout the nervous system, non-linear systems with memory can be found on many scales, from the biophysical properties of individual ion channels to entire neurons and even perhaps to networks. Understanding the nature of dynamic adaptation in the fly visual system has the potential to lead to a deeper understanding of many areas of neuroscience.

## 5 References

---

1. Adelson EH, Bergen JR (1985) Spatiotemporal energy models for the perception of motion. *J Opt Soc Am A* 2: 284-299.
2. Attneave F (1954) Some informational aspects of visual perception. *Psychological Review* 61: 183-193.
3. Baccus SA, Meister M (2002) Fast and slow contrast adaptation in retinal circuitry. *Neuron* 36: 909-919.
4. Barlow HB (1961) Possible principles underlying the transformation of sensory messages. In: *Sensory Communication* (WA Rosenblith, ed), pp 217-324. Cambridge, MA: MIT Press.
5. Barlow HB, Levick WR (1965) The mechanism of directionally selective units in rabbit's retina. *J Physiol* 178: 477-504.
6. Bausenwein B, Dittrich APM, Fischbach KF (1992) The optic lobe of *Drosophila melanogaster*. II. Sorting of retinotopic pathways in the medulla. *Cell Tissue Res* 267: 17-28.
7. Bausenwein B, Fischbach K-F (1992) Activity labeling patterns in the medulla of *Drosophila melanogaster* caused by motion stimuli. *Cell Tissue Res* 270: 25-35.
8. Bialek, W and de Ruyter van Steveninck, R. Features and dimensions: Motion estimation in fly vision. *Quantitative Biology* . 2-3-2005.
9. Borst A (2006) Correlation versus gradient type motion detectors: the pros and cons. *Philosophical Transactions of the Royal Society of London Series B-Biological Sciences*.
10. Borst A (2003) Noise, not stimulus entropy, determines neural information rate. *J Computat Neurosci* 14: 23-31.
11. Borst A, Egelhaaf M (1993) Detecting visual motion: Theory and models. In: *Visual Motion and its Role in the Stabilization of Gaze* (Miles FA, Wallman J, eds), pp 3-27. Elsevier Science Publishers.
12. Borst A, Flanagan VL, Sompolinsky H (2005) Adaptation without parameter change: Dynamic gain control in motion detection. *PNAS* 102: 6172-6176.
13. Borst A, Haag J (1996) The intrinsic electrophysiological characteristics of fly lobula plate tangential cells :I. Passive membrane properties. *J Computat Neurosci* 3: 313-336.

## References

14. Borst A, Haag J (2001) Effects of Mean Firing on Neural Information Rate. *J Computat Neurosci* 10: 213-221.
15. Borst A, Haag J (2002) Neural networks in the cockpit of the fly. *J Comp Physiol A Neuroethol Sens Neural Behav Physiol* 188: 419-437.
16. Borst A, Reisenman C, Haag J (2003) Adaptation of response transients in fly motion vision. II: Model studies. *Vision Res* 43: 1311-1324.
17. Braddick OJ (1980) Low-level and high-level processes in apparent motion. *Phil Trans R Soc Lond B* 290: 137-151.
18. Brenner N, Bialek W, Steveninck RRv (2000) Adaptive Rescaling Maximizes Information Transmission. *Neuron* 26: 695-702.
19. Buchner E (1976) Elementary movement detectors in an insect visual system. *Biol Cybern* 24: 85-101.
20. Buchner E (1984) Behavioural analysis of spatial vision in insects. In: *Photoreception and vision in invertebrates* (Ali MA, ed), pp 561-621. New York, London: Plenum Press.
21. Buchner E, Buchner S, Bülthoff I (1984) Deoxyglucose mapping of nervous activity induced in *Drosophila* brain by visual movement. *J Comp Physiol A* 155: 471-483.
22. Chance FS, Abbott LF, Reyes AD (2002) Gain modulation from background synaptic input. *Neuron* 35: 773-782.
23. Chklovskii DB, Koulakov AA (2004) MAPS IN THE BRAIN: What Can We Learn from Them? *Ann Rev Neurosci* 27: 369-392.
24. Chubb C, Sperling G (1988) Drift-balanced random stimuli: a general basis for studying non-Fourier motion perception. *J Opt Soc Am A* 5: 1986-2006.
25. Cuntz H, Haag J, Borst A (2003) Neural image processing by dendritic networks. *PNAS* 100: 11082-11085.
26. Dan Y, Atick JJ, Reid RC (1996) Efficient coding of natural scenes in the lateral geniculate nucleus: experimental test of a computational theory. *J Neurosci* 16: 3351-3362.
27. de Ruyter van Steveninck R, Zaagman WH, Mastebroek HAK (1986) Adaptation of transient responses of a movement-sensitive neuron in the visual system of the blowfly *Calliphora erythrocephala*. *Biol Cybern* 53: 451-463.
28. Douglass JK, Strausfeld NJ (2003) Retinotopic pathways providing motion-selective information to the lobula from peripheral elementary motion-detecting circuits. *J Comp Neurol* 457: 326-344.
29. Eckert H (1980) Functional properties of the H1-neurone in the third optic ganglion of the blowfly, *Phaenicia*. *J Comp Physiol* 135: 29-39.

## References

30. Egelhaaf M, Borst A (1989) Transient and steady-state response properties of movement detectors. *Journal of the Optical Society of America A-Optics Image Science and Vision* 6: 116-127.
31. Egelhaaf M, Borst A, Reichardt W (1989) The non-linear mechanism of direction selectivity in the fly motion detection system. *Naturwiss* 76: 32-35.
32. Exner S (1868) Über die zu einer Gesichtswahrnehmung nöthige Zeit. *Sitzungsberichte der kaiserlichen Akademie, Math Naturw Classe* 58: 601-631.
33. Fairhall AL, Lewen GD, Bialek W, de Ruyter van Steveninck R (2001) Efficiency and ambiguity in an adaptive neural code. *Nature* 412: 787-792.
34. Farrow, K. Lateral interactions and receptive field structure of lobula plate tangential cells in the blowfly. 1-106. 2005. Ludwig-Maximilians Universität. Thesis/Dissertation
35. Farrow K, Haag J, Borst A (2003) Input organization of multifunctional motion-sensitive neurons in the blowfly. *J Neurosci* 23: 9805-9811.
36. Fermi G, Reichardt W (1963) Optomotorische Reaktionen der Fliege *Musca domestica*. Abhängigkeit der Reaktion von der Wellenlänge, der Geschwindigkeit, dem Kontrast und der mittleren Leuchtdichte bewegter periodischer Muster. *Kybernetik* 2: 15-28.
37. Fischbach KF, Dittrich APM (1989) The optic lobe of *Drosophila melanogaster*. I. A Golgi analysis of wild-type structure. *Cell Tissue Res* 258: 441-475.
38. Gauck V, Egelhaaf M, Borst A (1997) Synapse distribution on VCH, an inhibitory, motion-sensitive interneuron in the fly visual system. *J Comp Neurol* 381: 489-499.
39. Götz KG (1964) Optomotorische Untersuchungen des visuellen Systems einiger Augenmutanten der Fruchtfliege *Drosophila*. *Kybernetik* 2: 77-92.
40. Grzywacz NM, Koch C (1987) Functional properties of models for direction selectivity in the retina. *Synapse* 1: 417-434.
41. Haag J, Borst A (2002) Dendro-dendritic interactions between motion-sensitive large-field neurons in the fly. *J Neurosci* 22: 3227-3233.
42. Haag J, Borst A (2003) Orientation tuning of motion-sensitive neurons shaped by vertical-horizontal network interactions. *J Comp Physiol A Neuroethol Sens Neural Behav Physiol* 189: 363-370.
43. Haag J, Borst A (2005) Dye-coupling visualizes networks of large-field motion-sensitive neurons in the fly. *Journal of Comparative Physiology A: Sensory, Neural, and Behavioral Physiology* 191: 445-454.
44. Haag J, Denk W, Borst A (2004) Fly motion vision is based on Reichardt detectors regardless of the signal-to-noise ratio. *Proceedings of the National Academy of Sciences of the United States of America* 101: 16333-16338.

## References

45. Harris RA, O'Carroll DC, Laughlin SB (2000) Contrast gain reduction in fly motion adaptation. *Neuron* 28: 595-606.
46. Hausen K (1982) Motion sensitive interneurons in the optomotor system of the fly. I. The Horizontal Cells: Structure and signals. *Biol Cybern* 45: 143-156.
47. Hausen, K. The neural architecture of the lobular plate of the blowfly *Calliphora erythrocephala*. 1984. Unpublished Work
48. Hecht S (1931) *Retinal Processes Concerned with Visual Acuity and Color Vision*. Cambridge: Harvard University Press.
49. Hengstenberg R (1982) Common visual response properties of giant vertical cells in the lobula plate of the blowfly *Calliphora*. *J Comp Physiol A* 149: 179-193.
50. Hengstenberg R, Hausen K, Hengstenberg B (1982) The number and structure of giant vertical cells (VS) in the lobula plate of the blowfly *Calliphora erythrocephala*. *J Comp Physiol A* 149: 163-177.
51. Hildreth EC, Koch C (1987) The analysis of motion: From computational theory to neuronal mechanisms. *Ann Rev Neurosci* 10: 477-533.
52. Hodgkin AL, Nunn BJ (1988) Control of light-sensitive current in salamander rods. *J Physiol (Lond)* 403: 439-471.
53. Hosoya T, Baccus SA, Meister M (2005) Dynamic predictive coding by the retina. *Nature* 436: 71-77.
54. Kim KJ, Rieke F (2003) Slow Na<sup>+</sup> inactivation and variance adaptation in salamander retinal ganglion cells. *J Neurosci* 23: 1506-1516.
55. Kirschfeld K (1972) The visual system of *Musca*: studies on optics, structure and function. In: *Information Processing in the Visual Systems of Arthropods* (Wehner R, ed), pp 61-74. Berlin, Heidelberg, New York: Springer.
56. Land MF (1997) Visual acuity in insects. *Annu Rev Entomol* 42: 147-177.
57. Land MF, Collett TS (1974) Chasing behavior of houseflies (*Fannia canicularis*). *J Comp Physiol* 89: 331-357.
58. Land MF, Eckert H (1985) Maps of the acute zones of fly eyes. *J Comp Physiol A* 156: 525-538.
59. Laughlin S (1981a) A simple coding procedure enhances a neurons information capacity. *Zeitschrift fur Naturforschung C-A Journal of Biosciences* 36: 910-912.
60. Laughlin S (1981b) Neural principles in the peripheral visual system. In: *Handbook of sensory physiology VII/6B* (Autrum H, ed), pp 133-280. Berlin, Heidelberg, New York: Springer.

## References

61. Lindemann JP, Kern R, Michaelis C, Meyer P, van Hateren JH, Egelhaaf M (2003) FliMax, a novel stimulus device for panoramic and highspeed presentation of behaviourally generated optic flow. *Vision Res* 43: 779-791.
62. Maddess T, Laughlin SB (1985) Adaptation of the motion-sensitive neuron H1 is generated locally and governed by contrast frequency. *Proc R Soc Lond B* 225: 251-275.
63. Mante V, Frazor RA, Bonin V, Geisler WS, Carandini M (2005) Independence of luminance and contrast in natural scenes and in the early visual system. *Nat Neurosci* 8: 1690-1697.
64. Marr D, Ullman S (1981) Direction selectivity and its use in early visual processing. *Proc R Soc Lond B* 211: 151-180.
65. Pirenne MH (1967) *Vision and the Eye*. London: Chapman & Hall.
66. Potters M, Bialek W (1994a) Statistical mechanics and visual signal processing. *Journal of Physiology France* 4: 1755-1775.
67. Reichardt W (1961) Autocorrelation, a principle for the evaluation of sensory information by the central nervous system. In: *Sensory Communication* (Rosenblith WA, ed), pp 303-317. New York: M.I.T Press; John Wiley & Sons.
68. Reichardt W, Poggio T (1976) Visual control of orientation behaviour in the fly I. A quantitative analysis. *Quart Rev Biophys* 9: 311-375.
69. Reisenman C, Haag J, Borst A (2003) Adaptation of response transients in fly motion vision. I: Experiments. *Vision Res* 43: 1293-1309.
70. Ruderman DL, Bialek W (1994) Statistics of natural images: Scaling in the woods. *Phys Rev Lett* 73: 814-817.
71. Sekuler R, Anstis S, Braddick OJ, Brandt T, Movshon JA, Orban G (1990) The perception of motion. In: *Visual perception: The neurophysiological foundations* (Spillmann L, Werner JS, eds), pp 205-230. San Diego, New York, Berkeley, Boston, London, Sydney, Tokyo, Toronto: Academic Press.
72. Shannon CE, Weaver W (1949) *The mathematical theory of communication*. Chicago: The University of Illinois Press.
73. Sharpee TO, Sugihara H, Kurgansky AV, Rebrik SP, Stryker MP, Miller KD (2006) Adaptive filtering enhances information transmission in visual cortex. *Nature* 439: 936-942.
74. Simmons PJ (1993) Adaptation and responses to changes in illumination by second- and third-order neurones of locust ocelli. *J Comp Physiol A* 173: 635-648.
75. Smirnakis SM, Berry MJ, Warland DK, Bialek W, Meister M (1997) Adaptation of retinal processing to image contrast and spatial scale. *Nature* 386: 69-73.

## References

76. Sperling G (1989) Three stages and two systems of visual processing. *Spatial Vision* 4: 183-207.
77. Srinivasan MV, Bernard GD (1976) A proposed mechanism for multiplication of neural signals. *Biol Cybern* 21: 227-236.
78. Srinivasan MV, Laughlin SB, Dubs A (1982) Predictive coding: a fresh view of inhibition in the retina. *Proc R Soc Lond B* 216: 427-459.
79. Strausfeld NJ (1984) Functional neuroanatomy of the blowfly's visual system. In: *Photoreception and vision in invertebrates* (Ali MA, ed), pp 483-522. Plenum Publishing Corporation.
80. Strausfeld NJ (1989) Beneath the compound eye: Neuroanatomical analysis and physiological correlates in the study of insect vision. In: *Facets of Vision* (Stavenga DG, Hardie RC, eds), pp 317-359.
81. Strausfeld NJ, Lee JK (1991) Neuronal basis for parallel visual processing in the fly. *Vis Neurosci* 7: 13-33.
82. Torre V, Poggio T (1978) A synaptic mechanism possibly underlying directional selectivity to motion. *Proc R Soc Lond B* 202: 409-416.
83. van Hateren JH, Kern R, Schwerdtfeger G, Egelhaaf M (2005) Function and coding in the blowfly H1 neuron during naturalistic optic flow. *J Neurosci* 25: 4343-4352.
84. Van Rullen R, Thorpe SJ (2001) Rate coding versus temporal order coding: What the retinal ganglion cells tell the visual cortex. *nc* 13: 1255-1283.
85. Victor JD, Purpura KP (1996) Nature and precision of temporal coding in visual cortex: a metric- space analysis. *J Neurophysiol* 76: 1310-1326.
86. Warzecha AK, Egelhaaf M, Borst A (1993) Neural circuit tuning fly visual interneurons to motion of small objects. I. Dissection of the circuit by pharmacological and photoinactivation techniques. *J Neurophysiol* 69: 329-339.
87. Yu YG, Lee TS (2003) Dynamical mechanisms underlying contrast gain control in single neurons. *Physical Review E* 68: 011901-1-7.
88. Zanker JM (1996) On the elementary mechanism underlying secondary motion processing. *Phil Trans R Soc Lond B* 351: 1725-1736.

## 6 Acknowledgements

---

The PhD was the first real struggle in my academic career and I found it a good lesson in my own strengths and weaknesses and in the value of friends and colleagues. Therefore, I would like to thank first and foremost, my “Doktorvater” Prof. Dr. Alexander Borst for being patient with me through the struggle. He offered me the opportunity to start again after a catastrophe and always gave me a second chance although I often disappointed him. His excitement and interest in all forms of science is contagious and it has been an honor to have worked so closely with him.

I am exceedingly grateful to Dr. Jürgen Haag for teaching me about electrophysiological recording and about the fly visual system. Also to Tanja Martin for showing me how she prepares a blowfly. Thanks also to Haim Sompolinsky for making my stay in Jerusalem memorable. I am indebted to the ‘bigfly’ lab, especially Hermann Cuntz, Karl Farrow, Yong Choe and Deusdedit Spavieri. I thank Hermann for bringing me to Germany in the first place and for being an amazing friend. I thank Yong and Dedi for their fruitful discussions and non-patronizing manners, I respect both of you as people and as scientists. And thank you Renate Gleich for your constant vigilance.

I am very grateful to everyone in the Borst lab for creating such a friendly and open atmosphere. I am indebted to Alexandra Ihring for my German and for the drive to actually complete this work. I am grateful to Eva Naumann for brightening up everything around her and being a kindred spirit. I would also like to thank members of other labs especially Katrin Deininger for always being there for me and generally for being a wonderful friend.

Last but certainly not least I would like to thank my family, each one as much as the other and each one for the unique roll that they have played in bringing me to this point in my life. I could not have done it without all of you, and yet each of you has been essential in his own way.

I dedicate this work, this struggle to my grandfather, Alfred Amorosi, who inspired many people to think for themselves. He motivated me to ask questions about the world around me and especially to not believe every answer I get.

## 7 Curriculum Vitae

---

### Virginia L. Flanagin

Max-Planck Institute of Neurobiology  
Systems and Computational Neurobiology  
Am Klopferspitz 18  
82152 Martinsried, Germany

virginia@neuro.mpg.de  
Tel: (089) 8578-3294

#### EDUCATION

**Ludwig-Maximilians Universität**, Munich, Germany, *Ph.D.* Neurobiology, **2006**  
Max-Planck Inst. of Neurobiology, Martinsried  
Thesis: Dynamic adaptation in fly motion vision  
Supervisor: Prof. Alexander Borst

**University of California, Berkeley**, USA, *M.Sc.* Epidemiology, **2002**  
Dept. Environmental Science, Policy & Management  
Topic: Socio-economic factors influencing AIDS transmission in South Africa  
Committee: Dr. Wayne M. Getz (advisor), Dr. Louise Fortmann, Dr. Cheryl Briggs

**Illinois Wesleyan University**, Bloomington, IL USA, *B.A. (Honors)* **1999**  
Emphasis: Theoretical Ecology GPA 3.8/4.0  
Supervisor: Dr. Given Harper

#### RESEARCH EXPERIENCE

**Interdisciplinary Center for Neural Computation**, Jerusalem, Israel **2004-2005**  
**Exchange Student**  
Worked with Haim Sompolinsky on the response properties of the correlation-type motion detector model to dynamic motion stimuli

**École de Physique**, les Houches, France **8/2003**  
Student Participant  
Section 80: Methods and Models in Neurophysics

**Illinois State University**, Vero Beach, FL, USA **Summer 1999**  
NSF-NIH Research Assistant  
Field and laboratory research with Steven Juliano investigating mosquito competition and community ecology

**Kansas State University**, Manhattan, KS, USA **Summer 1998**  
NSF-REU Undergraduate Fellowship  
Field biology and analysis studying the effects of grazing and fire management on prairie bird populations

Curriculum Vitae

**Illinois Wesleyan University**, Bloomington, IL, USA **1998-1999**  
Undergraduate Honors Thesis  
Quantification of Organochlorine Pesticides in Costa Rican Avifauna

**Illinois State University**, Normal, IL, USA **1997-1999**  
NSF-CRUI Undergraduate Fellowship  
Examined models for grasshopper growth in sub-optimal environments.  
Supervisor: Steven Juliano

FELLOWSHIPS & AWARDS      Max-Planck Fellowship, Max-Planck Inst. of Neurobiology  
2002-2006 College of Nat. Resources Fellowship, Univ. of California, Berkeley  
1999-2002 McKinsey & Co. Start Social Project Stipend, Munich, Germany  
2002 Wayne Wantland Biology Award, IWU  
1999 Howard Hodges Mathematics and Science Award, IWU  
1999 Alumni Scholarship, IWU  
1996-1999 Phi Kappa Phi Honors Society  
Sigma Xi Research Society  
Beta Beta Beta Biological Society

PUBLICATIONS      Borst, A, VL Flanagan, H. Somplinsky. (2005) Adaptation without parameter  
change: dynamic gain control in motion detection. **PNAS**. 102(17): 6172-  
6176.  
Klemens, JA, ML Wieland, VL Flanagan, JA Frick, RG Harper. (2003) A cross-  
taxa survey of organochlorine pesticide contamination in a Costa Rican  
wildland. **Journal of Environmental Pollution**. 122: 245-251.  
Flanagan, VL, SP Haase, SA Juliano. (2000) Effects of growth rates on  
development to metamorphosis in the lubber grasshopper, *Romalea*  
*microptera*. **Oecologia**. 125 (2): 162-169.

TEACHING      **University of California, Berkeley, USA**  
*Developmental Biology MCB131* **2001**  
**Illinois Wesleyan University**, Bloomington IL, USA  
*Introductory Ecology* **1997-1999**  
*Developmental Biology* **1998-1999**

TALKS      Max-Planck Institute for Dynamics and Self-Organization, Göttingen, Germany  
2006  
First Bernstein Center for Computational Neurosc. Meeting, Freiburg, Germany  
2005  
Entomological Society of America Annual Meeting  
1998

LANGUAGES      English and German: proficient in writing, reading and speaking